FFI-RAPPORT

MODITIC

simulation report on operational urban dispersion modelling

—

Stephane Burkhart, Direction Générale de l'Armement (DGA)
Arnaud Gousseff, Direction Générale de l'Armement (DGA)
John Aasulf Tørnes, Forsvarets forskningsinstitutt (FFI)
Oscar Björnham, Totalförsvarets forskningsinstitut (FOI)

MODITIC

simulation report on operational urban dispersion modelling

Stephane Burkhart, Direction Générale de l'Armement (DGA)
Arnaud Gousseff, Direction Générale de l'Armement (DGA)
John Aasulf Tørnes, Forsvarets forskningsinstitutt (FFI) Oscar
Björnham, Totalförsvarets forskningsinstitut (FOI)

Norwegian Defence Research Establishment (FFI)   20 September 2016

Keywords

Ammoniakk
EDA
Modellering og simulering
Spredning

Approved by
Hanne Breivik, *Research Manager*
Janet M Blatny, *Director*

Summary

The European Defence Agency (EDA) project B-1097-ESM4-GP "Modelling the DIspersion of Toxic Industrial Chemicals in urban environments" (MODITIC) has from 2012 to 2016 studied the release and transport of neutral and non-neutral chemicals in complex urban environments, in order to enhance the understanding of the dominating physical processes involved, and to support improvements in modelling techniques. This is important in order to improve the operational urban dispersion modelling tools in use by the EDA countries.

In work package WP6000, the capabilities of the current national members' operational models to handle complex urban dispersion of dense gas releases were assessed. The different operational models QUIC, PUMA, ARGOS and PMSS used in this study require different skill and expertise levels. The execution time for the simulations varies from minutes to hours. The most time consuming and demanding part is the setup of the models and to couple them to meteorology and source term descriptions. These models are usually conservative, and overestimation of the concentration levels close to the source may lead to exaggerated response.

In the ammonia field tests at INERIS, the QUIC software seems to work well using the included dense gas sub-model. The latest developments on PUMA have been tested with promising results in the scope of this project, dealing with dense puff interaction in a semi-linearized way to keep the response fast enough. ARGOS heavy puff model also provides good results for dense gas on open field but cannot handle obstacles in combination with dense gas.

Wind tunnel experiments of the dispersion of neutral and non-neutral gases in a part of Paris were also used for comparison. In this case, it was observed that the models tested tend to overestimate the concentration by a factor of three to five close to the source, and underestimate by the same factor in far field. ARGOS and PMSS were tested against the Paris case for neutral gas only and behave quite satisfyingly. Overestimations of concentrations behind buildings and underestimations in main streets were usually observed. A dense gas module exists for PMSS but was not available at the time.

In conclusion, as far as we tested our models, only QUIC has proved able to handle both obstacles and dense gas at the same time. PUMA was modified to handle dense gas characteristics but lacks functionalities on urban geometries. PMSS and ARGOS were partially validated with neutral gas on urban scenarios, but the dense gas modules remain to be tested and developed. The ARGOS URD model is mainly suited for densely built urban-like areas, but can only handle neutral gas. The tested models are not push-button tools and require various levels of expert skills. The advantage against models using computational fluid dynamics is the cheap computer cost, but they still need relatively large set-up times compared to the run-time. Development of software that can handle dispersion of dense gases in an urban environment is needed in the future.

Sammendrag

European Defence Agency prosjektet B-1097-ESM4-GP "MOdelling the DIspersion of Toxic Industrial Chemicals in urban environments" (MODITIC) har i perioden 2012—2016 studert utslipp og transport av nøytrale og ikke-nøytrale kjemikalier i et komplekst bymiljø for å øke forståelsen av de dominerende fysiske prosessene som er involvert. Dette er viktig for å forbedre de verktøyene som benyttes for urban spredningsmodellering i EDA-landene.

I arbeidspakke WP6000 ble det undersøkt hvilke muligheter deltakerlandene har til å benytte operasjonelle modeller for å håndtere spredning av tunge gasser i et komplekst bymiljø. De operasjonelle modellene QUIC, PUMA, ARGOS og PMSS som ble brukt i denne studien, krever ulik grad av ekspertise og ferdigheter. Gjennomføringstiden for simuleringene varierer fra minutter til timer. Den vanskeligste og mest tidkrevende delen er oppsett av modellene og å kople dem til meteorologiske data og beskrivelse av kildetermen. De operasjonelle modellene er generelt konservative og overestimerer konsentrasjonsnivåene nær utslippet. Dette kan føre til overdrevne beskyttelsestiltak.

Programvaren QUIC synes å fungere bra ved bruk av den tilhørende tung-gass-undermodellen for felttestene med ammoniakk ved INERIS. Den seneste utviklingen av PUMA, som håndterer tunge gasser på en semi-lineær måte for å gi svar raskt nok, har blitt testet med lovende resultater innenfor dette prosjektet. Tung-gass-modellen i ARGOS gir også gode resultater fra tunge gasser spredt på et åpent område, men kan ikke samtidig håndtere hindringer.

Vindtunneleksperimenter med spredning av nøytrale og ikke-nøytrale gasser i en del av Paris ble også benyttet. Her ble det observert en tendens for modellene til å overestimere konsentrasjonen med en faktor tre til fem nær utslippet og underestimere tilsvarende på større avstander. ARGOS og PMSS ble testet kun på nøytral gass i Paris-eksempelet og oppførte seg tilfredsstillende. Overestimering av konsentrasjonen på baksiden av bygninger og underestimering av konsentrasjonen i hovedgatene ble vanligvis observert. Det eksisterer en tung-gass-modell for PMSS, men denne var ikke tilgjengelig for bruk i løpet av dette prosjektet.

Så langt som disse modellene ble testet, konkluderes det med at kun QUIC kan håndtere både hindringer og tunge gasser samtidig. PUMA ble modifisert til å håndtere tunge gasser, men mangler funksjonalitet for bruk i bymiljøer. PMSS og ARGOS ble delvis validert i et bymiljø ved bruk av en nøytral gass, men en modell for håndtering av tung gass må testes (PMSS) eller utvikles (ARGOS). ARGOS URD er egnet for å brukes i tettbebygde områder, men kan kun håndtere nøytrale gasser. Disse modellene er ikke automatiserte og krever varierende grad av ekspertise for å kunne benyttes. Fordelen framfor CFD-modeller er at de har lave krav til datakraft, men krever forholdsvis lang tid for oppsett av modellen sammenlignet med kjøretid. I framtiden er det nødvendig å utvikle programvare som kan håndtere spredning av tunge gasser i et bymiljø.

Content

Preface

This work is part of the European Defence Agency (EDA) project B-1097-ESM4-GP "Modelling the dispersion of toxic industrial chemicals in urban environments" (MODITIC). The scientific objective of this project is the systematic study of the release and transport of neutral and non-neutral chemicals in complex urban environments, to enhance understanding of the dominating physical processes involved, and to support improvements in modelling techniques. The participating organisations are:

- Direction Générale de l'Armement (DGA), DGA CBRN Defence, France
- Institut National de l'Environnement Industriel et des Risques (INERIS), France
- Norwegian Defence Research Establishment (FFI), Norway
- Swedish Defence Research Agency (FOI), Sweden
- University of Surrey (UoS), United Kingdom

FFI is the lead organisation. The project was initiated 1 September 2012 with duration of three-and-a-half years. The project is funded by the Norwegian Ministry of Defences, the Swedish Ministry of Defence, the French Ministry of Defence, and the French Ministry of Ecology, Sustainability and Energy.

This report describes work and results from WP6000 "Operational Urban Dispersion Modelling". Chapter 2 contains common setup of the operational models; chapter 3 is authored by FOI Sweden, chapter 4 by DGA CBRNC defence France and chapter 5 by FFI Norway. Chapter 6 gives conclusions and operational recommendations. Each institute has conducted a validation of the quality of their own contribution. Stephane Burkhart (DGA) is the main author and combined the various contributions into a single report, while John Aa Tørnes (FFI) has transferred the report to the FFI-report template.

1   Introduction

We want to assess the capability of urban operational models in use in our national institutes, to give confident results on the dispersion of neutral or dense gas in a real urban environment.

For validation purposes, we will use some of the experimental data issued from 1) INERIS outdoor ammonia experiment [1] [2] and 2) the ENFLO wind tunnel data in the MODITIC project and described in WP4000 report [3].

The chosen wind tunnel models are a 1:200 scale array of idealized building shapes (hereafter called demi-complex) and a 1:350 scale Paris district. The first one will help assess the local properties of the dispersion, and the second one the complexity of a real city (although already simplified).

For practical (operational) purposes, in order to be able to treat realistic scenarios as the one described in WP1000 (release of chlorine following a tank failure in the middle of a densely built area) [4], we need to scale the release to full scale. This requirement stems also from the operational models themselves, which were parameterized for scale 1:1.

We will finally try to get a better understanding of the limitations and possibilities of such models, and give some recommendation for operational use.

2   Common setup

The different models used for the work described in this report require different input parameters. It was tried to set up the software packages to match the scenario description as closely as possible.

2.1   Scenario description

The complete descriptions of the chosen scenarios are described in [4] but we can summarize them as follows:

1) Outdoor release of ammonia (with/without obstacle wall) from INERIS data treated with PUMA, ARGOS and QUIC software
2) Demi-complex scenario treated with PMSS
3) Paris scenario treated with PMSS and ARGOS software.

Scenarios 2 and 3 have been scaled to scale 1:1 from wind tunnel data. Details of scaling procedures will be given below.

Scenarios considered in the wind tunnel involve a neutral atmosphere with neutral or dense gas (CO_2) released from a 10 cm diameter circular source. Several orientations of the buildings towards the incoming wind are considered.

2.2   Specific modelling of wind flow, turbulence and dense/neutral gas transport

Below we describe the main features of the models tested in this study.

ARGOS

ARGOS is sold by PDC-ARGOS (Denmark) and is an operational commercial software for crisis analysis involving CBRN agents. It deals with scenarios such as gas releases (no liquid discharge), fires, explosions and nuclear accidents. The dispersion sub-model Rimpuff is a local scale puff model taking into account local wind variations and turbulence levels. It can also calculate dry and wet deposition. ARGOS includes models for estimating the releases from containers and pipes as well as evaporation of spills on the ground and also has a special model for dispersion of heavy gasses. Heavy gases behave quite differently than normal aerosols or smokes from fires. ARGOS can geo-reference a domain and import user specified meteorological profiles, weather profiles from meteorological towers or numerical weather prediction (NWP) data. A database of properties is included for a number of substances. Based on the properties in the chemical database, ARGOS can calculate suggestions for hazard areas based on the toxicities of the substances involved in the incident. Obstacles can be taken into account through the sub-model Urban Dispersion Model (URD) which has been used for the Paris scenario. Since ARGOS cannot use URD for dense gas releases, only the neutral gas release has been modelled in the Paris scenario. For the INERIS case, the heavy-gas module was used for the release of ammonia without any obstacle present, while neutral gas only was released against the obstacle.

QUIC

QUIC (Quic Urban and Industrial Complex) is developed at Lawrence Livermore National Laboratory (LANL) (US) and is specifically designed for treating urban crisis scenarios with TICs, C, B and R agents and a number of source terms (gas release, liquid discharge, explosion, aerosol dispersion,…). A materials database is not provided, so users have to enter their own material properties. Wind is computed from a diagnostic mass preserving model. QUIC-PLUME uses a Lagrangian random-walk dispersion model, accounting for building-induced turbulence to reconstruct the chemical concentration field.

Buildings are constructed manually, based on simple available geometrical forms (that can be added vertically and horizontally), or automatically imported from shape files. Wind can be

specified from calculated wind profiles or imported as discrete data points. Multiphase releases are also available in addition to basic source terms.

A dense gas dispersion model is provided in version 5.92 of QUIC accounting for turbulent entrainment into the dense gas cloud.

PUMA

The Swedish Defence Research Agency (FOI) develops a custom made program suit for atmospheric dispersion called FOI Dispersion Engine (DE). Several models are included in DE that together span the entire spectrum of temporal and spatial scales needed when dealing with dispersion issues. The model PUMA is designed to operate in real-time and utilizes Gaussian puffs in a Lagrangian approach. The puffs are semi-symmetrical discrete puffs that collectively represent the entire concentration field from one or several sources. In the case of neutral gas the puffs are independent of each other and evolve due to parameterized turbulence as they are transferred according to the meteorological circumstances.

PUMA has been extended to also include dense gas physics. The main parameters that capture the nonlinear dense gas case have been developed and implemented. The introduction of dense gas implies a transition from independent to dependent puffs. The main idea with PUMA is that the puffs are still treated individually to a high extent. Basically each puff is first treated separately and independently with the inclusion of dense gas physics. In the next step dependencies between overlapping puffs are treated. The model is still under development and the results here represent the model status at the end of 2015.

PMSS

ARIA Technologie in France has developed PMSS as a micro-scale version of its own models of wind computation (SWIFT) and agent atmospheric dispersion modelling (SPRAY). This version allows taking into account obstacles in a simplified way and performs the dispersion computation in Lagrangian mode. Obstacles can be isolated or representing a town district. This version is named PMSS (Parallel Micro Swift Spray). PMSS software is thus constituted by two modules: Micro Swift, computing diagnostic 3D wind field and Micro SPRAY, computing 3D dispersion. It is necessary to pre-process building description files to be readable by PMSS through the translator SHAFT provided by ARIA.

A dense gas module exists, but is not available in the version currently in use at DGA CBRN Defence.

It is worth mentioning that PMSS is part of the CERES software (CEA, FR) and also integrated in a HPAC version not available in France.

2.3 Wind tunnel experiment

We refer to the report from WP4000 [3] and WP1000 [4] about the description of the experiments and scaling factor used in the wind tunnel.

2.4 Comparison of the methods

The methods used for comparison are described in the MODITIC WP1000 report on scenario definition and dissemination strategy [4].

Accent is put on using Warner methodology (Measures of Effectiveness) using all the experimental sensors (scaled) locations, but also using plots of observed versus predicted data for normalized concentrations, with FAC2 or FAC5 lines[1] plotted. Horizontal cuts of filled iso-contours of concentrations, eventually wind fields at sensor heights are to be presented (in street and roof levels).

---

[1] FAC2 and FAC5 are fractions of prediction within a factor of two or five, respectively

3 Results obtained by FOI Sweden

3.1 Introduction

The Swedish Defence Research Agency, FOI, has a long tradition of research and investigations in the field of atmospheric dispersion. This includes the usage of external commercially available programs as well as the development of custom models and implementations thereof. Different models are required to be able to face a wide variability of problems. The model *Puff Model of Atmospheric Dispersion* (PUMA) is a Lagrangian dispersion model utilized for real-time simulations. The extension of PUMA to include dense gas effects is described in this report.

Models for dense gas dispersion have been developed since the middle of the 20th century. The problem is nonlinear and complex in its nature which means that it is necessary to insert simplifications in the models. This can be done in many different ways which has led to a myriad of models over the years. One approach is to give an analytic steady-state solution [5-8] which is not a trivial task given the nonlinearity of the problem. Another more popular and useful approach is to adopt the Lagrangian method where discrete distributed parcels are dynamically transported from the source downwind following the physical laws included in the model. The cloud can be represented by cylinders [9, 10], particles with no inherent sizes [11-15] or by means of a more complex formulation using Gaussian puffs [16-18]. As the use of Computational Fluid Dynamics (CFD) has grown rapidly recently, the dense gas problem has also become the subject of several such studies. In this area there is not necessarily new dense gas models per se that have been developed. The dense gas effect is instead captured by the introduction of a state equation, which may be constructed and used in different ways, in terms of density or temperature. The ability of CFD to handle complex geometry is often included in the studies which then becomes very situational [19-23].

PUMA uses horizontally symmetrical discrete puffs with a Gaussian concentration distribution that collectively represent the entire concentration field from one or several sources. We start by the dense gas description of one individual puff and continue with the interactions between puffs as a future development.

3.2 Dense gas

The model implementation for dense gas discussed in this report refers to atmospheric dispersion and hence the expression *dense gas* implies a gas that is denser, *i.e.*, has higher density, than the surrounding air. There are two common situations that give rise to dense gases. The first and most straightforward includes the case where the released gas has a higher molecular weight than air. The second situation, which is in particular addressed here, includes a gas that is a dense gas mainly due to the fact that it has a significantly lower temperature than the surrounding air. This is typically the case when liquefied gas is released. A sudden drop in

pressure in combination with a limited heat exchange with the surroundings leads to a quick adiabatic expansion process in which the temperature drops drastically leading to a dense gas scenario.

3.2.1 Release characterization

The dense gas implementation in PUMA uses a defined volume as a source term where air and the released substance, are mixed at a temperature provided by the user. This means, that given a certain substance the user only needs to define the flow rate, the volume and the temperature as the source term.

- The flow rate means the mass per unit of time of the released substance, the mixed air is not included. This rate may be arbitrarily time dependent.
- The size of the source determines the initial puff size. In combination with the parameter n_{std}, *i.e.*, the number of standard deviations of the so-called effective volume, the model will calculate the amount of entrained air for the density and the thermodynamical calculations.
- The temperature of the source defines the shared temperature of the gas and the entrained air at the source.

3.2.2 Effective volume

The concept of an *effective volume* is mainly introduced for the calculations of the thermodynamical phenomena that are present. An effective volume is defined for every puff and the relative size of this volume is controlled by the constant parameter n_{std}. The effective volume is used to calculate energy exchange with the surroundings, temperature equalization due to air entrainment and the slumping velocity of the puff. The concentration distribution of the puff is not directly affected by this concept but remains unrestricted. The effective volume is described as an ellipsoid, see Figure 3.1, according to

$$\frac{1}{n_{std}^2}\left[\frac{x^2}{\sigma_x^2}+\frac{y^2}{\sigma_y^2}+\frac{z^2}{\sigma_z^2}\right]=1 \tag{1}$$

with the volume

$$V=\frac{4}{3}\pi\sigma_x\sigma_y\sigma_z n_{std}^3 \tag{2}$$

Non-restricted puff

Restricted puff with
an effective volume
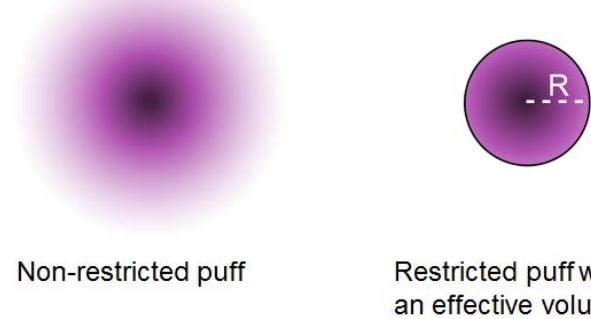
*Figure 3.1   Illustration of the concept with effective volume. A cut off radius R is defined and
the thermodynamics in the model is applied to the effective volume. Note that the
concentration is still kept unrestricted.*

3.2.3   Effective height

PUMA utilizes *effective heights* on the puffs. This effect is introduced to account for situations
where part of the puff becomes located below the surface or above the planetary boundary layer
(PBL). Since this causes a model error in concentration calculations, the part located in a
forbidden region is *mirrored* back into the allowed region. This means that it is virtually
reflected perpendicular to the limiting border and that the geometrical centre of the puff is not
the actual mass centre of the puff anymore. Hence, the puff centre is not used to obtain the mean
velocity and turbulence for the puff in these situations. An analytic expression has been
developed (by vertical integration of the sum of the original and the mirrored concentration) that
provides the effective height which corresponds to the weighted mean value in the vertical
direction, illustrated in Figure 3.2. This property is not particularly compiled for dense gas
modelling but becomes more prominent here since the dense gas puffs are located close to the
ground more frequently than neutral puffs.
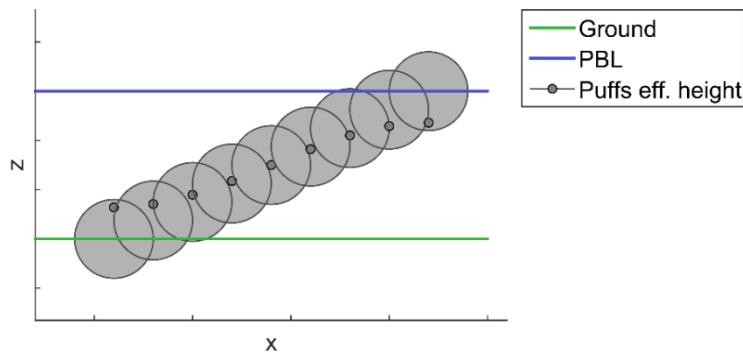
*Figure 3.2   Illustration of the effective heights (dots) for puffs (grey circles) at different
heights. The circles are drawn at one standard deviation from the puff centre.*

3.2.4 Puff mean position assumption

The environmental conditions, often defined by the current meteorology, vary within the dispersion region, in particular they vary vertically. This property is included in PUMA when it comes to neutral turbulence effects for instance. However, this phenomenon is disregarded in several calculations where the environmental value at the coordinate determined by the horizontal puff centrum and the effective height of the puff is used for the entire puff.

It would be possible to use the vertical weighted mean for properties such as wind velocity and turbulence. This would require a vertical integration of the plane concentration multiplied with the property of interest as described by equation (3).

$$\overline{\zeta}_{xy} = \frac{1}{m} \int_0^{pbl} c(z) \zeta_{xy}(z) dz \tag{3}$$

where ζ_{xy} is an arbitrary property of the puff that varies with height, c is the concentration and m is the total mass. However, this expression is in general not analytically solvable and a numerical approach will be far too demanding for a fast model like PUMA. The approach is therefore to calculate the effective height, z_{Eff}, from the concentration profile and directly use

$$\overline{\zeta}_{xy} = \zeta_{xy}(z_{Eff}).$$

3.2.5 Slumping velocity

Due to a higher density than that of the surroundings, the dense gas puffs will descend towards the ground with a slumping velocity, U_{slump}. PUMA utilizes a commonly used expression given by equation (4).

$$U_{slump} = \gamma_{slump} \sqrt{g L_{EV} \frac{\rho - \rho_{air}}{\rho_{air}}} \tag{4}$$

where L_{EV} is the vertical radius on the effective volume, i.e., $L_{EV} \equiv n_{std} \sigma_z$. The slumping velocity is limited to maximum 0.5 m/s for numerical reasons. Note that U_{slump} is always positive in the dense gas case and that the parameter γ_{slump} is a positive constant that is given by empirical data and has been set to unity here.

3.2.6 Richardson number

The Richardson number, *Ri*, is a dimensionless entity that describes the relation between the buoyancy and the convective flows. The expression for the Richardson number is here defined as described by equation (5).

$$Ri \equiv \frac{(U_{slump})^2}{(u*)^2} \tag{5}$$

3.2.7 The F-factor

A factor called the *F-factor*, that describes to which extent a puff is regarded as a dense gas puff, is introduced as

$$F = \frac{Ri - Ri_{min}}{Ri_{max} - Ri_{min}} . \tag{6}$$

The F-factor takes values between 0 and 1, where 0 means no dense gas effects and 1 means maximum dense gas effects. The interval of transition between dense gas and neutral gas is determined by Ri_{min} and Ri_{max}. The lower limit sets the transition between turbulent and laminar dynamics. Ding *et al*. [24] showed by wind tunnel experiments and comparisons with experimental results from others that it was possible to establish a dimensionless relation between the scale of the flow, Re*, and the scale on the density variation relative to the mixing turbulence, Ri*. This resulted in a transition from turbulent to laminar regime at Ri*~8. More explicitly the limit is formulated as

$$Ri_{min} = 7.78 + \frac{0.51}{1000} \frac{u * z_0}{v} \tag{7}$$

where v is the dynamic viscosity of air, $u*$ is the friction velocity and z_0 is the roughness length. The factor 1000 in the denominator is a scaling factor for recalculation from model scale to real life scale where z_0 is scaled by 100 and $u*$ with $\sqrt{100}$ according to [25]. The upper limit, Ri_{max}, is interpreted as the limit to the transitional regime and defines the interval of Ri where the puffs smoothly transits between being a dense gas and a neutral gas. It has here been set to $Ri_{max} = 3Ri_{min}$.

F is used in:

- Damping of the horizontal velocity
- Damping of the vertical neutral turbulence
- Damping of the vertical movement
- Buoyancy generated turbulence
- Deformation against the ground

3.2.8 Puff horizontal velocity

A dense gas plume will interact with and alter the convective fields which is a phenomenon not explicitly utilized in PUMA. Instead, the factor F can be used to modify the horizontal velocities of individual puffs to capture this effect [16, 26].

$$u \rightarrow u(1 - 0.3F) \tag{8}$$

$$v \rightarrow v(1 - 0.3F) \tag{9}$$

3.2.9 Width of the puffs

In PUMA, it is assumed that the contributions to the increased width of the puffs can be written as linear contributions in the differential equation.

$$\frac{d\sigma_y}{dt} = \left(\frac{d\sigma_y}{dt}\right)_{Neutral} + \left(\frac{d\sigma_y}{dt}\right)_{DenseGas} \tag{10}$$

$$\frac{d\sigma_z}{dt} = \left(\frac{d\sigma_z}{dt}\right)_{Neutral} + \left(\frac{d\sigma_z}{dt}\right)_{DenseGas} \tag{11}$$

The last term actually consists of two separate contributions from the dense gas model: turbulence effects and deformations caused by compression towards the ground.

$$\left(\frac{d\sigma_y}{dt}\right)_{DenseGas} = \left(\frac{d\sigma_y}{dt}\right)_{DenseGas\_Turb} + \left(\frac{d\sigma_y}{dt}\right)_{DenseGas\_Ground} \tag{12}$$

Note that the widths in x- and y-direction are always equal due to horizontal symmetry in PUMA.

3.2.10 Damped vertical neutral turbulence

A dense gas puff is stable on the upper side and unstable on the lower side. This means that there will be considerable mixing between the puff and the surrounding air on the bottom side while the upper side will experience less exchange. When the puff is in contact with the ground, there will be a stable boundary on both the lower and upper sides. This stable gradient results in a substantial decrease in the vertical turbulence and dispersion of the puff. A damping factor, D, is introduced that takes values in the interval between 0 and 1 and represents the decrease in turbulence mixing due to dense gas effects and the effect of the ground.

$$\left(\frac{d\sigma_z}{dt}\right)_{Neutral} \rightarrow D\left(\frac{d\sigma_z}{dt}\right)_{Neutral} \tag{13}$$

The damping coefficient D is written as

$$D = 1 - \gamma_{damp} F^{0.5}\left(\frac{L_{EV} - z}{L_{EV}}\right)^{0.5} \qquad\qquad z \le L_{EV} \tag{14}$$

where γ_{damp} is a constant between 0 and 1, here set to 0.95. A plot of the dampening factor as a function of the F-factor and the relative closeness to the ground is shown in Figure 3.3.
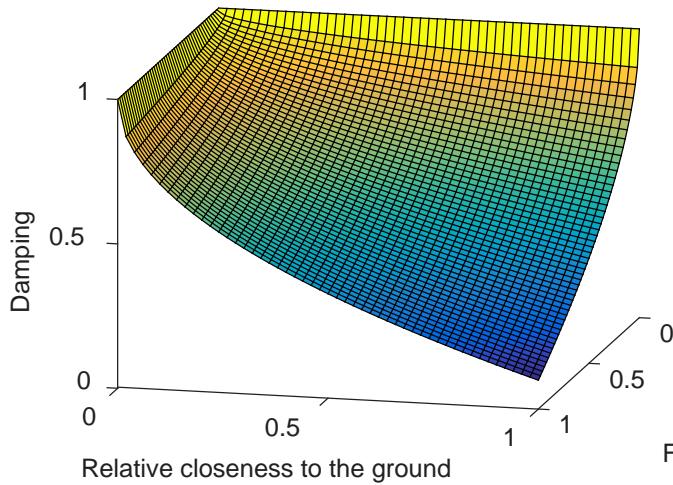
Figure 3.3   A two-dimensional surface plot of the damping factor D that depends on the F-factor and the closeness to the ground. The minimum value of D is determined by the parameter γ_{damp}. Blue colour represents large dampening and yellow colour little dampening.

3.2.10.1 Mass centrum dynamics

The vertical neutral turbulence gives rise to vertical puff movement towards a steady-state height. Due to the induced boundary layer of the puff, *i.e.*, the stable gradient, the turbulence becomes compromised, which is modelled by a damping of the volume integral of the vertical turbulent flow by the D-factor. This will reduce the vertical movement of the puff center.

$$\left\langle \overline{w'c'} \right\rangle \to D \left\langle \overline{w'c'} \right\rangle \tag{15}$$

3.2.11   Buoyancy generated turbulence

The internal turbulence of a dense gas causes an extra contribution to the growth of the puff [16]. The term introduced to the dynamic equations, see equation (12), takes slightly different form in case the puff is determined to be in contact with the ground or not.

$$\left(\frac{d\left(\sigma_y^{\,2} \right)}{dt} \right)_{DenseGas\_Turb} = 2K_{DGturb} \tag{16}$$

Equation (16) can be rewritten as

$$\left(\frac{d\sigma_y}{dt} \right)_{DenseGas\_Turb} = \frac{K_{DGturb}}{\sigma_y} \tag{17}$$

where K_{DGturb} takes different forms depending on whether the puff is in contact with the ground or not.

$$K_{DGturb} = \begin{cases} 0.15 q_p 1.75 & \text{no ground contact} \\ 0.15 q_d 1.75 & \text{ground contact} \end{cases} \qquad (18)$$

where q_p and q_d are introduced and defined below.

Equations (17) - (18) give

$$\left(\frac{d\sigma_y}{dt}\right)_{DenseGas\_Turb} = 0.15 q_{p/d} 1.75 \qquad (19)$$

This contribution is equal in all geometric directions, which implies

$$\left(\frac{d\sigma_z}{dt}\right)_{DenseGas\_Turb} = \left(\frac{d\sigma_y}{dt}\right)_{DenseGas\_Turb} = \left(\frac{d\sigma_x}{dt}\right)_{DenseGas\_Turb} \qquad (20)$$

3.2.11.1 No ground contact

For a puff that is not constricted by ground contact, the following expression is utilized

$$q_p^{\,2} = (1+F) U_{slump}^{\,2} \left(c_{q1} + c_{q2} \frac{V_{xy}^2}{V_{xy}^2 + w_s^{\,2}} \right) \qquad (21)$$

The coefficients c_{q1} and c_{q2} are empirically estimated from jet rise experiments and are attributed the values $c_{q1} = 0.4$ and $c_{q2} = 3.0$ [16].

3.2.11.2 Ground contact

For a puff that is determined to be in contact with the ground equation (22) is used.

$$q_d^{\,2} = c_{q1} (1-F)^2 U_0^{\,2} \qquad (22)$$

where U_0 is the horizontal spread induced by the compression of the puff towards the ground and the coefficient c_{q1} has empirically been found attributed the value 0.4 [16].

3.2.12 Compression against the ground

When a puff experience a slumping velocity and is in contact with the ground it will start spreading horizontally and contract vertically. This takes place when the requirement

$$z < L_{EV} = \sigma_z n_{std} \qquad (23)$$

is fulfilled. The Lagrangian horizontal front velocity, U_0 is written as

$$U_{down} = F\left[U_{slump} - D\left\langle \overline{w'c'} \right\rangle \right] \qquad (24)$$

$$U_0 = \gamma_{comp} \frac{U_{down}}{\pi} \left(\frac{\sigma_z}{\sigma_y} \right)^{\gamma_{ce}} \tag{25}$$

where the model specific coefficients γ_{comp} and γ_{ce} have been introduced, with which one can tune the compression behaviour. The velocity U_0 describes the extra horizontal front velocity of the puff due to the compression and is held at maximum 2 m/s for numerical reasons. This phenomenon will not affect the centrum position of the puff but rather deform the puff. This Lagrangian horizontal velocity equals the dense gas contribution to the time derivative of the width of the puff and is illustrated by Figure 3.4.

$$\left(\frac{d\sigma_y}{dt} \right)_{DenseGas\_Ground} = \frac{U_0}{n_{std}} \tag{26}$$
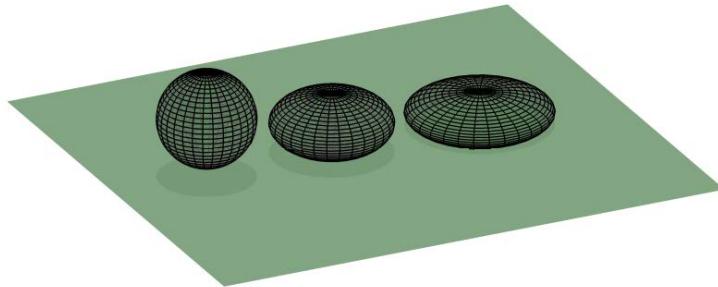
Figure 3.4   The compression of a puff against the ground causes the puff to increase its horizontal width and decrease its vertical height. The puff is moving with the wind towards the right side in the figure and three snap-shots of its effective volume are depicted as it becomes deformed.

The compression effect does not imply any change in the puff volume. For an unrestricted puff there is no defined volume. However, we can consider the effective volume, V, to find an expression for the puff height.

$$V = \frac{4\pi}{3} \sigma_x \sigma_y \sigma_z n_{std}^3 \tag{27}$$

$$\frac{d\sigma_y}{dt} = \frac{U_0}{n_{std}} \tag{28}$$

$$\frac{dV}{dt} = \frac{4\pi}{3} n_{std}^3 \left[\frac{d\sigma_x}{dt} \sigma_y \sigma_z + \frac{d\sigma_y}{dt} \sigma_x \sigma_z + \frac{d\sigma_z}{dt} \sigma_x \sigma_y \right] = 0 \tag{29}$$

Using the model specific constraint $\sigma_x = \sigma_y$ implies that

$$2 \frac{d\sigma_y}{dt} \sigma_y \sigma_z + \frac{d\sigma_z}{dt} \sigma_y^2 = 0 \tag{30}$$

and an expression for the change of the puff height due to the compression is obtained.

$$\left(\frac{d\sigma_z}{dt} \right)_{DenseGas\_Ground} = -\frac{2}{\sigma_y^2} \frac{d\sigma_y}{dt} \sigma_y \sigma_z = -2 \frac{U_0}{n_{std}} \frac{\sigma_z}{\sigma_y} \tag{31}$$

An alternative method that is numerically more precise is to calculate σ_z from the new volume given by the change in σ_x and σ_y.

Finally, for numerical stability reasons a lower limit of the vertical puff size has been implemented such that $\sigma_z \geq 0.4$ m is always valid.

3.2.13 Energy exchange with the ground

As mentioned above, the temperature of the puff describes both the released gas and the entrained air and is considered constant in the entire effective volume. The energy exchange, Q, with the ground is assumed to be proportional to the temperature difference, ΔT, and the contact area, A, between the puff and the ground which equals the cross-section area, see equation (32). This assumption is called the Newton's Law of Cooling [27].

$$Q = hA\Delta T \tag{32}$$

The parameter h is the convective heat transfer coefficient.

The effective volume is an ellipsoid which can be described by equation (33).

$$\frac{1}{n_{std}^2} \left[\frac{x^2}{\sigma_x^2} + \frac{y^2}{\sigma_y^2} + \frac{z^2}{\sigma_z^2} \right] = 1 \tag{33}$$

The cross-section area to the ground is given by a constant value of z which gives rise to a two-dimensional ellipsoid described as

$$\frac{1}{n_{std}^2} \left[\frac{x^2}{\gamma^2 \sigma_x^2} + \frac{y^2}{\gamma^2 \sigma_y^2} \right] = 1 \tag{34}$$

where

$$\gamma^2 \equiv 1 - \frac{z^2}{n_{std}^2 \sigma_z^2}. \qquad\qquad 0 \leq z \leq n_{std}\sigma_z \tag{35}$$

The area on this ellipsoid equals

$$A = \pi n_{std}^2 \gamma^2 \sigma_x \sigma_y = \pi n_{std}^2 \sigma_x \sigma_y \left(1 - \frac{z^2}{n_{std}^2 \sigma_z^2} \right) \tag{36}$$

The convective heat transfer coefficient h depends on the wind speed, v, and may, by the use of empirical data for the heat exchange between air and solid objects [28], be written as

$$h = 10.45 - v + 10\sqrt{v} \tag{37}$$

which is a valid expression for wind speeds between 2 and 20 m/s. It is possible that the puffs have a lower velocity than 2 m/s, in which case the velocity is set to 2.0 m/s, resulting in a slight overestimation of the heat transfer.

The heat exchange leads to a change in temperature of the puff, which depends on the heat transfer following equation (32), the heat capacities, c_p, and masses, m, for the released gas and the entrainment air (with subindices G and A, respectively) and the time step Δt.

$$\Delta T = \frac{Q\Delta t}{c_{p\_G}m_G + c_{p\_A}m_A} \tag{38}$$

3.3 Multiple puffs

The puffs are independent of each other for a neutral gas in PUMA. With the introduction of dense gas effects, PUMA becomes nonlinear, which means that the puffs are no longer entirely independent of each other and cannot be updated separately without compensation for other puffs. There are four main areas of dependencies:

- Local concentration calculations
- Overestimation of air entrainment
- Overestimation of energy exchange with the ground
- Discrepancy in temperature description

A more detailed description of these areas and how PUMA takes the nonlinear effects into account is given below.

Finally, the process of concentration field compilation is always linear and the puffs are independent of each other in both the neutral and the dense gas cases.

3.3.1 Local concentration

The local concentration for a puff has impact of the thermodynamical and kinetic processes. For instance, the relation between the mass released gas and entrained air collectively affect the temperature change due to heat transfer to the ground. This implies that when the dynamics of a certain puff is to be updated, neighbouring puffs may have a noticeable impact on the outcome. At the current state, PUMA ignores this phenomenon and assumes that the mass given by the puffs themselves is a good enough description of the total mass of the released gas in their effective volumes. This may be a subject for future development of PUMA regarding dense gas.

3.3.2 Entrainment air

As already mentioned, surrounding air will be mixed into the puffs causing dilution of the released gas, which is shown by an increase of the standard deviations of the puffs. When puffs grow they begin to occupy new volumes, which contain surrounding air and also cause an equalization in temperature. However, the new volume of an arbitrary puff may already be occupied by another puff. This causes an overestimation of the temperature equalization if this issue is not addressed. In PUMA, an ad hoc damping factor, γ_{ent} is introduced as an exponent of the increase in volume to compensate for the over-counting of entrained air. The value of this factor depends on the amount of overlapping between the neighbouring puffs and thereby varies as the puffs evolve. However, in the current state of PUMA, this parameter is treated as a constant throughout the simulations.

3.3.3 Energy exchange with the ground

A similar situation occurs when considering the energy exchange with the ground as with the entrainment of air. That is, the same energy may be counted multiple times due to overlapping puffs. In this case, the heat transfer from the ground to the plume may be too large if this issue is not addressed. The same approach is chosen here as in the entrainment case, *i.e.*, the introduction of an ad hoc damping factor, γ_{ground}, that lowers the heat transfer. As is the case with the entrainment air, this factor is here set to a constant value.

3.3.4 Heat exchange between overlapping puffs

The effective volumes of puffs may overlap, see Figure 3.5, which means that the gas mix in the shared volume may be described by different temperatures since PUMA utilizes effective volumes for the puffs with constant temperature inside. This ambiguous description is, of course, not physically correct.

Normally, however, the temperature difference is negligible between neighbouring puffs. Even so, a functionality has been included in PUMA that conducts a heat transfer between puffs depending on their effective volume overlap and their temperature difference.
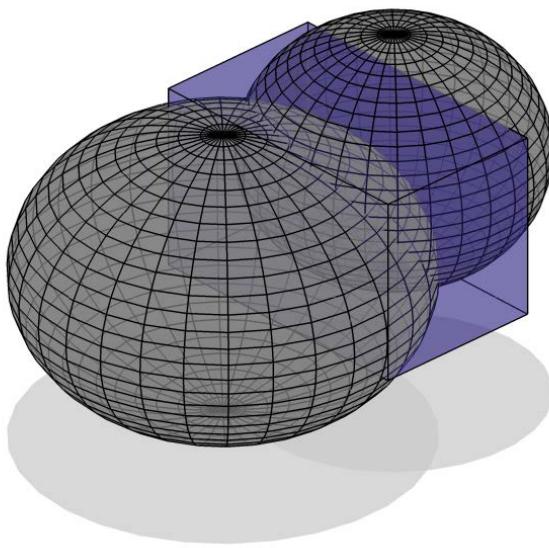
Figure 3.5   Two puffs that overlap within the blue cuboid.

3.4   Validation

Experiments with the release of liquefied ammonia were conducted at the CEA-CESTA, Bordeaux, France, during the period of 1996-2012 [29-31]. The comprehensive experiments include both temperature and concentration measurements at a large number of masts up to 1700 meters from the source. In this chapter, a detailed comparison between the measured data and model data from PUMA is presented. The source and environmental conditions have been reproduced as closely as possible.

It is mentioned in the reports that test no.4 was considered the most successful and this is therefore chosen as the comparison data set here. Selected data from the measurements are here presented with the permission of INERIS. Concentration is given in the unit of volumetric ppm, which is sensitive to local temperatures [32]. PUMA applies metric units and the concentrations are converted separately for each puff since they have individual temperatures.

To further validate the dense gas implementation of PUMA, CFD simulations were conducted that also mimicked the INERIS test no.4. These simulations were executed using the commercial program PHOENICS, where LES was used as turbulence model to capture the dynamic behaviour of the plume within an intermittent high Reynolds number atmospheric boundary layer. The CFD-simulation used synthetic turbulence at the inflow boundary to establish the intermittent properties of the boundary layer.

3.4.1 Meteorology

The meteorological data for INERIS test no.4 [31] is presented here together with settings in the simulations. The average temperature was measured to be 12.5 ^{0}C and the relative humidity was 82%. The same values were used in the simulations. The Pasquill atmospheric stability class[2] was estimated by two different methods for the experimental data, one method results in class C (slightly unstable conditions) and the other results in class D (neutral conditions) [31]. In the simulation process class D has been used. The measured wind velocity and wind direction for the time period of the measurement are shown in Figure 3.6.
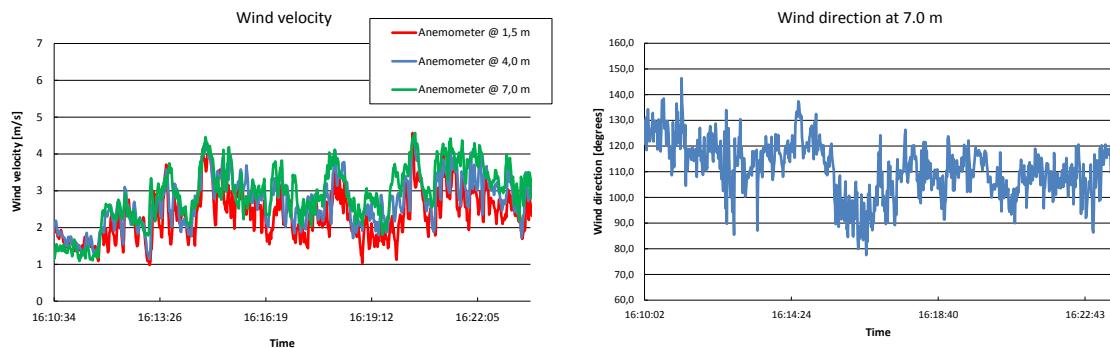
*Figure 3.6   Wind velocity and wind direction for test no.4 in the left and right panels,
respectively.*

The wind profile used in PUMA is developed by Thaning (unpublished) and is an improvement of the similarity theory of Zilitinkevich *et al.* [33]. The mean wind velocities at different vertical positions are presented in Table 3.1 for both measurements and simulations.

Height [m]	INERIS average wind speed [m/s]	Simulation wind speed [m/s]
7.0	3.1	3.1
4.0	2.9	2.8
1.5	2.5	2.4

Table 3.1   Average wind speed at three different heights.

The wind angle is in line with mast #26 at 7.0 meters height according to information given in the INERIS report [31]. However, according to the concentration data the wind direction seems to be in line with mast #23 - #24. In the simulation, the line between these two masts is therefore used as both the x-axis and the wind direction at 7.0 meters height. This discrepancy might be a result from the fluctuations in wind direction seen in the right panel of Figure 3.6.

Since the experiments took place on a very flat surface, the roughness parameter has been assigned a value of 0.01 meters, which corresponds to a lawn [34] in the wind profile model.

---

[2] Atmospheric stability is classified according to the Pasquill Stability Classes from class A, extremely unstable conditions up to class G, extremely stable.

3.4.2 Source

A tank of 12 m^3 with liquefied ammonia stored at saturation pressure, approximately 5.8 bar, was employed during the INERIS experiments. Nitrogen gas was injected into the tank during the experiments to keep the inner pressure of the tank constant. A valve with an inner diameter of 50.8 mm was used to allow the release of liquefied ammonia, which was transported through a 10.4 meter long hose, with an inner diameter of 50 mm, to the release device. The release device was a 1.56 meter long rigid pipe with an inner diameter of 50.8 mm. The pressure was monitored inside the tank and at two different positions in the release device. The actual time-resolved release rate is not available due to practical measurements issues caused by rapid phase transitions of the fluid in the system. The release height was 1.015 meters above the ground. However, the time averaged release rate was measured to 4.2 kg/s.

3.4.2.1 Jet model

The jet model described in [35] was used to define the source term. The model used an adiabatic expansion scheme and standard thermodynamical processes to calculate a cross-section area for the jet, its distance from the orifice, the density of the released substance and its temperature. An illustration is given in Figure 3.7. PUMA utilized the source term provided by the jet model to initiate the puffs that thereafter evolved according to the dense gas model described in this report.
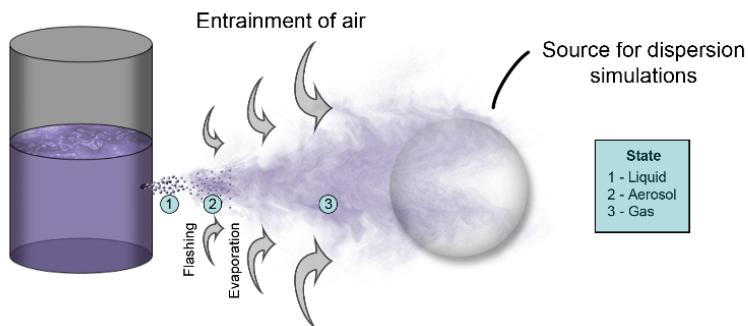

Figure 3.7   Illustration of the jet model where a leak gives rise to a two-phase jet that undergoes several processes before a final source description that is useful to FOIs dispersion models was obtained.

3.4.2.2 Input

There were a few parameters required as input data to the jet model. Most of them were directly provided from the meteorological conditions of the measurements and the release system. The entrainment factor and the edge factor for the hole were tuned to obtain a representative source for INERIS test no.4. The choice and motivation for these settings are described in section 3.4.3.2. In addition, a final condition was provided to the jet model. This condition determined at which jet velocity the source term was defined. This is not a critical parameter and was here chosen to give rise to velocities that corresponded to the ambient wind velocity when the

damping factor F took its maximum value of 1.0. A complete compilation of the input parameters are presented in Table 3.2.

Parameter		Value
Entrainment factor	χ	1.5
Hole edge factor	C_d	0.1774
Orifice diameter	d_{hole}	50.8 mm
Gas pressure	P_0	0.2 MPa
Air temperature	T_{atm}	12.5 ^{0}C
Relative humidity	Φ	82%
Ambient wind speed	u_{atm}	2.23 m/s
Final velocity limit (using a Lagrangian formulation of the jet)	F_{DG}	0.7

Table 3.2   Parameters used in the adiabatic jet model to reproduce the source term for test no.4 of the INERIS experiments. The jet model was run in Lagrangian mode.

3.4.2.3 Output

The output of the jet model included a cross-section area, where a mix of the released gas and air passed at a given velocity (determined by the final velocity speed in the input). The gas mix had a low temperature that originated mainly from an adiabatic expansion. Moreover, the distance from the orifice as well as the density of the released substance was provided. The jet model does not explicitly define the geometric shape of the cross-section area. The area was in this simulation treated as a circle, leaving all deformation of the puffs to be inflicted by the compression against the ground. The output of the jet model is described in Table 3.3.

Parameter	Value
Density of ammonia	0.0983 kg/m^3 ≈ 105 000 ppm
Position	11.1 m
Cross-section area	13.4 m^2
Radius of circle cross-section area	2.07 m
Temperature	-54 ^{0}C

Table 3.3   The output parameters from the jet model given the input data of Table 3.2.

3.4.3   Source comparison

A comparison with experimental data has been performed to validate that the source term has been successfully modelled. In addition, two input parameters are determined by an iterative

comparison process. These parameters are the entrainment factor and the edge factor for the hole, which are determined by comparison of the mass flow and propagation angle, respectively.

3.4.3.1 Mass flow

The experimental results clearly indicate that the pressure from the tank dropped on its way to the orifice, see the left panel in Figure 3.8. In addition, the temperature also dropped in a similar manner, see right panel in Figure 3.8. These facts suggest that there was an inner flash present in the pipe before the orifice. The main reason for the inner flash was the extensive hose present between the tank and the orifice. The outcome of such a situation is that the mass flux becomes substantially lower than what would have been the case without the inner flash [34].
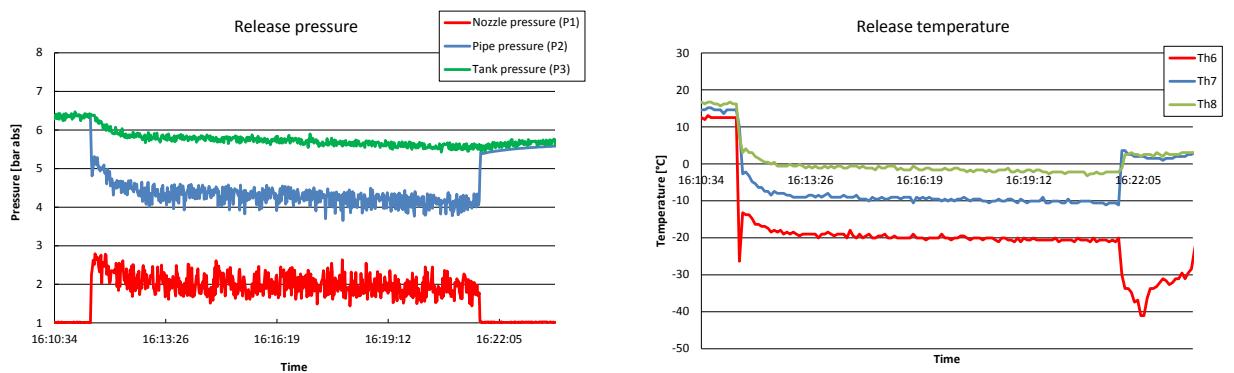
Figure 3.8   Left panel, the measured pressures at three different point in the release system. The most interesting is the nozzle pressure, which had an average of 2.0 bar during the release period. Right panel, the temperature at three different locations during the release. Th6, Th7, and Th8 correspond to three different positions in the outlet pipe where Th6 was the outlet temperature. The temperature dropped rapidly in the pipe.

When reproducing the INERIS source in the jet model, which has no explicit support for hoses or inner flash, the mass flux became 17 kg/s, which was to be compared to the measured mass flux of only 4.2 kg/s. By adding a friction term calculated for this specific hose, the mass flux in the model dropped down to 7.3 kg/s. This discrepancy seems to support the indication of inner flash. To compensate for this reduction in mass flux, the parameter C_d was attributed a value of 0.1774, which resulted in a model source with the same mass flux as in the experiments.

3.4.3.2 Angle of propagation

The width of the plume, w, was 5 meter at a distance, x, of 20 meters from the release point according to measurement data (see Figure 3.9). This corresponds to a propagation angle, α, of ~7 degrees. The width was here defined as the distance between the points where the concentration levels were half of the axial concentration. This means that, assuming a normal distribution of the concentration, the horizontal standard deviation of the plume at this distance was approximately 2.1 meters.
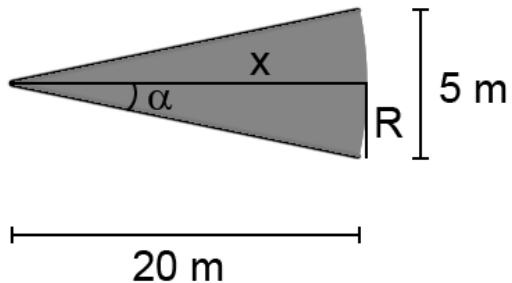
Figure 3.9   The jet expanded approximately linearly in the horizontal plane. The point of view in this illustration is from above with the source to the left. The plume depicted here corresponds to the width in test no.4 in the INERIS experiments.

The width equals twice the radius and can be written

$$w = 2R = 2x\tan(\alpha) \tag{39}$$

The plume was circular in the yz-plane close to the source, but transcended into a more elliptic shape with distance. It can be estimated from the data presented in Figure 3.11 that the vertical standard deviation was only ~1.1 meters, which means that the ellipsoidal INERIS plume at 20.0 meters distance from the orifice had a cross-section area that corresponded to that of a circular plume with a standard deviation of ~1.5 meters.

It was found that an entrainment factor of 1.5 gave results that agreed well with the experimental findings. The jet in the model then obtained a horizontal propagation angle of 14.8 degrees if the experimental proportions between width and height was maintained. Note that the propagation angle is not directly comparable between INERIS and PUMA jet source due to different definitions. The PUMA jet source width should be divided by 1.75 to establish a more comparable entity. This would imply a width in the model of 8.5 degrees, which is fairly close to INERIS' estimated value of 7 degrees. A comparison of the two distributions and the widths at a distance of 20 meters from the orifice is given in Figure 3.10. A normal distribution has been used for the INERIS data whilst the model distribution is uniform since the jet model is defined that way.

**Distribution comparison**
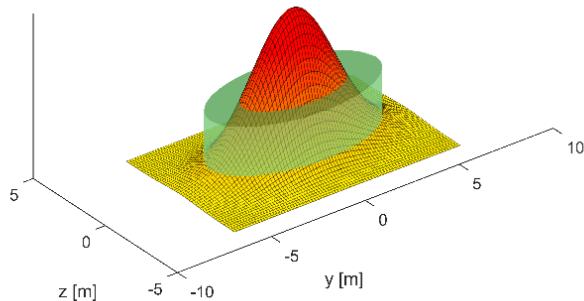
Figure 3.10 The width and distributions for the measurement and the model are depicted at a distance of 20 meters from the orifice. To make this comparison, the jet model was allowed to continue all the way to this point, i.e., no dispersion model has acted upon the plume.

As mentioned, PUMA used Gaussian puffs, which means that the concentration changed from uniformly distributed to a normal distribution in the intersection between the jet source and the Lagrangian dispersion model. This means that the flat surface of the green ellipse in Figure 3.10 changed into a Gaussian distribution as soon as the dispersion process began. The source in the model was defined as a cuboid with $\Delta x = \Delta y$ for PUMA since the model is symmetric in the horizontal plane. The model sets the standard deviation σ in any direction on newly created puffs to the source width in that direction divided by 3.5, which means that the edge of the source is located at 1.75σ.

3.4.3.3 Vertical concentration close to the source

The vertical concentration profile was compared at the distance of 20 meters from the orifice, see Figure 3.11. Since the wind direction was fluctuating, no single mast provided the maximum value of the plume over time. To compensate for this fact, the instantaneous maximum values of the different masts were collected as a time series on which the average was taken. However, the true maximum of the plume was always located in between the masts. Moreover, data is only available for a few masts, in this case #22 and #23 were used. The centre of the plume may have been, at least for some periods, outside this small interval.

The data for PUMA is the actual maximum value, *i.e.*, at the horizontal centre line. To make a fair comparison three sets of simulation data are therefore presented: one set located at the centre of the plume showing the maximum values and two sets with horizontal off-sets of 4.5 and 9.0 degrees, respectively. For these data sets, the jet model source term described by the parameters in Table 3.3 has been used. This means that puffs were created at the position x=11.1 meter and thereafter transported using the dense gas model. In addition, the

concentration profile for the jet is plotted. In this case the final condition of the jet source model was changed so that the jet reaches 20.0 meter. Puffs were inserted at this point to obtain the Gaussian distribution, but the dense gas model described in this report was not utilized.

Figure 3.11 shows that there is a clear difference between the concentrations between the pure jet model and the case where the jet has been followed by a brief dispersion model stage. This discrepancy is expected and originates from the discrete transition from jet to dense gas dispersion, which results in a plume closer to the ground due to the loss of inertia and introduction of negative buoyancy. The measured values have a shape of the vertical profile that is between the shapes of the PUMA dispersion model and the jet model, which suggests that the actual plume in the measurements had begun to transit into dense gas mode at the distance 20.0 meter. It is worth noticing that the experimental values indicate a lower total mass than that of the simulation, which is discussed further in chapter 3.4.
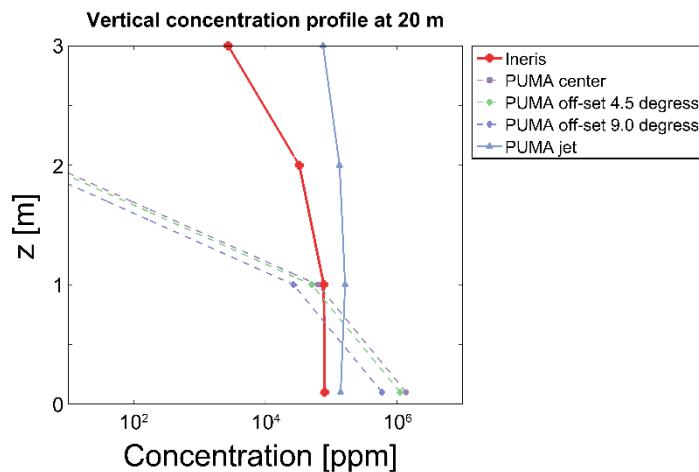
Figure 3.11 The vertical concentration profile. The three dashed lines correspond to simulated data located at the centre of the plume and with off-sets in y-direction of 4.5 degrees and 9.0 degrees, respectively. The vertical concentration profile is plotted for the jet if allowed to continue to 20.0 meters.

3.4.3.4 Numerical verification

To verify the numerical methods as well as the mass flow from the source, a control area was constructed, through which the plume was transported until steady-state was reached. In this process the puffs were not allowed to change size or position except in the wind-direction. First, the control area had the same size as the source term for the puffs. The mass flow through the control area was then 3.7 kg/s. The same test was then conducted using twice the size in both directions of the control area, in which case the mass flow was 4.2 kg/s, which is equal to the true release rate. This means that the process was able to catch the entire release and that approximately 12% of the mass was located outside of the source cross-section area, see Figure 3.12.
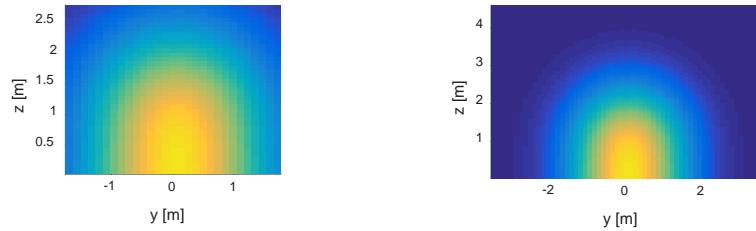
Figure 3.12 The concentration at a control cross-section in the yz-plane. The left panel shows the concentration using a cross-section area corresponding to the source size, while the right panel shows a cross-section area that has twice the size in both directions. The mass flow through the control areas were 3.7 and 4.2 kg/s, respectively. The colour scale is the same in both panels. A mirroring scheme is applied, which means that the part of the concentration field that is located below the ground is effectively reflected, which yields non-symmetrical fields as can be seen in this figure.

3.4.4 Dispersion

The jet stage is followed by a dispersion process where the ammonia is transported over a wide field. Concentrations and temperatures are compared between the model and the experimental values at distances of 20, 50, 100, 200, 500, and 800 meters in this chapter.

3.4.4.1 Time of arrival

A comparison between the times of arrival (TOA) of the plume at different distances was conducted. This is in general not an unequivocal observation. Detectors will normally increase their readings gradually when the plume begins to reach them. Moreover, the signals are also fluctuating and noisy, which makes it difficult to state with certainty which time to use. In this comparison the time point when the concentration reached, approximately, its maximum value for the first time was used. The determination was more straightforward for the simulation data, which was free of noise and meandering. For this data set, the short time for the plume to propagate through the jet stage was ignored.

Table 3.4 shows the times and the mean velocities in each interval for both measurements and simulations. There is a discrepancy, mainly in the interval 20-100 meters, where PUMA predicted significantly lower velocities than what was measured. This might be due to inertia effects from the jet that were not caught by PUMA. That is, the jet model ended at a point where the velocity was higher than the surrounding air. This difference in velocity was immediately lost in the transition between the models. In addition, there might be meteorology issues with the wind profile, since the puffs were located very close to the ground in this stage of the dispersion process. The fraction of the gas that was located relatively high above the ground experienced a higher velocity than the gas close to the ground. This vertical skewing of the front

of the plume can be an explanation for the higher velocities in the experiments, since the puffs could not capture this phenomenon.

The velocity was expected to decrease with distance during the first part of the release, since the plume descended towards the ground and thereby became subject to a weaker wind field. This is also what was seen with the exception of the initial interval for the INERIS data. This might be caused by the fact that the concentration data was given every fifth second (every second for the release data), which is a low resolution in this case. The maximum concentration might be located anywhere in the interval 4-9 seconds and if the true time of arrival was at ~6 seconds the velocity in the initial part exceeded the velocity in the second interval. The decrease in velocity took place somewhat earlier for PUMA. Eventually the velocity in the model started to increase again. This is due to the fact that the plume continuously transcended from dense gas to neutral gas. It experienced a decreased damping on its velocity and started to ascend vertically, which means that the wind speed was higher. It is not entirely clear why the transport velocity for the measurements never increased, but it might be explained by the fact that the vertical skewing effect caused the front to hit the detectors without ever being close to the ground. The uncertainty is extra high for the TOA for 800 m in the INERIS data, since a brief period of concentrations was recorded at ~300 seconds, where the concentrations reached 40% of the concentrations that arrived later.

Distance [m]	INERIS TOA [s]	INERIS Velocity [m/s]	PUMA TOA [s]	PUMA Velocity [m/s]	PUMA eff. Height [m]
20	9	2.2	12	1.67	0.32
50	17	3.8	50	0.79	0.35
100	33	3.1	80	1.67	0.68
200	85	1.9	140	1.67	1.8
500	249	1.8	250	2.73	9.4
800	441	1.6	340	3.33	15.0

Table 3.4   *Comparison between the time of arrival for the plume in measurements and simulations at 1.0 meters above the ground level. The time was taken when the concentration roughly reached the maximum value for the first time. The velocities refer to the last interval till that point, i.e., the velocity for "distance 100 m" refers to the mean velocity for 50-100 m.*

3.4.4.2 Centreline concentration

The concentrations in the centreline of the plume were given from the INERIS experiment and reproduced with PUMA, see *Table 3.5*. This data was compiled from different masts at every distance to obtain the maximum values for every distance.

Distance [m]	INERIS [ppm]	PUMA [ppm]	PUMA 4.5⁰ off-set [ppm]	PUMA 9.0⁰ off-set [ppm]
20	65000	62300	60000	53000
50	27000	38300	32900	20800
100	16000	51100	41800	23100
200	10000	13800	10500	4740
500	1200	1040	4740	158
800	500	394	158	39

Table 3.5   Centreline concentrations at different distances at a height of 1.0 meters above ground level. The off-set columns show point values with an off-set from the centreline by 4.5 degrees and 9.0 degrees which correspond to one half and one distance between masts in the field far from the source, respectively

Assuming that the distribution in the cross-section plane was normal, the experimental values seem to underestimate the concentration for, at least, the shortest distance. Given that the standard deviations of the distribution was 2.1 and 1.1 meters, respectively, and that the wind speed was ~2.5 m/s, the maximum value of the cross-section must have been in the order of 130.000 ppm for the plume to be mass consistent with a flow of 4.2 kg/s. The measured value was only about half of that value. There are several possible explanations to this large discrepancy; the maximum value was not located at 1.0 meters above the ground, the measurement was horizontally off-centre, the devices could only measure up to 100.000 ppm, there was meandering in the wind, and the profile might not been normally distributed to begin with or the widths were underestimated. Another reason was the method of collecting the experimental data. The maximum value of any sensor was identified, and the time average of that particular sensor was used as the centre of plume value. This means that fluctuations of the true plume centre over the ten minute course of the experiment were not caught. Since the data from the simulation was, inherently, more precisely measuring the true maximum value in the plume, it is expected that the model over-predicted the experimentally measured concentration values. However, at the shortest distance the puffs are small and located close to the ground causing the concentration at 1.0 meters height to be significantly below the maximum value. It seems that PUMA predicts a plume that is located somewhat lower than the measured plume.

The centreline concentrations at 1.0 meters height are depicted in Figure 3.13. Since the plume was quite flat in the near-field the concentration measurements became sensitive to the vertical height of the puffs. This is clearly shown for the first distances where the PUMA concentration curve fluctuates as the puff sizes increases. The maximum concentration of the plume was initially close to the ground and ascended towards the measuring height as the puffs grew. This

caused the concentration at 1.0 meters height to actually increase at 100 meters distance and thereafter keep decreasing. The point values close to the source is therefore not a good description of the plume. As the plume grew, the concentration measurements became less sensitive to the height at which they were sampled. To investigate the impact of the dense gas model in PUMA further, a simulation using the same settings where the gas was not treated as dense gas was conducted. The concentration close to the ground was significantly lower in this case, which illustrates the need of modelling a dense gas properly.
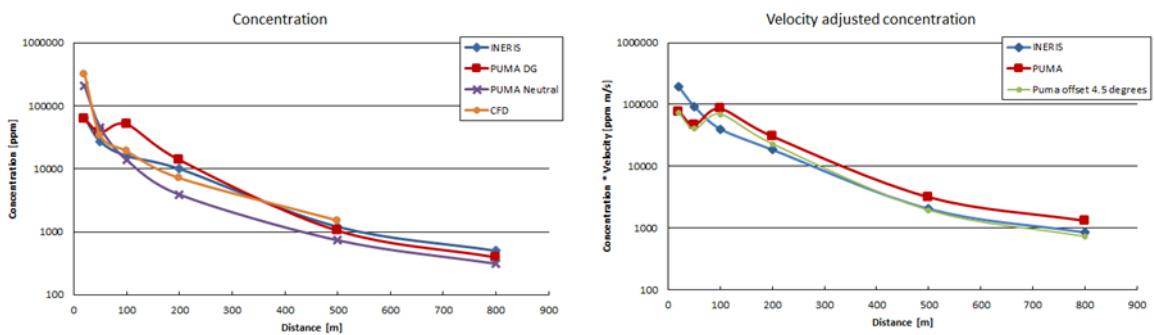
Figure 3.13 Centreline concentration values in measurements and simulations. Left panel, the corresponding concentration for PUMA without the dense gas model is included for comparison. Right panel, the centreline concentration values are multiplied with the local velocities in measurements and simulations. The off-set values correspond to 4.5 degrees translation in the y-direction.

The concentration depends linearly on the reciprocal of the velocity. As discussed above there are discrepancies between the measured and modelled velocities, which might introduce a systematic error in the comparison. To exclude this effect and focus on the dispersion process *per se*, selected series of point data have been multiplied with the velocities of the plume at the local positions, which gives slightly modified curves shown in the right panel. The data set, labelled *PUMA offset 4.5 degrees*, holds the concentration data for PUMA using a horizontal offset of 4.5 degrees, which corresponds to half the distance between masts in the far-field. These values can be regarded as a representation of the maximum values if the plume is located in between two masts. The off-set curve agrees very well with the experimental in the far-field, which indicates that the model is treating the dense gas phenomenon acceptably well under the well-grounded assumption that the experimental values underestimate the true maximum centreline values.

A common method to depict the degree of agreement between two sets of point measurements in atmospheric dispersion is to plot the values against each other at various distances. The diagonal then represents a perfect match. A relative discrepancy within a factor of two for the majority of the points is in general regarded as a good agreement. Figure 3.14 shows the degree of agreement for both PUMA and CFD against the measured centreline concentrations. The

white area indicates the desired region where the relative difference is within a factor of two and both series lies within this area with the exception of one point each.
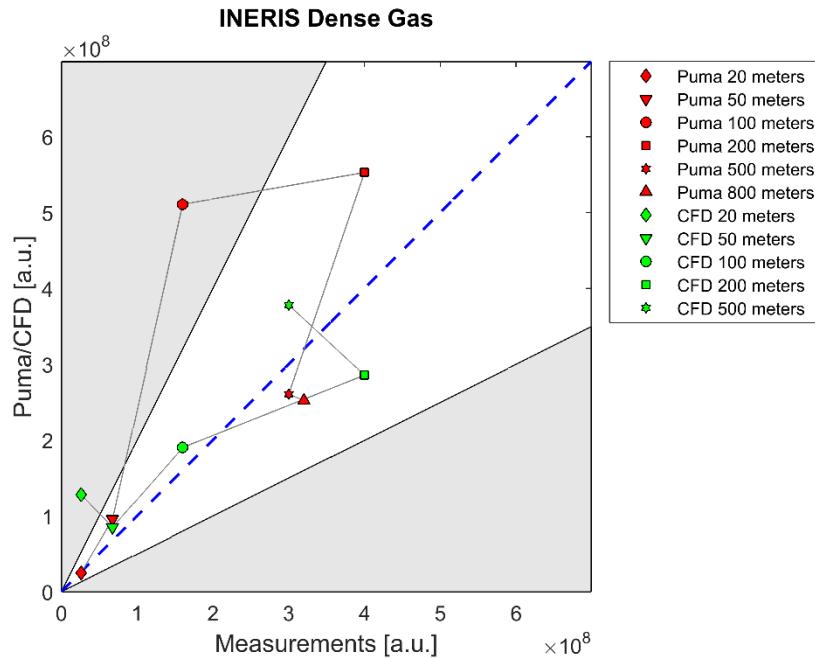

Figure 3.14 The centreline concentrations adjusted for the distance squared. A perfect match means that the points are located along the blue dashed diagonal line. The white cone indicated the area where the relative difference between measurements and simulations are within a factor of 2, which in general is considered as a good match.

3.4.4.3 Point concentration

Data from a subset of the masts was available and has been used to compare concentration data both in the near-field and the far-field. It is not straight-forward to draw conclusions from such a comparison, since there are a lot of uncertainties mainly regarding the meteorological conditions. The experiment was designed to obtain a steady-state plume, which implies that the mean concentration for the period of exposure was the key factor to inspect. Figure 3.15 shows the mean concentrations for both measurements and simulations in a logarithmic scale. The point data shows a varying degree of agreement mainly due to the stochastic nature of the meandering winds. Since the centreline concentration analysis already provides strong indications of a well modelled concentration decline with distance, the point concentration comparison serves mainly as an investigation of the width prediction. There are some discrepancies in the location of the plume, but the overall picture is satisfying in this regard as is shown in Figure 3.15.
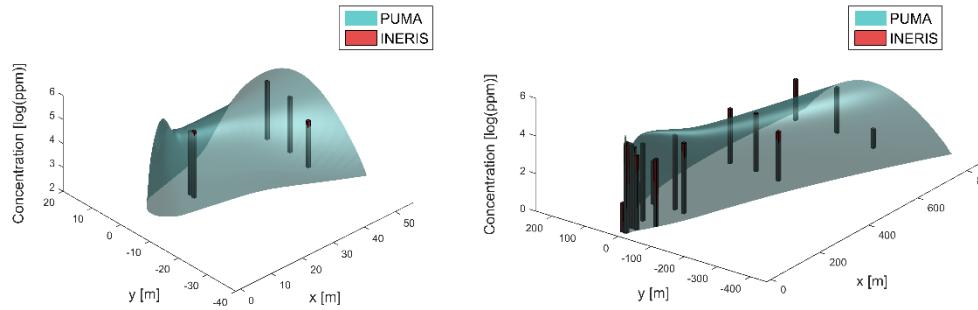
Figure 3.15 Bar diagram showing the concentrations from measurements and simulations at 1.0 meters height above ground. The left panel shows the area closest to the source, while the right panel shows the entire field. The concentration values are logarithmical.

3.4.4.4 Concentration isosurfaces

Experimental data is restricted to sparsely scattered point measurements, which gives too little information for a compilation of an entire plume. In contrast, plots of isosurfaces may readily be investigated for the simulation data. A comparison between the plumes with and without the dense gas model is presented in Figure 3.16. As expected, the dense gas plume stays close to the ground causing high concentration in a far wider region than the case for neutral gas.
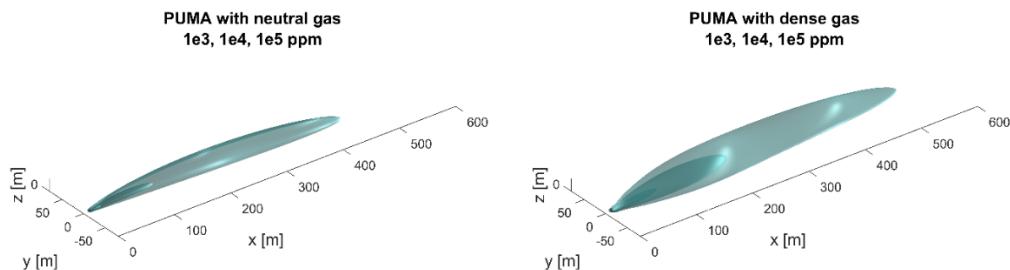
Figure 3.16 Comparison of isosurfaces for neutral and dense gas simulations. The high concentrations are found in an extensively larger area in the dense gas case than in the neutral case. There are three different isosurfaces plotted semi-transparently for the concentration values of 10^3-10^5 ppm.

3.4.4.5 Cross-section concentration

A comparison has been conducted of the cross-section concentrations of the CFD and PUMA plumes. The sections were chosen at 50 and 100 meters from the source. In contrast to the data of the centreline concentrations of the plume at a particular height, this method provides a 2D

view of the shape of the fields. The fields are plotted using isolines at three different concentration levels and are shown in Figure 3.17. The CFD field clearly predicts that the lower concentration regions are located higher above the ground than PUMA does. By inspection, the field CFD is non-Gaussian, which implies that the Gaussian puffs are inherently unable to create the same field. The best matches of the isolines are found for 10.000 ppm at 50 meters and for 50.000 ppm at 100 meters.
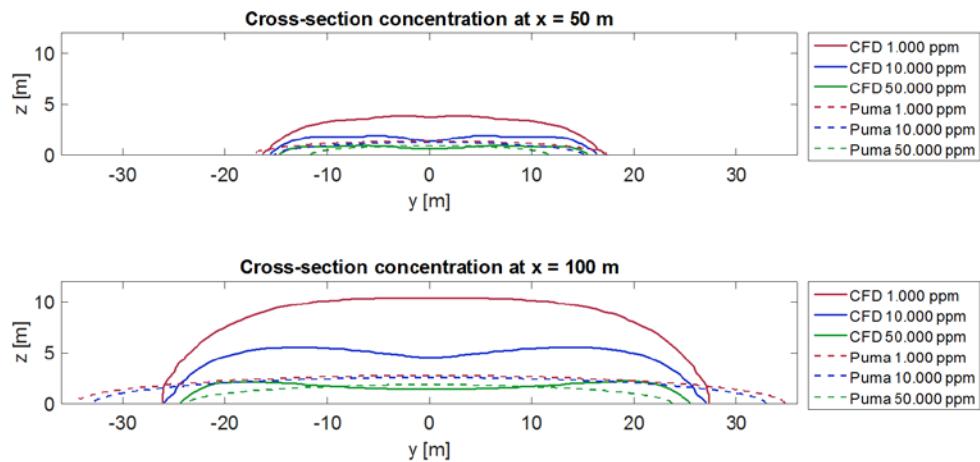

Figure 3.17 Comparison of cross-section concentrations for CFD and PUMA at 50 (top) and 100 (bottom) meters from the source.

Finally, a graphical illustration of the difference between neutral and dense gas cross-section concentration fields at 100 meters from the source is presented in Figure 3.18. As expected there is a distinct difference, which illustrates that a dense gas release is modelled poorly without consideration of the phenomena involved in this process.
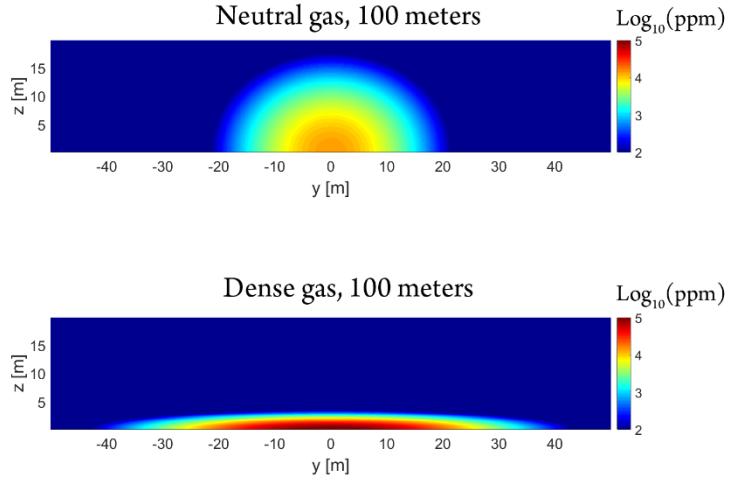
Figure 3.18 Comparison of neutral and dense gas treatment in PUMA. There is a significant difference in the cross-section concentration at a distance of 100 meters from the source.

3.4.4.6 How long is the gas dense?

A typical property of a dense gas close to the surface is that it has limited vertical spread due to the stable upper boundary layer. This implies that the plume is almost solely spreading in one dimension orthogonal to the axis of propagation. In contrast, a neutral plume is spreading in two dimensions. Further on, a dispersion process in a pipe would "spread" in zero dimensions orthogonal to the axis of propagation. Due to mass conservation, it can be argued that the concentration at any point in a plume will scale with the reciprocal of the distance, *x*, raised to the number of dimensions orthogonal to the axis of propagation, *n*, it is spreading in, since the cross-section area at that distance increases at the same relative pace.

$$C \propto \frac{1}{x^n} \tag{40}$$

This means that for the case with a pipe, the concentration will remain constant at all distances. More interesting, a dense gas will have $n \approx 1$ and the concentration will scale as the inverse of the distance. When the gas starts to behave as a neutral gas the dispersion will gradually change into a situation with $n \approx 2$, since there is now spreading in two dimensions (y and z in the coordinate system used here). The dimension of the spreading can be obtained by taking the logarithm on both sides of equation (40) and investigating the derivative.

$$\frac{d \ln(C)}{d \ln(x)} = -n \tag{41}$$

This effect is observable in the measurement when the centreline data is again used, see Figure 3.19. The transition is not as clear for the simulation data even though there is a change in the

slope. The increase in concentration at 100 meters is an artefact of the vertical width of the puffs reaching an optimal value in relation to the measuring height of 1.0 meters.
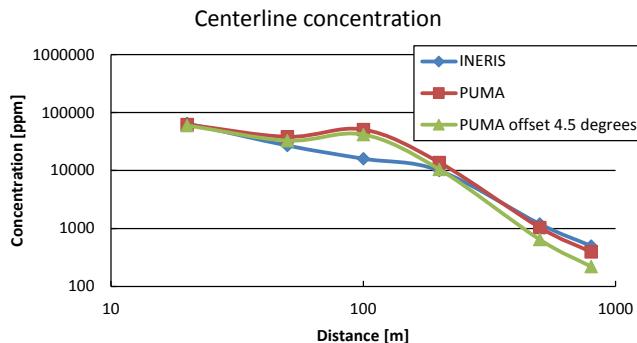

Figure 3.19 In a plot of the logarithm of the centreline concentration vs. the logarithm of distance, it is possible to estimate which type of dispersion that takes place at different positions by investigating the current slope.

There is a breaking point at the distance 100 and 200 meters for PUMA and INERIS data, respectively. For the initial intervals the slope, n, in equation (41) is ~0.81 for INERIS and ~0.6 for PUMA. At the second stage, the slope is ~2.2 for INERIS and ~2.4 for PUMA. This suggests that there is a transition from dense gas mode into neutral gas mode at approximately 200 meters from the source in the experiments, which agrees reasonably well with simulations results. The transition is not distinct but rather a gradual process in an interval and cannot be determined more precisely.

3.4.5   Temperature

In addition to the concentration, the temperature was also measured at the same positions as the concentrations. PUMA utilizes an effective volume in which the temperature always is considered to be evenly distributed. This means that the model provides a volume of constant temperature, which is to be considered as a measure for the mean temperature in that volume. Since this is not the case in real life measurements, it is expected that the model will overpredict the temperature in the centre of the puffs and underpredict the temperature in the outer regions of the effective volume. This property is clearly illustrated when looking at the vertical temperature profile at 20.0 meters from the source. Here, the plume was close to the ground and the measured temperature at z=0.1 m was below 40.0 degrees. Unfortunately the thermocouples were not able to measure below this limit, so the actual temperature at this position remains partly unknown with an upper limit of 40.0 °C. The temperature increased to -22.4, -14.4 and 7.2 °C for the heights 1.0, 2.0, and 3.0 meters, respectively. PUMA uses 1.75σ as the radius for the effective volume in each direction, which means that the effective volume reached 1.2 meters above the ground at this distance from the source. The temperature on the puffs at this position was -39.6 °C, which is between the real temperature at 0.1 and 1.0 meters. The model

property with effective volume holding a constant temperature aggravates the comparison with measurements. The results shown in Figure 3.20 indicate that the puff temperature matched the measured temperatures quite well despite the limitation caused by the discrete temperature distribution.
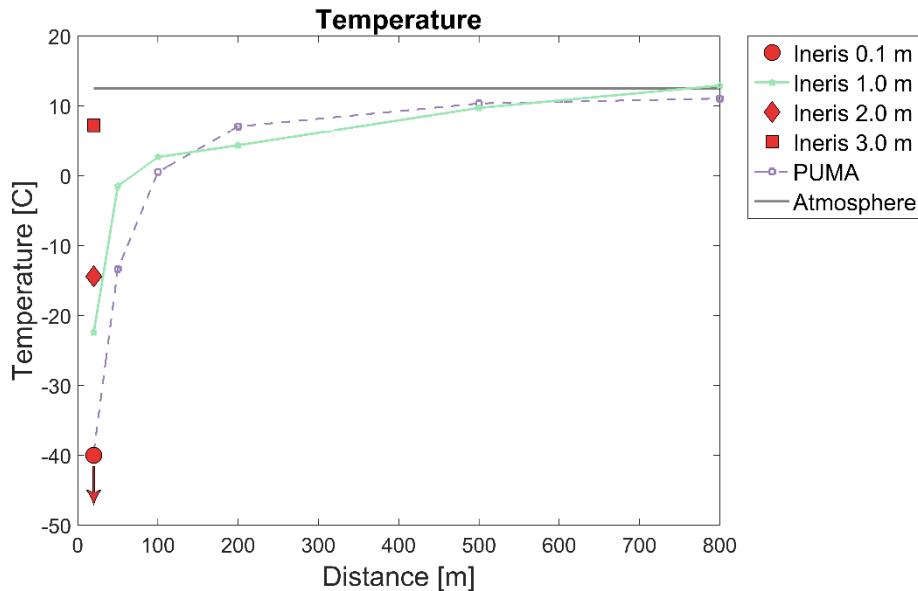

Figure 3.20 *The temperature from measurements and simulations. Note that the thermocouples could only measure down to -40 degrees Celsius. The actual experimental temperature at 0.1 m height and 20.0 meters from the source is below this temperature, which is indicated by the arrow.*

3.5 Discussion

The framework for a dense gas model has been presented in this work. The dense gas model has been developed for, and implemented into, an existing custom made Lagrangian puff model for atmospheric dispersion called PUMA. The physics required to capture the main features of dense gas behaviour have been described together with thermodynamical effects. In addition, model specific phenomena and issues that arise thereof have been discussed.

Since PUMA is a real-time model, the computational cost is always a key factor to consider when adding new functionalities. Although the dense gas model adds extra calculations, the additional computational time has been held back by linearization assumptions and a minimum of puff interactions. In accordance with the aim of keeping PUMA as quick as possible, constants have been implemented to compensate for effects caused by overlapping of puffs. It can be argued that the modelling of these effects would profit from a more sophisticated treatment. This is one aspect to consider in future developments.

A validation against full-scale experimental data has been conducted using the INERIS-measurements as an independent data set. It was found that the evolution of the centreline

concentration over distance agrees well with measurements. There is an over-prediction of the concentration levels which is, as discussed in section 3.4.4.2, expected and not considered a problem. For the centreline data, there are significant discrepancies between experimental data and simulation data in the near-field, which are mainly caused by the sensitivity of the vertical puff sizes in combination with the single measurement height of 1.0 meters above ground. An investigation was therefore conducted using the cross-section areas of the plumes for PUMA and CFD generated fields.

PUMA was executed with a puff frequency of 0.5 Hz. Ideally, the frequency would not influence the result, which also is the case with a neutral gas. However, there is an influence of the frequency in the dense gas case due to the nonlinear effects. When a puff is created it has a predefined size given by the source. The release rate of the substance is given, which means that the fraction of the released gas scales linearly with the inverse of the puff frequency. This is a model artefact, which cannot easily be eliminated but rather needs to be considered during the execution.

3.5.1 Important parameters

A set of model specific parameters have been introduced in PUMA that together regulate the dense gas behaviour in PUMA, see *Table 3.6*.

Parameter	Value	Description
γ_{ent}	0.3	The ad hoc parameter that describes the limited expansion effects
γ_{ground}	0.3	The ad hoc parameter that describes the limited heat transfer to the ground
γ_{slump}	1.0	The ad hoc parameter for the slumping velocity
γ_{comp}	2.0	The ad hoc parameter for horizontal spread
γ_{ce}	0.4	The exponential ad hoc parameter that defines the shape dependency of the compression
γ_{damp}	0.95	The ad hoc parameter that decides the maximum damping of vertical entrainment
n_{std}	1.75	The relative size of the puff in the thermodynamical aspect

Table 3.6   The main parameters to control the dense gas physics in PUMA.

The parameters γ_{ent} and γ_{ground} are coupled to the overlapping between puffs and therefore also to the frequency of the creation of puffs in comparison to the ambient wind speed. This relation and the optimal values for these parameters remain unclear and may be subject to future investigation. The parameters γ_{slump} and γ_{comp} are both coupled to the deformation of the puffs when compressed against the ground. However, the parameter γ_{slump} also affects the vertical positions of the puffs. The values presented in Table 3.6 for these parameters have been chosen by comparison to the empirical data presented in the validation chapter. A similar approach for

dense gas treatment as presented here is given by Hanna *et al*. [10]. By comparison it can be derived that their theory suggests the following expression for the two model parameters:

$$\gamma_{slump}\gamma_{comp} = \pi\sqrt{\frac{4\pi}{3}} \approx 6.4 \tag{42}$$

if the corresponding height of the puff is defined to be $H \equiv V/\pi R^2$ where $R \equiv n_{std}\sigma_x$ and $V = 4\pi\sigma_x\sigma_y\sigma_z/3$. Beauchemin *et al*. use a similar cylinder based model as Hanna *et al*., but with a slightly different expression which yields

$$\gamma_{slump}\gamma_{comp} = \pi\sqrt{\frac{4}{3}} \approx 3.6 \tag{43}$$

when the same comparison is conducted [9]. These three values differ, but are in the same order of magnitude. However, there are distinct differences in the architecture used in this work and in the works of Hanna *et al*. and Beauchemin *et al*., which means that parameter values are not readily transferable between the models.

Comparison to empirical data is not straight-forward and may be interpreted differently. Also, different measurements may give rise to different model agreement depending on the experimental setup and how it suits different model designs.

4 Results obtained by DGA CBRNC Defence France

4.1 Objectives

We want to assess a few operational urban models in use against neutral and eventually dense gas data at DGA CBRN Defense. QUIC (LANL) will be used for dense gas dispersion against the INERIS full scale ammonia release. PMMS (ARIA Tech.) will be used against MODITIC demi-complex case and the Paris case for neutral gas release only (the dense gas module needs to be tested separately first).

4.2 Scaling Procedure

No scaling has been needed for the INERIS field experiment case. For the MODITIC wind tunnel scale, data have been subjected to a 1:200 scaling for the demi-complex case, and 1:350 scaling factor for the Paris case. PMMS is included into a dispersion platform called OXER-BC at DGA CBRN Defence Centre, and geo-referencing is required to import a Computer Aided Design (CAD) into it. It has proved delicate to correctly scale and project the geometry into the right projection system (Lambert II wide).

4.3 Inflow conditions

Inflow conditions for the MODITIC scenarios are the same as for the wind tunnel and correspond to a neutral atmosphere. A scaling based on source Richardson number and vertical momentum flux ratios has been applied (see WP4000 report [3]). The comparison leads to quite large release rates at scale 1:1 that are here just used for validation purpose. Volumetric air speed, Q_{air}=1885 m^3/s through a 40 m diameter source, and air speed U(10m)=8.14 m/s for the demi-complex case; Q_{air}=2493 m^3/s through a 40 m diameter source and U(10m)= 10.77 m/s for the Paris case.

For the INERIS outdoor release of ammonia, conditions are set according to the scenario described in WE3300 [2]. For test no. 4, the Pasquill stability class is C/D (slightly unstable/neutral conditions) and the wind 3.0 m/s at 7 m. For test no. 5, the Pasquill stability class is A/B (extremely unstable/ moderately unstable conditions) and the wind 3.5 m/s at 7 m.

4.4 Dense gas modelling, obstacle treatment

With QUIC software, the only tool that was tested for dense gas release, the parameters are the following:

- Volumetric continuous release 5 cm side length, with mass rate 4.2 kg/s

- Ammonia diphasic, droplet spectra with mean mass diameter, MMD=300 µm and standard deviation, σ=1.7

- Perfect depositing gas

The physiochemical properties of liquid ammonia are recalled in Figure 4.1 and used by QUIC. The obstacle is a concrete wall (3 m x 3 m x 1 m) placed at 3 m from the pipe exit. QUIC is unable to provide a horizontal source term when dealing with neutral gas release in contrast to the case with dense gas release.

Ambient	1	atm
Saturation Pressure	850453	Pa
Heat of Vaporization	23323	J / mol
Surface Tension	2.13979e+0	N / m
Boiling Temperature	239.72	K
Molecular Weight	17.0306	g / mol
Liquid Viscosity	1.3803e+07	Pa*s
Liquid Density	0.61	g / cm^3
Diffusivity	2.16e-05	m^2/s
Contact Angle	0	degrees
Droplet Fraction	1	
Re-Evaporation Exp	0.1	
Evaporation Threshold	0.001	
Retention Fraction	0.1	

Figure 4.1 Physiochemical properties of the ammonia multiphase model.

4.5 Calculation set-up and control

The setup of QUIC cases takes about a half day for preparation and 25 min for execution (principally dispersion).

The end of calculation control is made visually by looking at the stationary time results of flow and plume concentration in surfaces of interest.

The setup of PMSS cases takes about one day preparation for the complex area case and two days for Paris case. The execution (principally dispersion) takes about one hour for the complex area case and four hours (largely depending on the number of particles released, on the street configuration) for the Paris case.

4.6 Results and discussion

4.6.1 Using QUIC (LANL) with dense gas model of INERIS test case no. 4 and no. 5

QUIC reconstructs a mass consistent flow field around obstacles and treats the dispersion with a Lagrangian particles model modified by the diphasic module.

An example of flow and pressure field around the wall is shown in Figure 4.2.
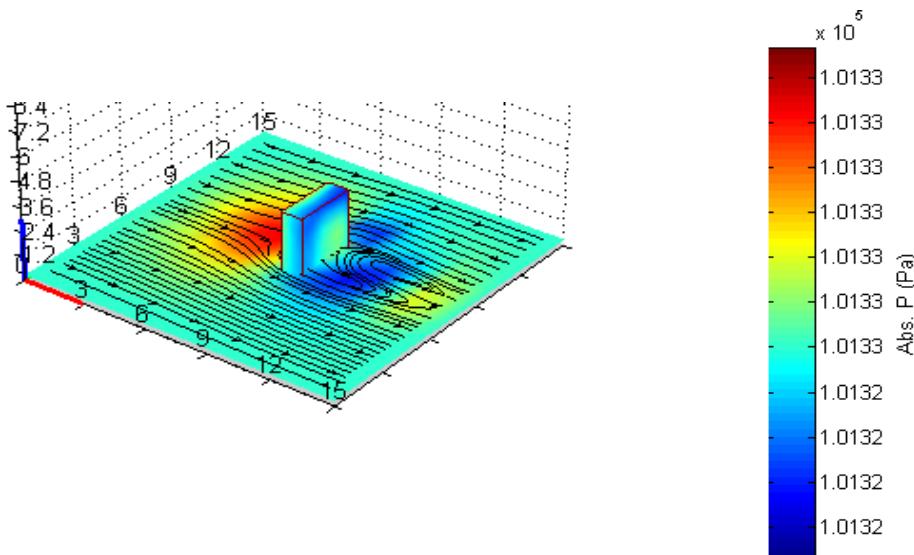
Figure 4.2   Flow and pressure behind the obstacle as computed by QUIC.

Results for concentrations are presented by comparing the converged plume picks along the arcs of sensors at different distances downwind. Temperature simulation outputs are not available.

Without obstacle (test no. 4), a neutral gas release shows a net underestimation of the concentrations from the experimental results, shown in red colour (Figure 4.3). This is probably due to the vertical momentum imposed for this kind of neutral source in QUIC, not representing the horizontal jet orientation.

On the Figure 4.4 (left panel), using the multiphasic model, the jet direction is well taken into account and leads to a good correlation for the case without obstacle (test no. 4), at least in close field (distance <100m). In far field, too much deposition in the model leads to strong underestimation.

With obstacle (test no. 5 shown in Figure 4.4, right panel) in close field and using multiphasic model, the correlation is not as good as the no-obstacle case, because of rainout not considered in the model (lower gas rate); but still some dilution by obstacle appears to be effective (compared with "no obstacle") and a good far field correlation is retrieved, thanks to lower experimental levels.
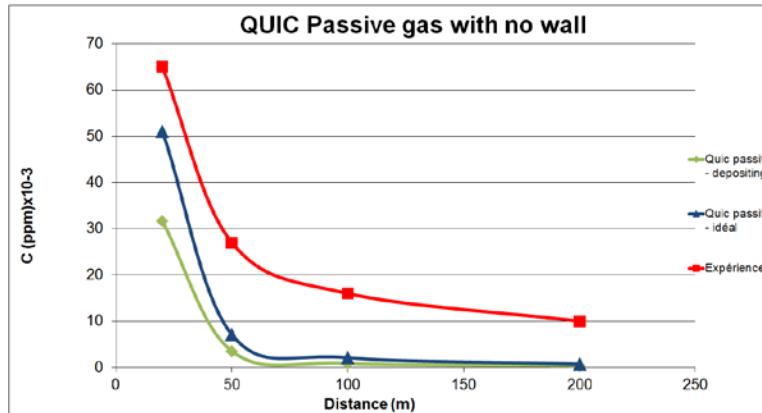
Figure 4.3   QUIC neutral gas release without obstacle.
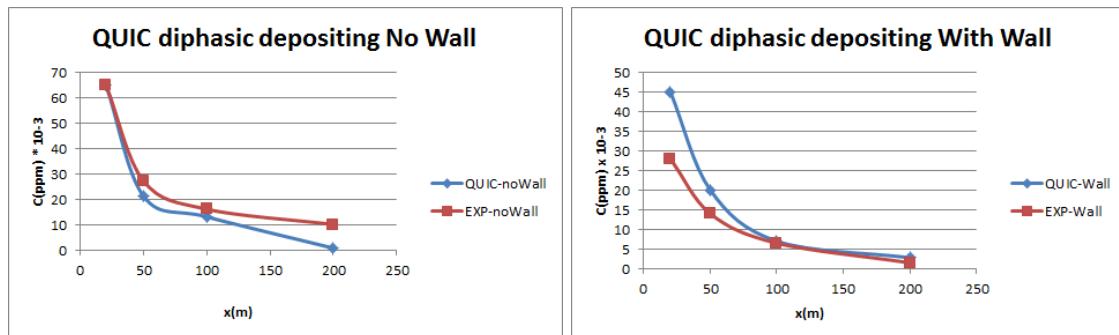
Figure 4.4   QUIC dense gas release without wall (left) and with wall (right).

4.6.2   Complex array case using PMSS (Aria Tech.) and passive scalar

We recall that in PMSS, the wind field is calculated with building wakes effect and verification of mass consistency. A particle Lagrangian dispersion model is used to compute the concentration of gas.

The MODITIC complex array with source S1 and neutral gas is here used for comparison.

The PMMS parameter choices and hypothesis are:

- No trees
- Chimney release (diameter=20m, continuous release of 1885 m^3/s)
- Mesh size 2m x2 m
- « Real » wind profile from the scaled wind tunnel one
- 40 000 particles emitted per unit time (the number is estimated by requiring the "well mixed" criteria be fulfilled everywhere in the domain)

An instantaneous plot of the particle distribution at level of interest is shown on Figure 4.5.
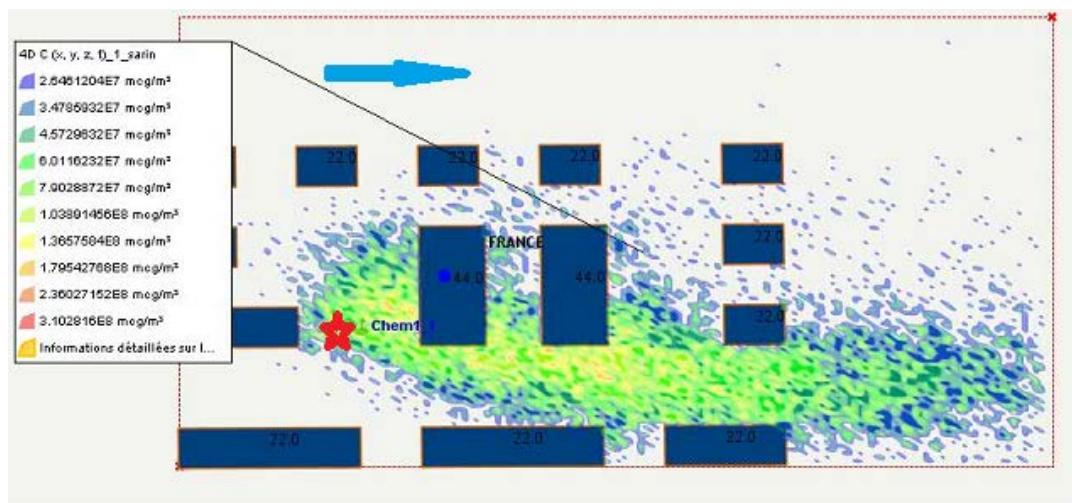
Figure 4.5   Plot of PMSS particles distribution for the S1 neutral source in complex array case. The wind direction is shown with a blue arrow and the source position with a red marking.

Two lateral normalized concentration profiles (equivalent wind tunnel scale) are presented on Figure 4.6, at the array and just after the array. The correlation is rather satisfying, showing the ability of PMSS to deal with neutral gas dispersion in an array like urban zone.
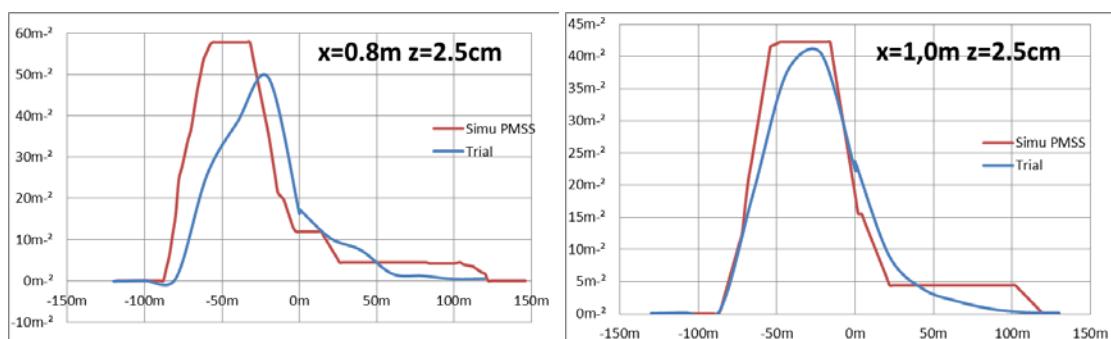
Figure 4.6   Lateral concentration profiles for the S1 complex array case.

4.6.2.1 Complex array, release S1, False Alarm rate, Measures of Effectiveness 1

In Figure 4.7 (left), measures under 1 m^{-2} have been eliminated because they correspond to extremely low concentrations, some even given as negative values[3]. The MOE1[4] is satisfying far from the array (at the array exit, a plume shift may explain the collapse of MOE1; the occurrence rate is also very low), and the false alarm rate, slightly over 50% up to a concentration 50 m^{-2} is principally due to PMMS overestimation of concentration behind buildings (low observed concentrations), and underestimation downstream of the main street where the plume go through, as shown in Figure 4.9.

4.6.2.2 Complex array, release S1, Measures of Effectiveness 2

For analogue reasons (overestimation behind buildings, underestimation in main street), we observe a non-negligible number of false positives (points below the horizontal blue line) and false negatives (points to the left of vertical blue line), see Figure 4.7 (right).

4.6.2.3 Complex array, release S1, probability that the ratio of simulation over measure be in a given range

Globally, almost 40% of the simulation/measure ratio is within ½ and 2 range, almost 70% between 1/10 and 10. The «bad» ratios are principally found at low concentration measured values (Figure 4.8).
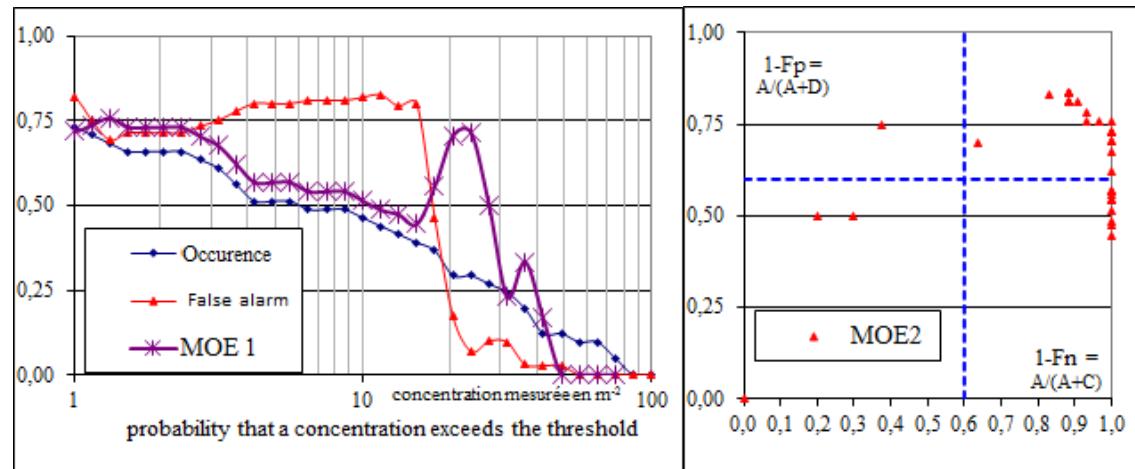
*Figure 4.7   False alarm and MOE1 (left), MOE2 (right).*
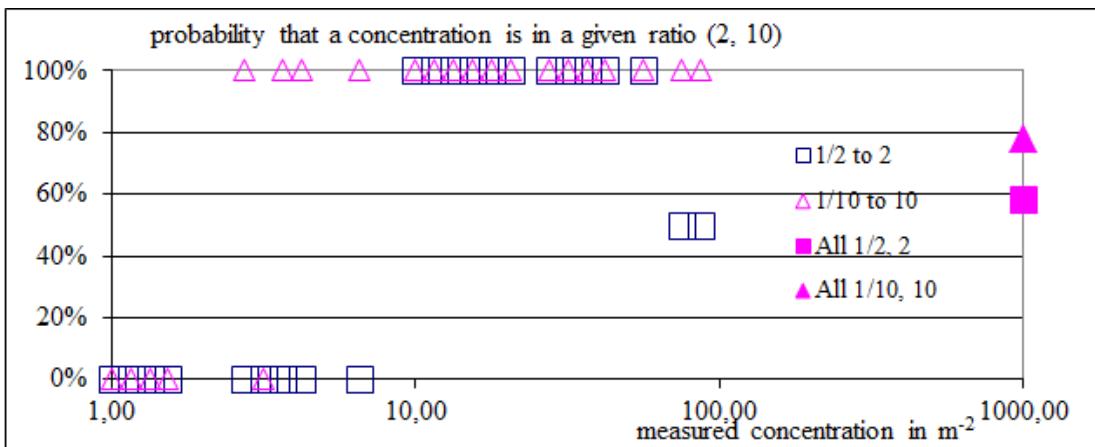
Figure 4.8   Probability that the ratio of simulation over measure be in a given range.
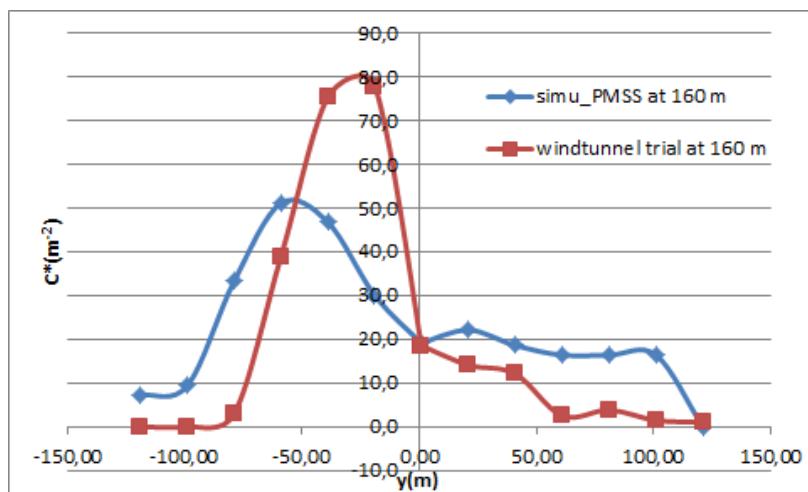

Figure 4.9   Lateral profile of measured and computed concentrations at 160 m from the source perpendicular to the wind, at ground level.

4.6.3   Paris case with PMSS and passive scalar

4.6.3.1 Champs-Elysées release S1

In Figure 4.10 (left), we see that false alarms represent ~60% for low concentrations < $10m^{-2}$ in streets a few hundred meters from the source: low concentrations are measured in the street parallel to Champs-Elysées, where PMMS predicts non negligible concentrations, in green colour on Figure 4.12. Much better False Alarm rates (< 25%) are obtained if we cut at $10m^{-2}$. MOE1 > 50% is acceptable for validation purpose.

In Figure 4.10 (right), we see that globally the points are centred in a 60% square. A few False Positives and False Negatives in far field are probably due to an orientation shift between experiment and simulation. False positives (points below the horizontal blue line) are principally due to measurements in the streets situated left from Champs-Elysées. In these streets, PMMS models concentrations rather high, when sensors measure extremely low concentrations, points in blue or green colour in Figure 4.12. False negatives (points left from the vertical blue line) are principally due to measurements in the streets situated to the right of the Champs-Elysées. In these streets, PMMS models concentrations extremely low, when sensors measure non negligible concentrations, points in red colour in Figure 4.12.

In Figure 4.11, we see that all concentration values represent 35% within a factor of 2, but get closer to 50% if we truncate at 10 m^{-2}. The scattered results for individual concentrations may come from the limited number of sensors or a high sensitivity to the ratios.
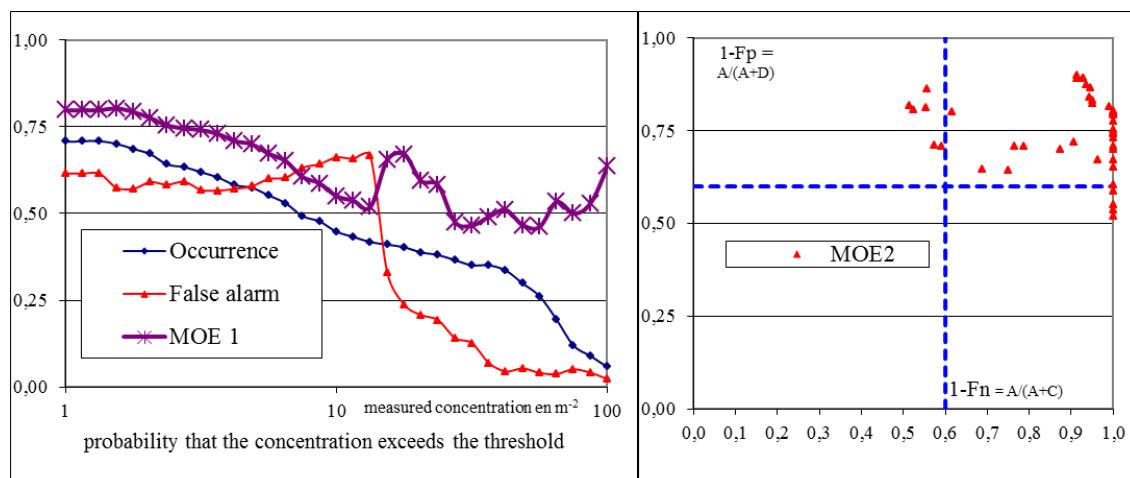
*Figure 4.10 False alarm, MOE1 (left) – MOE2 (right).*

probability that the concentration is in a given ratio

measured concentration in m^{-2}
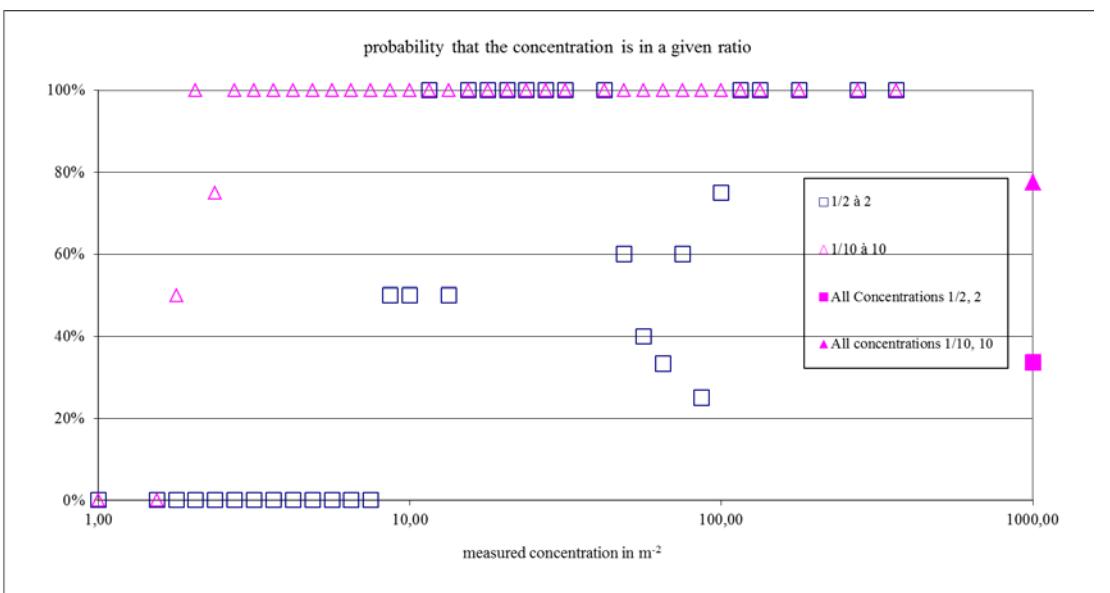
Figure 4.11 Probability that the ratio of simulation over measure be in a given range.

Source

Measured concentrations zero or very low, simulated concentration rather high

wind

Simulated concentration rather low, measured concentration rather high
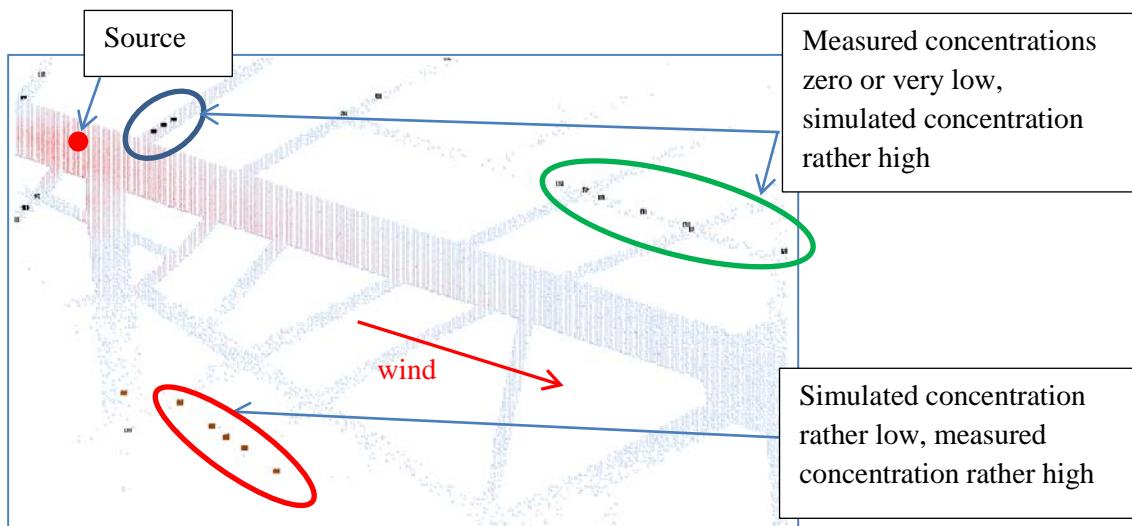
Figure 4.12 Concentrations computed by PMSS color scaled from red (high) to blue (low)levels.

4.6.3.2 Champs-Elysées release S3

In Figure 4.13 (left), we see that for the S3 source case, PMSS overestimates concentrations, especially far from the source as shown in Figure 4.15, which yields >50% of False Positives for low levels (<10m^{-2}).

In Figure 4.13 (right), we see that the same remarks for False Positives (see Figure 4.15) can be made. A few False Negatives are visible (left of vertical blue dotted line) and correspond to the

source surrounding sensors, located in a circular place where the unsteady flow is difficult to reproduce exactly by this model.

In Figure 4.14, we see that 40% of the results are within a factor of 2, 70% in a factor of 5. As shown on Figure 4.16, some measured concentrations are zero or quasi zero, when simulated concentration are not, which explains the ratio over 100. These values improve when we put a threshold at 10 m^{-2}. This threshold value is case dependent, and corresponds here to a much too large release when scaled up to scale 1. The right threshold value of interest would be dictated by toxicity levels.
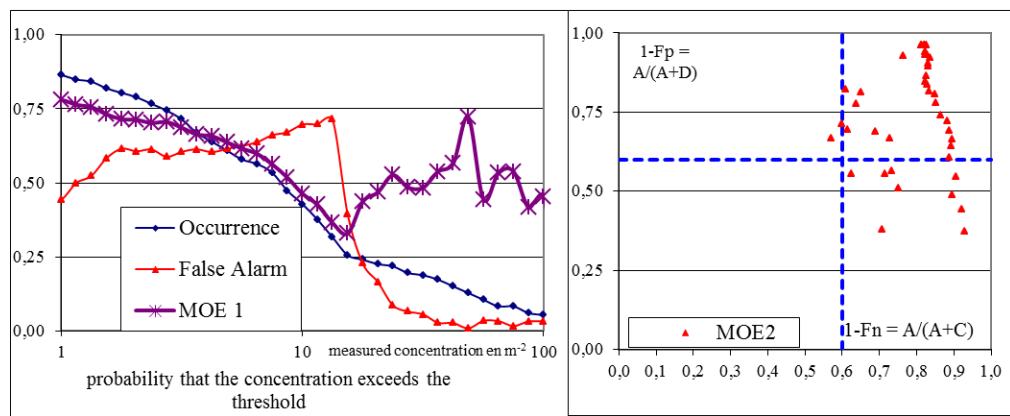
Figure 4.13 False alarm, MOE1 (left) – MOE2 (right).
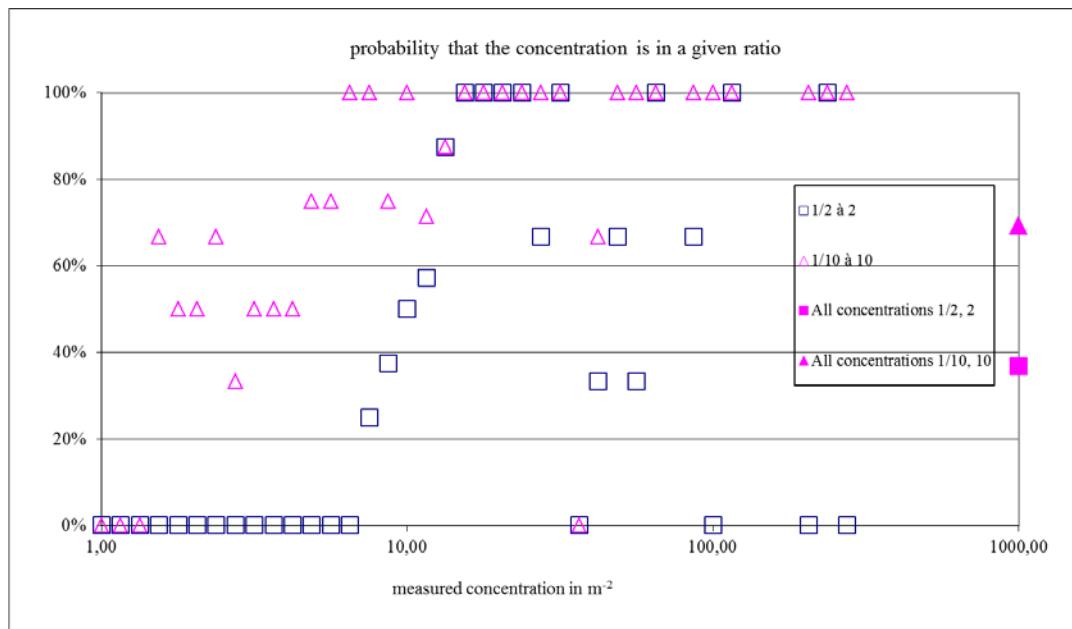
Figure 4.14 Probability that the ratio of simulation over measure be in a given range.
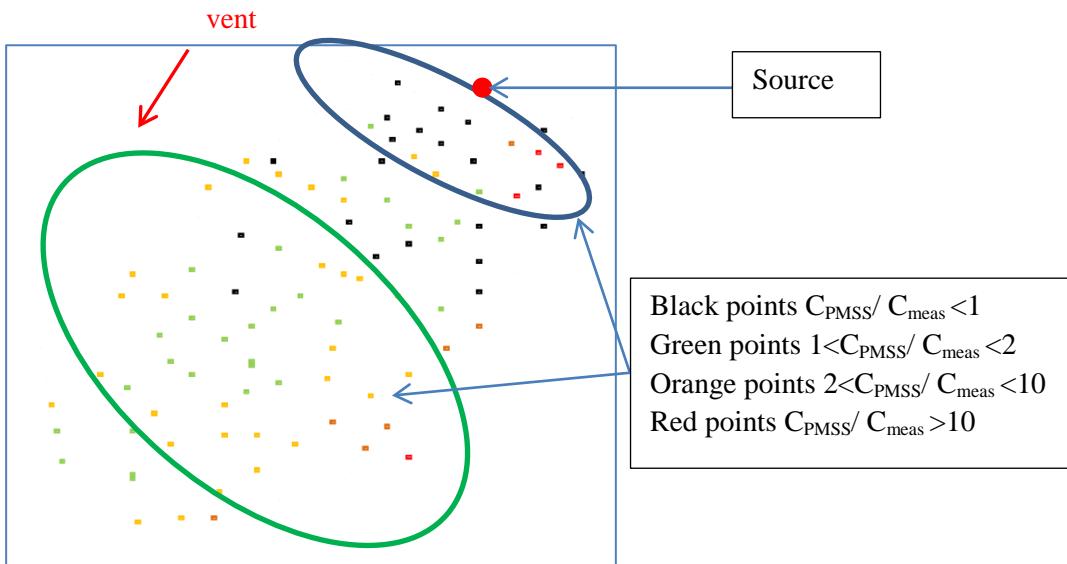
Figure 4.15 Ratios of concentrations C_{PMSS}/C_{meas}.

Black points $C_{PMSS}/C_{meas}<1$
Green points $1<C_{PMSS}/C_{meas}<2$
Orange points $2<C_{PMSS}/C_{meas}<10$
Red points $C_{PMSS}/C_{meas}>10$

Measured concentration zero or very low, simulated concentrations non negligible
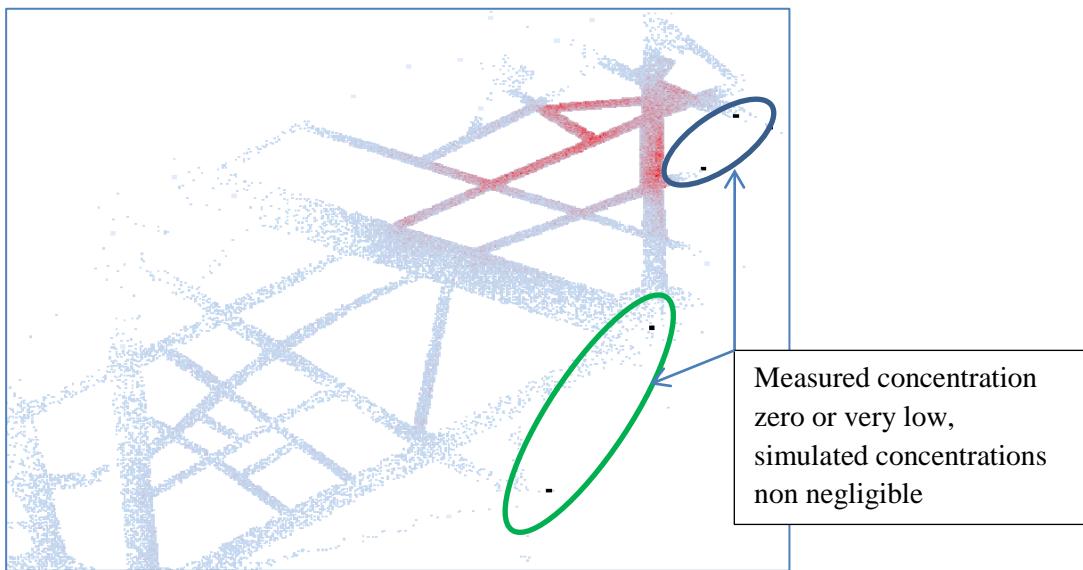
Figure 4.16 Concentrations computed by PMSS.

QUIC and PMSS reconstruct a mass consistent flow field around obstacles and treat the dispersion with a Lagrangian particles model. Even if they are simpler and quicker than CFD models, they are not real-time models, so the computational cost is very important in treating operational cases. Although both can treat the dense gas model, we have only used the dense gas model with QUIC in the simpler cases of INERIS experiments (in open field and only with a wall).

Verifications against full scale and small scale experimental data have been done. It was found that the magnitude of the results is essentially the same, whatever the model or the experiment. The quality of the comparison depends highly on the concentration (or dosage) threshold chosen, under which data are discarded.

As mentioned above, the set-up time and computational time is about 2 days, after getting the shapefiles of the buildings.

The risk analysis capability requires important cartographic and meteorological skills. It's not so easy to treat an operational case, but it could be done if all specific skills and input data (meteorological, geographic) are in the operational unit. The results are faster than with CFD models and provide a better understanding of the cloud crossing the streets than with a Gaussian model or a Lagrangian transport and diffusion model using Gaussian puffs as SCIPUFF (HPAC).

Some real testing need to be done on specific operational scenarios, but is not included here in this study report.

5 Results obtained by FFI Norway

5.1 ARGOS applied to INERIS dense gas ammonia release

Two cases of outdoor release of ammonia at the Centre of Scientific and Technical Studies of Aquitaine (CEA-CESTA) in France were simulated using the Accident Reporting and Guiding Operational System (ARGOS) version 9.2.7.5 from PDC-ARGOS. The simulations in ARGOS were performed with Urban Release and Dispersion module (URD) versions 8b [5]. The releases were conducted at the TEE test site at CEA-CESTA, an area which has a radius of approximately two kilometres, is flat and free from any obstacles. The releases were conducted at the centre of this site. Ammonia was released through a release device placed on a square (10 m x 10 m) concrete slab, approximately 15 cm thick as shown in Figure 5.1 [1].
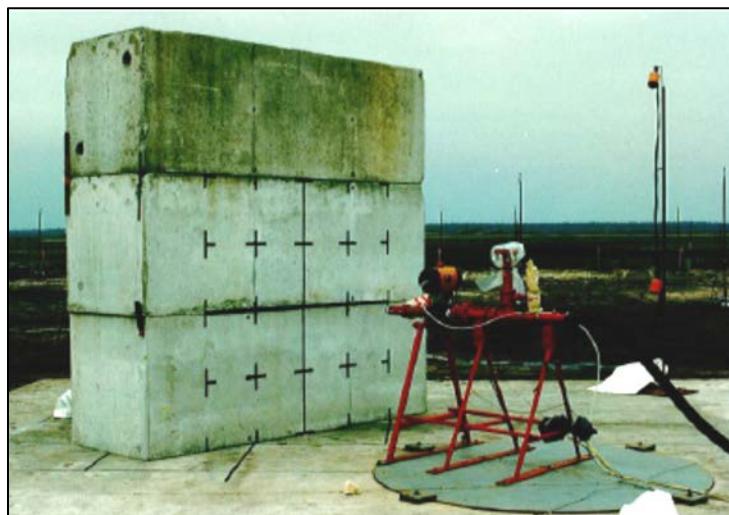

Figure 5.1   Release device and concrete wall (picture from INERIS report [2]).

Test no. 4 was a reference case with a horizontal release through a 50.8 mm diameter orifice without any obstacles. Test no. 5 was a release through the same orifice, but towards a 3 m x 3 m concrete wall placed 3 m from the release point (as shown in Figure 5.1)[6].

The meteorological parameters reported by INERIS [2] and shown in Table 5.1 were entered in the "advanced manual dialogue" in ARGOS. The parameters used in ARGOS for test no. 5 are shown in Figure 5.2. Note that a surface roughness of 0.05 was used, corresponding to grassland.

---

[5] A newer version of URD (version 8c), where the modelling of puff growth and puff position has been improved, is now available
[6] See also description in Chapter 3.4.2.

Test	Temperature [°C]	Relative humidity [%]	Solar flux [kW/m^2]	Wind velocity at a height of 7 m [m/s]	Wind direction at a height of 7 m [°C]
4	12.5	82	0.25	3.1	290
5	20	50	0.65	3.5	310

Table 5.1   Meteorological parameters during the ammonia releases, taken from the INERIS test report [2].
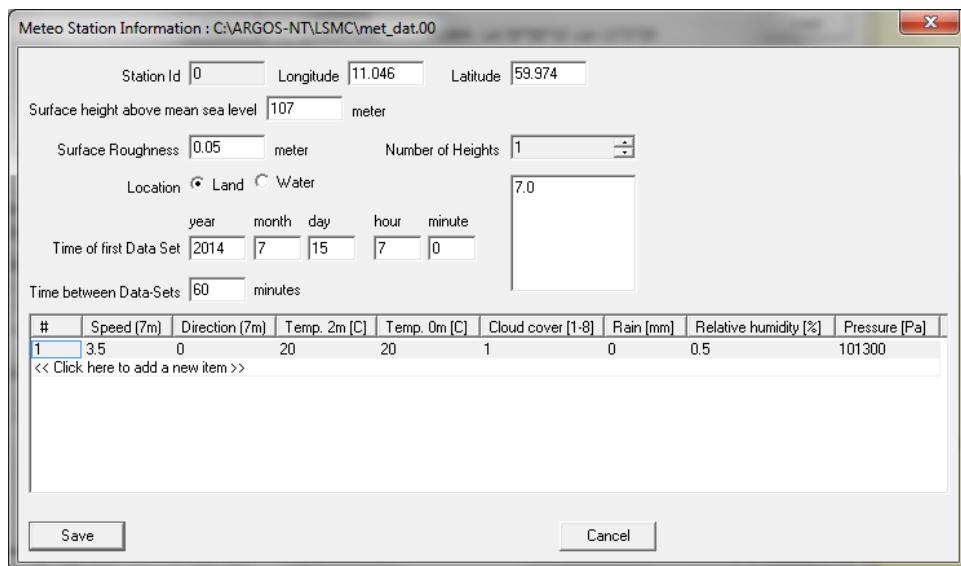
Figure 5.2   Advanced manual weather parameters used in ARGOS for test no. 5.

The experiment in test no. 4 was performed in slightly unstable/neutral atmospheric conditions (Pasquill-Gifford class C/D), whereas the experiment in Test no. 5 was performed under extremely unstable/moderately unstable atmospheric conditions (Pasquill-Gifford class A/B).

The release rate from test no. 4 was calculated with the source term module in ARGOS based on the information of the release system given by INERIS [2]. The given parameters were followed as closely as possible and the resulting release rates calculated by ARGOS are shown in Table 5.2. The result from this simulation fits well with the average flow rate of 4.2 kg/s given by INERIS and was used by the ARGOS dispersion modelling for release no. 4. A separate simulation using the average release rate for the whole period was also conducted.

Elapsed time (min)	Release rate (kg/s)
0-3	4.18
3-11	4.03
11-18	0.09
18-29	0.06
29-49	0.05
49-97	0.03
97-165	0.03
165-166	0.00

Table 5.2   Release rates calculated by ARGOS.

The URD in ARGOS was used with the input parameters shown in Figure 5.3.
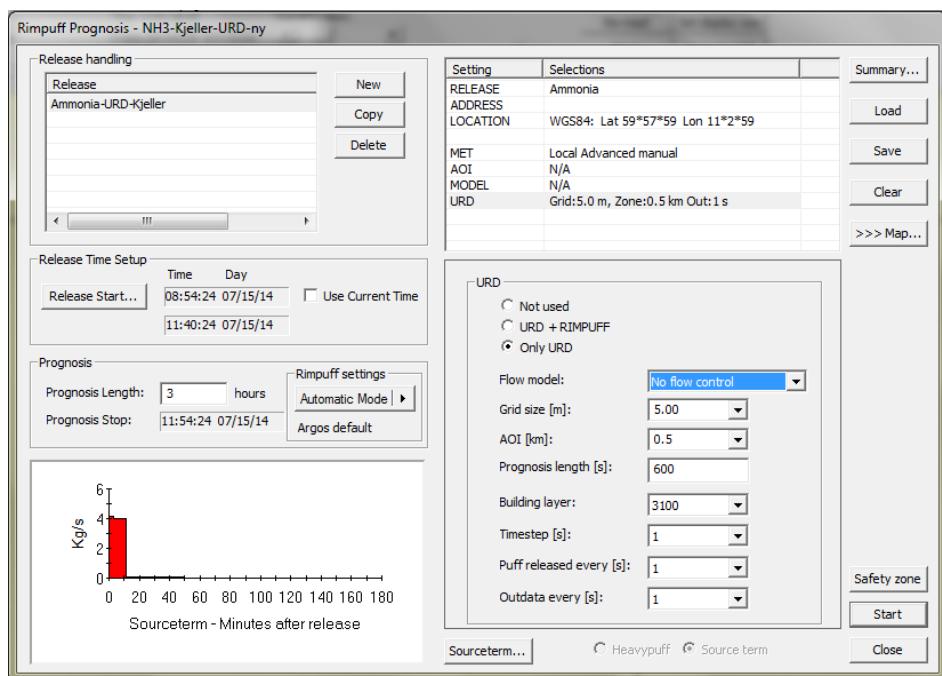
Figure 5.3   Parameters used for Urban Release and Dispersion (URD) in ARGOS.

The concentrations obtained by ARGOS are given at ground level, whereas the results from INERIS are read out at a height of 1 m.

5.1.1   Release no. 4

This was a horizontal release with no obstruction (no concrete wall). The module *URD with no flow control* was used in ARGOS because the other options (*FOI flow without wakes* and *FOI flow with wakes*) needed buildings at the site. ARGOS uses normally a Gaussian puff model (RIMPUFF), but has also a heavy-gas model (box-model). This heavy-gas model cannot be

used in combination with urban releases. The heavy-gas module was, therefore, tested without using the URD module.

5.1.1.1 Results

When using the heavy-gas module, the height of the plume was read out from the "Sourcemodeltester" program and plotted as shown in Figure 5.4. Argos uses in this case the HeavyPuff module up to 500 m from the release site, where Rimpuff takes over. According to the calculations shown in Chapter 3.4.4.6, in reality the transition between heavy and neutral gas takes place at approximately 200 m. The prediction plotted in Figure 5.4 shows that the plume height measured from the ground reaches a minimum of 0.8 m at 6.5 m from the release site.
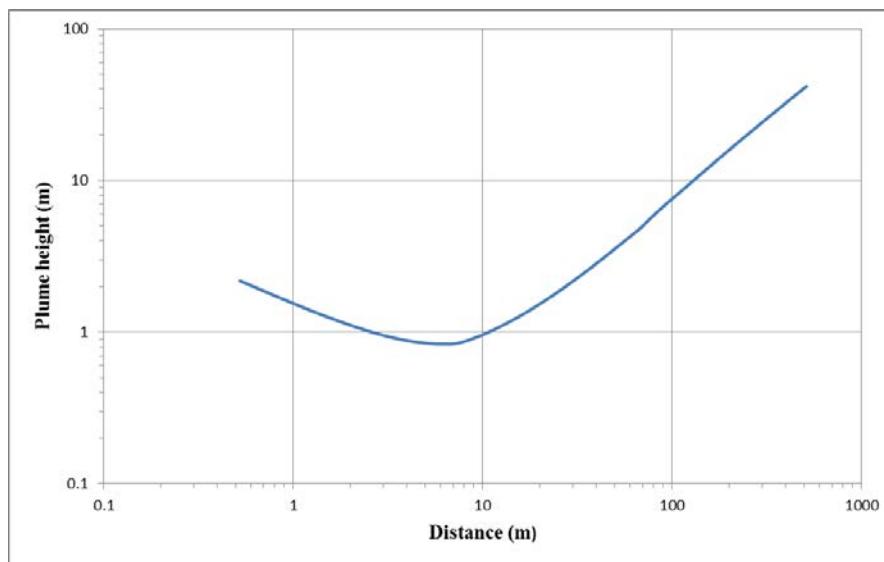
Figure 5.4   Plume height as a function of distance from the release site using the Heavypuff module in ARGOS.

The results from the ARGOS runs are shown in Table 5.3 and compared with the measurements reported by INERIS (Figure 5.5). In addition, a simulation with a constant release rate of 4.2 kg/s over 10 min in ARGOS was conducted. This is the average mass flow rate reported by INERIS [2]. As a comparison, results from the ARGOS runs with a constant release rate of 4.2 kg/s and the HeavyPuff run are shown in Table 5.3. In the ARGOS runs without HeavyPuff, the URD module was used up to 1 km where RIMPUFF takes over.

Distance from release site (m)	Maximum ammonia concentration at cloud centreline at ground level (INERIS at 1 m)				
	INERIS measured (mg/m^3)	ARGOS simulated (mg/m^3)	Time to reach maximum concentration in ARGOS (min)	ARGOS simulated rate 4.2 kg/s (mg/m^3)	ARGOS HeavyPuff (mg/m^3)
At nozzle		100000			
20	45000	16000	0.5	19000	75000
50	19000	4000	1	6300	20000
100	11000	1700	2	2400	7200
200	7000	630	3	1000	2200
500	830	170	6	170	1700
800	350	83	7	64	920
1500				23	135
2000				9.2	65
5000				0.83	10

Table 5.3   ARGOS results from the reference case (release no. 4) compared to the measured data by INERIS.
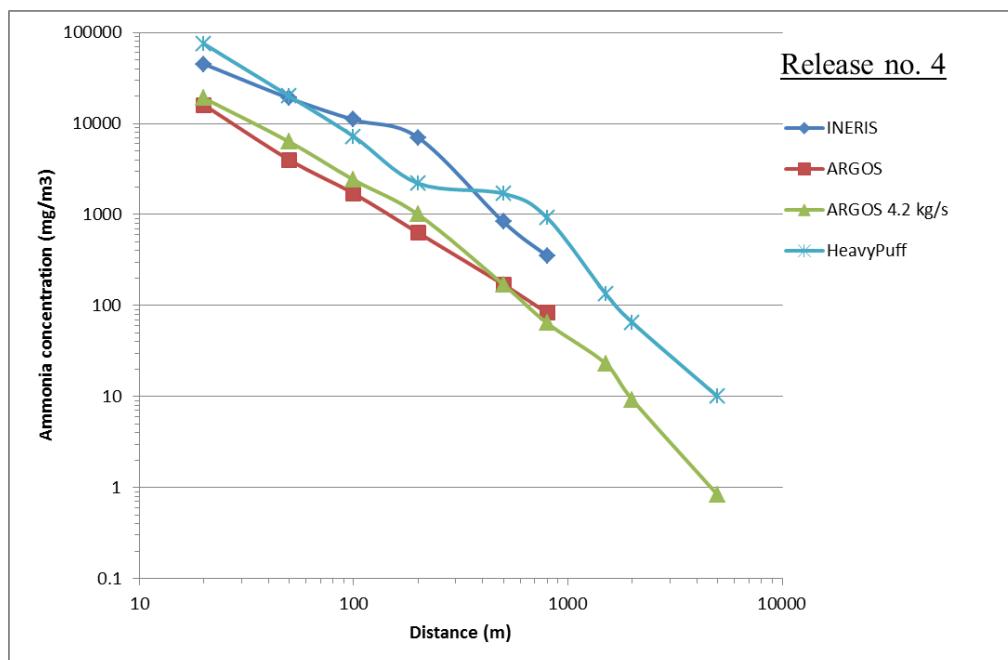
Figure 5.5   Ammonia concentration as a function of distance from the release site with no obstruction, including an ARGOS-run with constant release rate of 4.2 kg/s.

Figure 5.5 shows that the results from the HeavyPuff module in Argos are much closer to the measurements done at INERIS than the results from Argos using the URD module version 8b. It is, however, not possible to use the HeavyPuff module in ARGOS together with the URD module and ARGOS can therefore not be used to see any effects from the concrete wall in release no. 5.

The relationships between the ARGOS simulations and the real results from INERIS are shown in Figure 5.6.
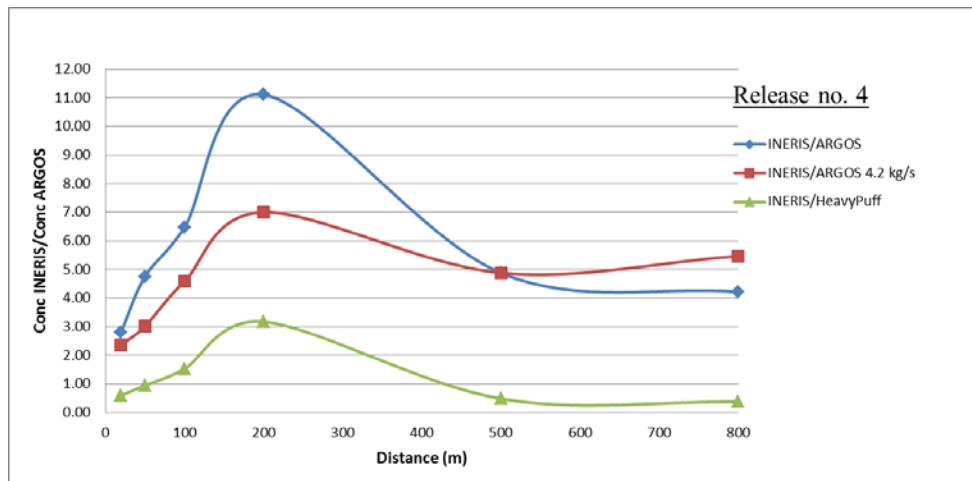

Figure 5.6   Relationship between the maximum ammonia concentration calculated by INERIS and ARGOS using both the release rate calculated by ARGOS and a constant release rate of 4.2 m/s.

Figure 5.6 shows that the ratios between the measurements at INERIS and the calculated concentrations by ARGOS increase with distance from the source and seem to level out and decrease after 200 m. When using the URD module, ARGOS has underpredicted the ammonia concentration during this release by a factor 2-11 depending on distance from the source. When using the HeavyPuff module, the results correspond much better with the real release, with differences by a factor 1/3 to 3.

The cloud width 20 m from nozzle, defined as the distance where the concentration has dropped to half the maximum concentration, was also compared: INERIS = 5 m, ARGOS approx. 10 m. This shows that the ammonia cloud simulated by ARGOS initially is wider and therefore less concentrated compared to the experiment. This could be the reason for the underprediction of the maximum concentration in this release. As described by INERIS [1], the ammonia release is a two-phase mixture, where the evaporation of ammonia aerosols keeps the plume temperature low so it stays close to the ground over a long distance. This behaviour is not captured by ARGOS. The height of the cloud could furthermore not be estimated by ARGOS when using the URD module.

The width of the plume simulated by ARGOS using the URD module was read out at different distances from the release point for both release no. 4 and release no.5 using the URD module and from release no. 4 using HeavyPuff. The results are compared and shown in Figure 5.9 in the next chapter.

5.1.2 Release no. 5

Since the ARGOS calculations of scenario no. 4 (shown in Figure 5.6 above) show that a constant release rate of 4.2 kg/s over 10 min gave a marginally better correlation with the measurements from the real release than using the source term module in ARGOS, a constant release rate was selected for scenario no. 5.

During release no. 5, the meteorological conditions were different from the reference case (release no. 4). The advanced manual meteorological parameters used in ARGOS for release no. 5 are shown in Figure 5.2.

The resolution in ARGOS using the URD module is 5 m x 5m with time steps down to 1 sec. Some initial runs showed that the original wall (3 m x 3 m) was too small to influence the dispersion in ARGOS. Therefore, the wall dimensions were scaled with factors 5, 10 and 20.

5.1.2.1 Scaling parameters

When upscaling the wall size, other variables should be scaled as well to keep the correct relationship between all the input parameters.

1. The height and width of the wall was scaled up equally in both directions
2. The distance between the nozzle and the wall was scaled proportional to the wall size as shown in Table 5.4)
3. The release rate was scaled proportional to the wall dimensions.
4. The wind speed was scaled up from the real measurements at INERIS, keeping the relationship between the (wind speed)^2 and the wall dimension constant:

$$\frac{u_{Argos}^2}{h_{Argos}} = \frac{u_{Ineris}^2}{h_{Ineris}} \Leftrightarrow u_{ARGOS} = u_{INERIS}\sqrt{\frac{h_{ARGOS}}{h_{INERIS}}} \text{ , where}$$

u_{INERIS} is wind speed measured by INERIS,
u_{ARGOS} is wind speed used in ARGOS calculations and
h_{ARGOS} / h_{INERIS} is the scaling factor used for the wall size

The scaled parameters used in ARGOS were: Wall size, release distance from wall, wind speed and release rate. These parameters are shown in Table 5.4.

Scaling factor	Wall height and width (m)	Release distance from wall (m)	Wind speed (m/s)	Release rate (kg/s)
Unscaled	3	3	3.5	4.2
5	15	15	7.8	21
10	30	30	11.1	42
20	60	60	15.7	84

Table 5.4   Scaled parameters.

5.1.2.2 Results

In order to compare the results with the real measurements, the following non-dimensional variables are introduced:

$$C^*_{ARGOS} = \frac{c_{ARGOS}\, u_{ARGOS}\, h^2_{ARGOS}}{Q_{ARGOS}},$$

$$C^*_{INERIS} = \frac{c_{INERIS}\, u_{INERIS}\, h^2_{INERIS}}{Q_{INERIS}},$$

$$x^*_{ARGOS} = \frac{x}{h_{ARGOS}} \text{ and}$$

$$x^*_{INERIS} = \frac{x}{h_{INERIS}} \text{ where}$$

C_{ARGOS} is concentration read out from ARGOS (in kg/m³),
u_{ARGOS} is wind speed used in ARGOS (in m/s),
h_{ARGOS} is scaled height or width of the wall (in m, where height and width is equal),
Q_{ARGOS} is release rate (in kg/s) and
C_{INERIS} is concentration reported by INERIS (in kg/m³),
u_{INERIS} is wind speed reported by INERIS (in m/s),
h_{INERIS} is original height or width of the wall (in m, where height and width is equal) and
Q_{INERIS} is release rate reported by INERIS (in kg/s)

Table 5.5 and Figure 5.7 show the dimensionless ammonia concentrations C^* as a function of the dimensionless distance (x^*). The concentrations from ARGOS are given at ground level, whereas the concentrations at INERIS were measured at 1 m above ground. A release without a wall, using the meteorological conditions for release no. 5, was also simulated by ARGOS and the results are shown in Table 5.5.

Real distance from wall (m)	Dimensionless ammonia concentration C* at cloud centreline at ground level (INERIS at 1 m)					
	INERIS	ARGOS without wall	ARGOS unscaled	ARGOS scaling factor = 5	ARGOS scaling factor = 10	ARGOS scaling factor = 20
20	210000	206250	131250	3144471	9913740	9928142
50	105000	68250	55425	1685436	5407495	7446106
100	48750	26250	23250	737902	2585162	4568287
200	11250	8850	8625	278390	1088614	2495452
500	1050	1950	2070	72616	286977	892191
800	225	750	720	30942	123803	390417
1000				20460	82773	333398
1300				12997	52415	216675
1600				8469	34390	145568
1900				4109	16602	64399

*Table 5.5   The dimensionless concentrations from INERIS and ARGOS.*
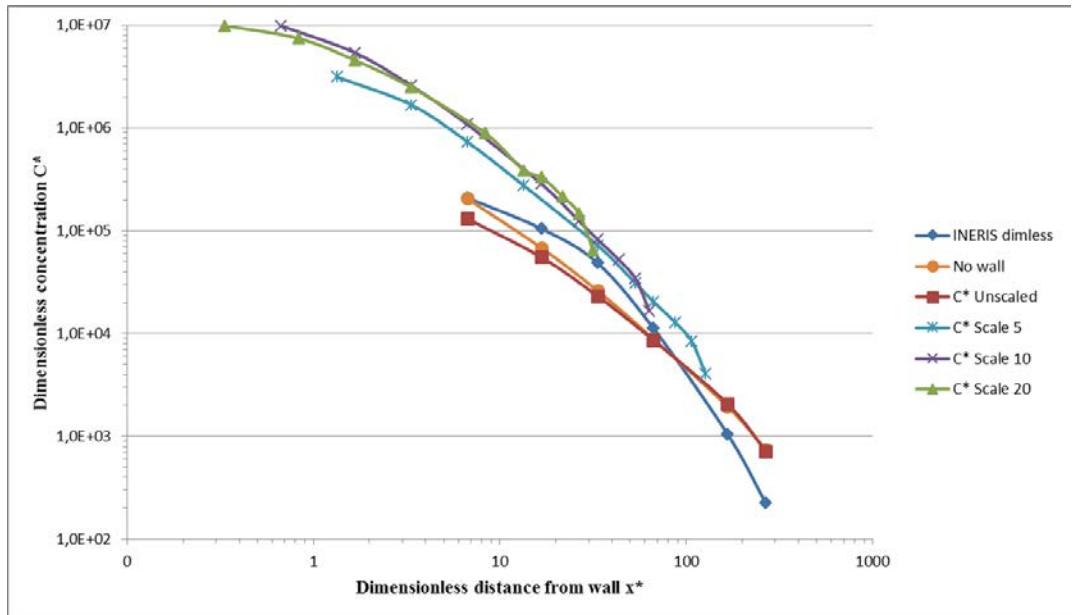
Figure 5.7 The dimensionless concentration C* as a function of dimensionless distance from wall x*.

Figure 5.7 shows that the predicted concentrations by ARGOS generally are higher than the actual concentration read out from INERIS. The exceptions are the concentrations at short distances from the wall (less than approximately 80 m) with no wall and with no scaling. This observation is opposite to what was observed during release no. 4, where ARGOS predicted lower ammonia concentrations than was measured in the experiment. The ratios between the predicted and real concentrations are given in Figure 5.8 and show that the difference between the reported and the calculated concentrations are between 1 and 5, increases with scaling factor and is generally higher at the smallest distances from the wall.
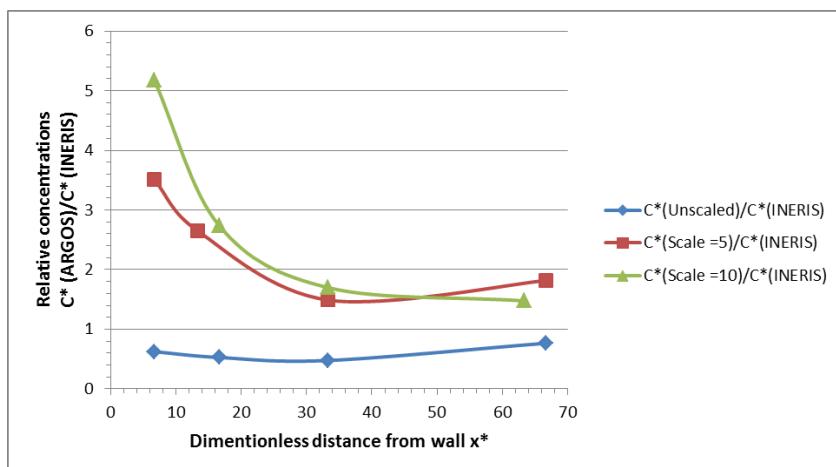
Figure 5.8 Ratio between the dimensionless concentrations predicted by ARGOS and the dimensionless concentrations measured at INERIS.

The results in Figure 5.7 and Figure 5.8 also show that ARGOS underpredicts the ammonia concentration close to the release site from release no. 5 when the wall was not scaled, similar to what was seen during release no. 4. Without scaling, the resolution in ARGOS is not high enough to recognise the presence of the wall. When the wall size is scaled up, the effect of the wall is seen and ARGOS overpredicts the ammonia concentration.

The reason for the overprediction of the ammonia concentration during release no. 5 could be that the recirculation and wakes around the wall will dilute the gas more effectively during the release than predicted by ARGOS. Another reason might be the possible rainout of liquid ammonia when the jet hits the obstacle. This was observed during the release at INERIS, but is not captured by ARGOS.

The ARGOS plume widths for the two meteorological conditions used in releases no. 4 and no. 5 are shown in Figure 5.9. In addition, the plume width using the HeavyPuff function for Release no. 4 is shown. The plume width is defined as the distance where the concentration has dropped to half the maximum concentration. A simulated ammonia release without obstacles was used for release no. 5.
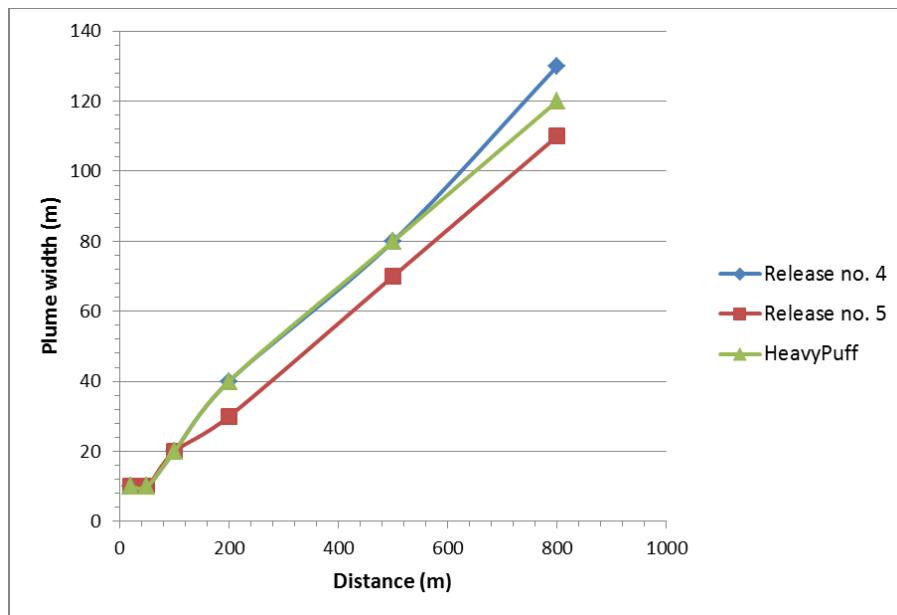
Figure 5.9   Plume widths simulated by ARGOS at different distances from the release point at the two meteorological conditions used in release no. 4 and release no. 5. In addition, the HeavyPuff function was used for release no. 4. All releases were simulated without obstacles.

The results plotted in Figure 5.9 show that the plume width from ARGOS was somewhat smaller (narrower plume) in release no. 5 without obstacles compared to what was produced from release no. 4. The reason might be a larger wind speed during release no. 5. When the HeavyPuff function was used, the plume width was similar to what was produced without the

HeavyPuff function. ARGOS uses the HeavyPuff function up to 440 m from the release site, where RIMPUFF takes over.

5.1.3 Conclusions on Argos applied to INERIS data

During release no. 4, without the concrete wall present, the ammonia centreline concentration was heavily underpredicted by ARGOS when using the Urban Release and Dispersion module (URD) version 8b instead of the HeavyPuff module. The reason might be that the Gaussian puff model in ARGOS (RIMPUFF) does not handle the ammonia release as a heavy gas and therefore predicts a larger and more dilute plume than was the case in reality. When the HeavyPuff module was used in ARGOS, the predicted centreline concentration was much closer to the measurements made by INERIS. The HeavyPuff module in ARGOS can, however, not be used together with the URD module. ARGOS (URD and RIMPUFF) does not take into account that the ammonia release is a two-phase mixture, where the evaporation of aerosols keeps the plume temperature low so it stays close to the ground over a long distance.

The ARGOS simulations using the URD module presented in this paper show that a wall with dimensions 3 m x 3 m is not large enough to affect the ammonia plume produced during the releases at INERIS. It was necessary to scale up the wall dimension by a factor of at least five in order to see any effects from the wall (i.e. 15 m x 15 m). When using this scaling factor, the ammonia centreline concentration from release no. 5 was constantly overpredicted by ARGOS. The reason for this might be that the recirculation and wakes around the wall will dilute the gas more effectively during the release than predicted by ARGOS, and the possible rainout of liquid ammonia when the jet hits the obstacle.

5.2 ARGOS applied to the Paris case

The objective has been to use ARGOS (Accident Reporting and Guidance Operational Systems) for simulating the neutral gas release for the Paris scenario. Obstacles can be taken into account through the sub-model Urban Dispersion Model (URD) which has been used for the Paris scenario. Since ARGOS cannot use URD for dense gas releases, only the neutral gas (air) released in the Paris scenario has been modelled.

5.2.1 Scaling Procedure

ARGOS has been used in full scale for the calculation of the Paris scenario. The spatial dimensions from the wind tunnel have therefore been scaled by a factor 350 [3]. Propane has been added to the air flow in the wind tunnel at a concentration of 1/1000 for detection purposes [3, 36]. The measured concentration of propane was therefore multiplied by 1000 to obtain the air concentration in the wind tunnel. The Paris building data used in ARGOS was obtained from DGA in ESRI shape format and converted to ARGOS-specific format by The Norwegian Radiation Protection Authority (NRPA).

5.2.2 Inflow conditions

The ARGOS results were compared with the wind tunnel experiments [36] carried out with a reference air velocity of 1 m/s. The air release rate in the wind tunnel was 0.11 m/s from a source with a diameter of 0.103 m, giving a release rate of 50 l/min.

In the calculations by ARGOS the release rate was scaled accordingly, giving a release rate of 2493 m^3/s air, corresponding to 2992 kg/s (air density 1.204 kg/m^3 at 20 °C [37]). A continuous release from a point source on the ground with a source duration of 30 min was used in the calculations.

The meteorological conditions used for the release in Paris are given in Table 5.6 below. Advanced manual meteorological setup was selected in ARGOS, using wind data from only one height (10 m).

Parameter	Value
Temperature	20 °C
Time of release	Mid-day in July
Atmospheric stability	Slightly unstable (C)
Wind speed	10.77 m/s (at 10 m height)
Surface roughness	0.10 m
Cloud cover	4/8
Precipitation	0 mm
Relative humidity	80 %
Atmospheric pressure	101300 Pa

Table 5.6   Meteorological conditions during the release.

5.2.3 Dense gas modelling, Obstacle treatment

It is not possible to use ARGOS to model dense gas dispersion in an urban environment. Only modelling of neutral gas dispersion (air) was therefore carried out.

5.2.4 Calculation set-up and control

The resolution in ARGOS using URD is 5 x 5m, with time steps down to 1 s. The parameters used for the calculations in this report are:

Flow model: FOI Flow without wakes
Resolution = 5.00 m
Area of interest (AOI) = 1.0 km

Prognosis length = 600 s
Building layer representing Paris buildings
Timestep = 1 s
Puff release every 1 s
Outdata every 15 s or 20 s

5.2.5 Results and discussion

ARGOS is a quick model that gives results within seconds or a few minutes when the input parameters are defined and entered into ARGOS. Using the URD with high resolution will result in longer runtime (a few minutes) compared to Rimpuff (seconds). Normally the most time-consuming step is definition of the scenario itself and finding the input parameters needed to run ARGOS. This set-up time could be shortened in a real case by reading actual weather from a weather service provider and by using predefined release-scenarios in ARGOS.

The results from ARGOS from the three different source positions are given in Figure 5.10 Figure 5.11, Figure 5.12 and Figure 5.13 for source S1; Figure 5.16, Figure 5.17, Figure 5.18 and Figure 5.19 for source S2 and Figure 5.21, Figure 5.22, Figure 5.23 and Figure 5.24 for source S3. Concentrations below 100 mg/m^3 are treated as noise in these plots.

5.2.5.1 Source S1: Position Champs Elysees

In Figure 5.10, the air concentration as a function of distance from the source is shown. The distances are calculated as straight lines as the crow flies. This figure shows that some concentrations predicted by ARGOS between 300 m and 400 m from the source are much higher than the wind tunnel measurements. Note that one very high concentration predicted by ARGOS close to source (7 740 000 mg/m^3 at 35 m) is not plotted in Figure 5.10.

Actually, the huge release rate was obtained by direct conversion of the wind tunnel conditions to full scale giving an unrealistically high release rate. A more realistic release is shown during the release of hydrogen cyanide (HCN) in Chapter 5.2.6.

In Figure 5.11, the air concentration in the wind tunnel (one minute averaging time) is plotted against the air concentration predicted by ARGOS, using logarithmic scales. Note that the highest concentrations in the lower left corner represent readings closest to the source. The results in this figure show that ARGOS give relatively good correlation with the wind tunnel measurements close to the source (most readings within FAC5), but overpredicts the concentrations farther away from the source.
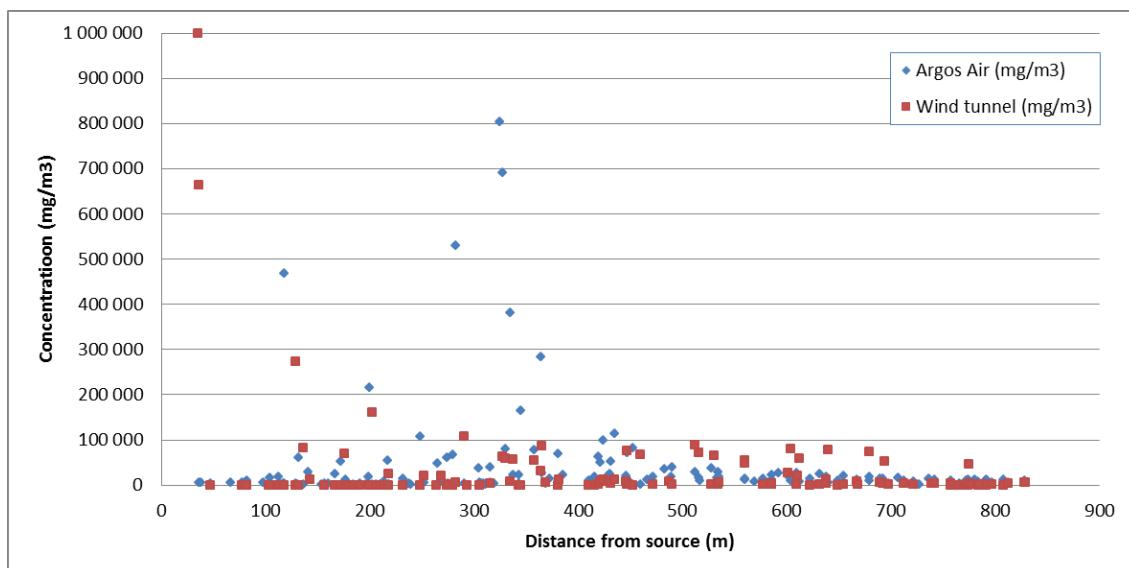
Figure 5.10 Air concentration as a function of distance from the source S1 position. One ARGOS reading close to the source is omitted (7 740 000 mg/m³ at 35 m from the source).
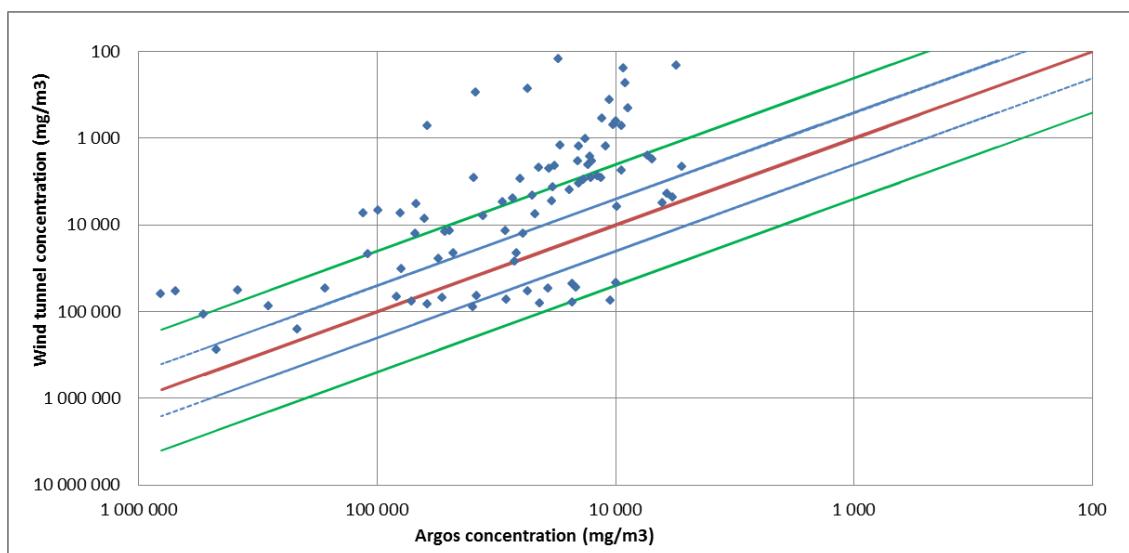

Figure 5.11 Air concentration predicted by ARGOS compared with the air concentration measured in the wind tunnel at different distances from the source S1. Note that the points close to origo represent the highest concentrations found close to the source. The red line represents exact match between predicted and measured concentrations. The blue and green lines represent two times and five times over- and underprediction (FAC2 and FAC5).
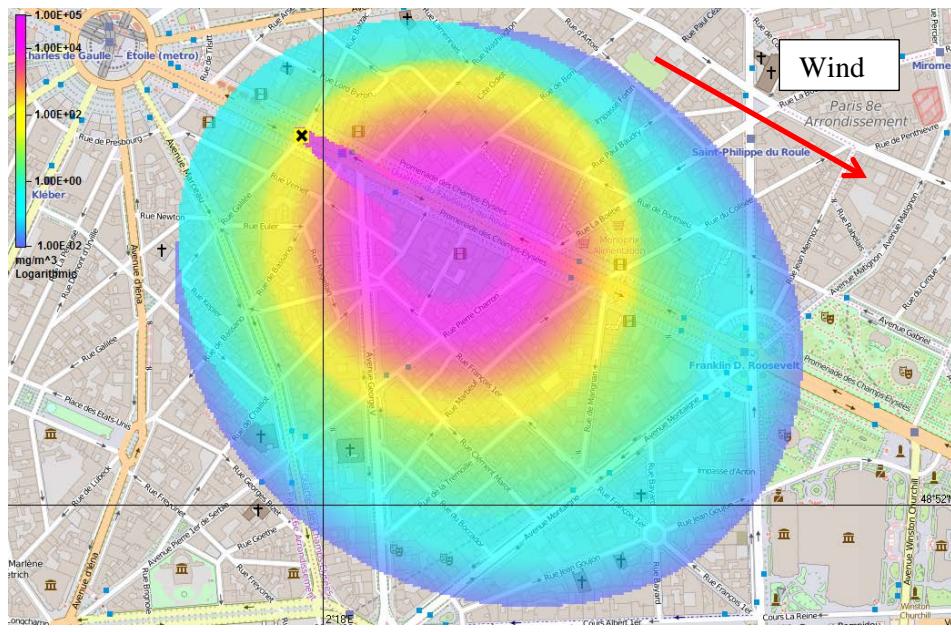
Figure 5.12 ARGOS concentration plot from the release at source position S1.
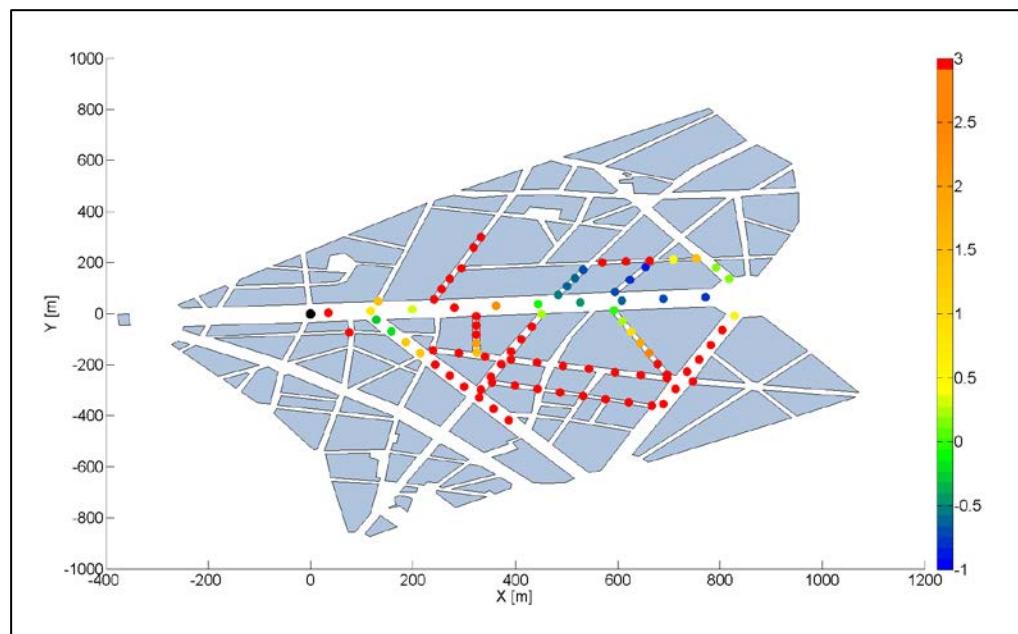
Figure 5.13 Comparison of ARGOS concentrations with wind tunnel measurements. Positive values indicate factors of overprediction and negative values indicate factors of underprediction. The black dot shows the position of the source. The wind direction is from left to right in the figure.

In Figure 5.13 a comparison of ARGOS predictions with wind tunnel measurements are shown graphically on a layout of the area of interest in Paris. Red dots indicate overprediction, green dots similar values and blue dots indicate underprediction. As most of the significant concentrations of air in the wind tunnel are in a narrow channel along Champs Elysees (see Figure 5.14), a large portion of the predicted ARGOS concentrations are higher than in the wind tunnel.
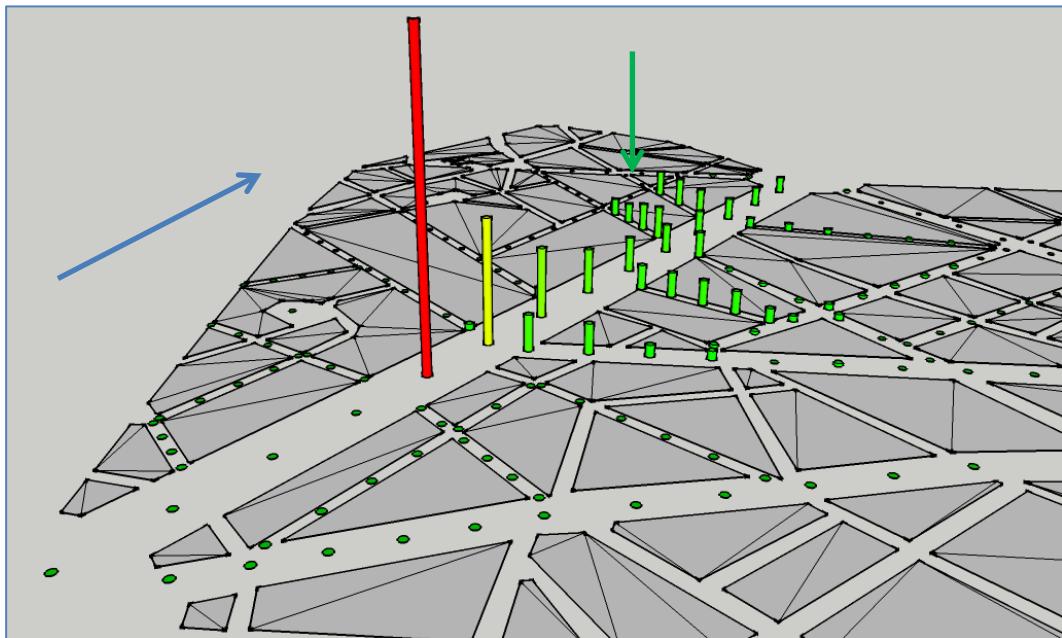
Figure 5.14 Column plot of street level measurements of air, source S1 (taken from J Benson, 2015). The blue arrow shows the wind direction in the tunnel. The green arrow shows the position of Rue la Boétie and Rue du Colisée.

The relative concentrations in Figure 5.14 also show that ARGOS predicts a quicker decrease of the agent concentration along Champs Elysees compared to the results from the wind tunnel. This will result in underprediction of the air concentration at the longest distances from the source as seen in Figure 5.15. The same observation was made during a recent COST project [38]. The reason for this underprediction might be that ARGOS predicts a spread of the released gas over a wider area, which gives a lower concentration compared to the wind tunnel where the gas is channeled along Champs Elysees.
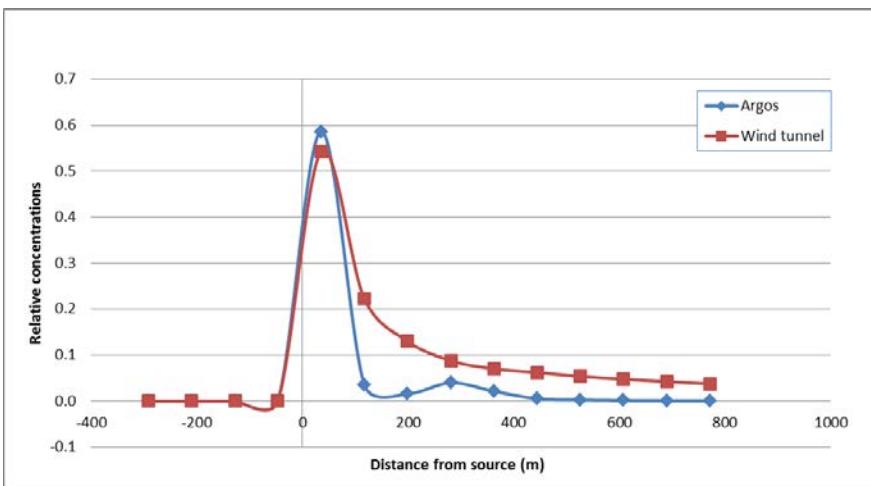
Figure 5.15 Relative concentrations along Champs Elysees.

In addition, the results from the wind tunnel show relative high concentrations of air north of Champs Elysees 500-700 m from the source in Rue la Boétie and Rue du Colisée (Green arrow in Figure 5.14) that are not observed in ARGOS. This pattern is due to the specific geometry for this source position, which generates a very complex wind field, not captured by ARGOS.

5.2.5.2 Source S2: Position Avenue George V

In Figure 5.16, the air concentration as a function of distance from the source is shown. The distances are calculated as straight lines as the crow flies. This source position shows better agreement between the wind tunnel concentrations and the concentrations predicted by ARGOS. Some overpredictions are observed as shown in Figure 5.17, where the air concentration in the wind tunnel (one minute averaging time) is plotted against the air concentration predicted by ARGOS, using logarithmic scales. Note that the highest concentrations in the lower left corner represent readings closest to the source. There are only a few overpredictions for this source location (see Figure 5.19). Farther away from source, ARGOS in general underpredicts the concentration, more to the left of the wind direction (upwards in Figure 5.19) than to the right.
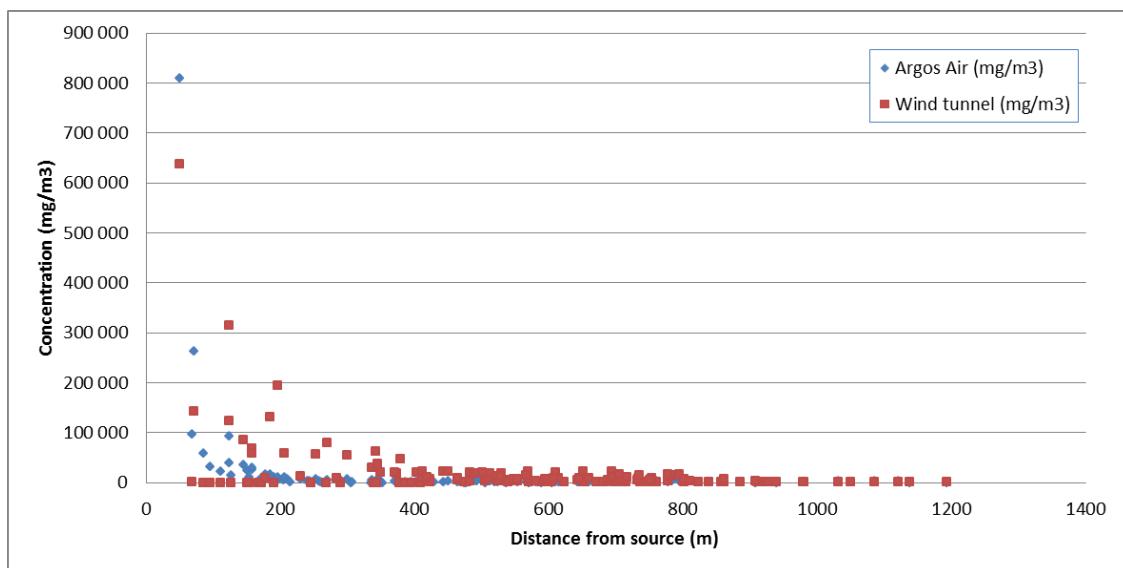
*Figure 5.16 Air concentration as a function of distance from the source S2 position.*
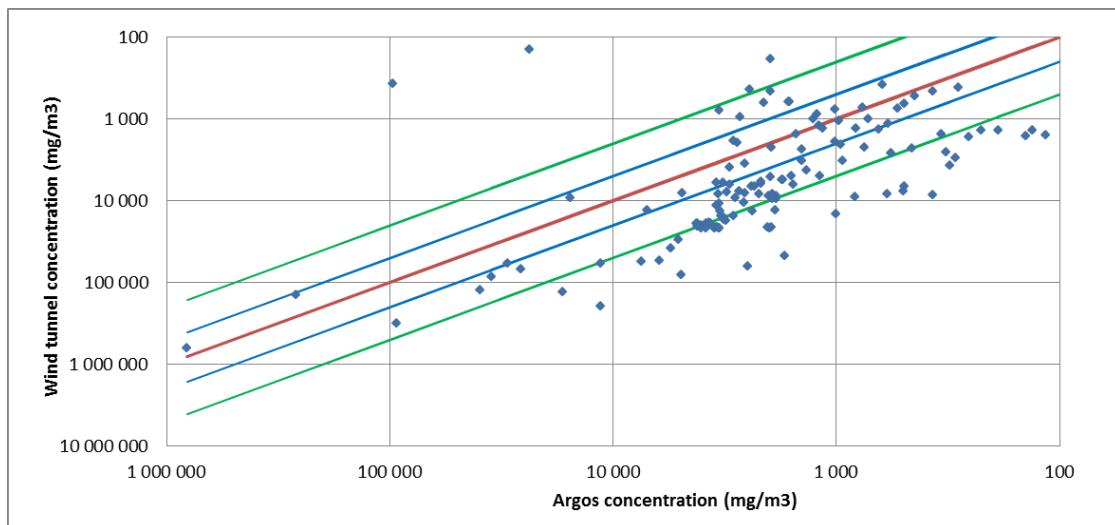
Figure 5.17 Air concentration predicted by ARGOS compared with the air concentration measured in the wind tunnel at different distances from the source S2. Note that the points close to origo represent the highest concentrations found close to the source. The red line represents exact match between predicted and measured concentrations. The blue and green lines represent two times and five times over- and underprediction (FAC2 and FAC5).
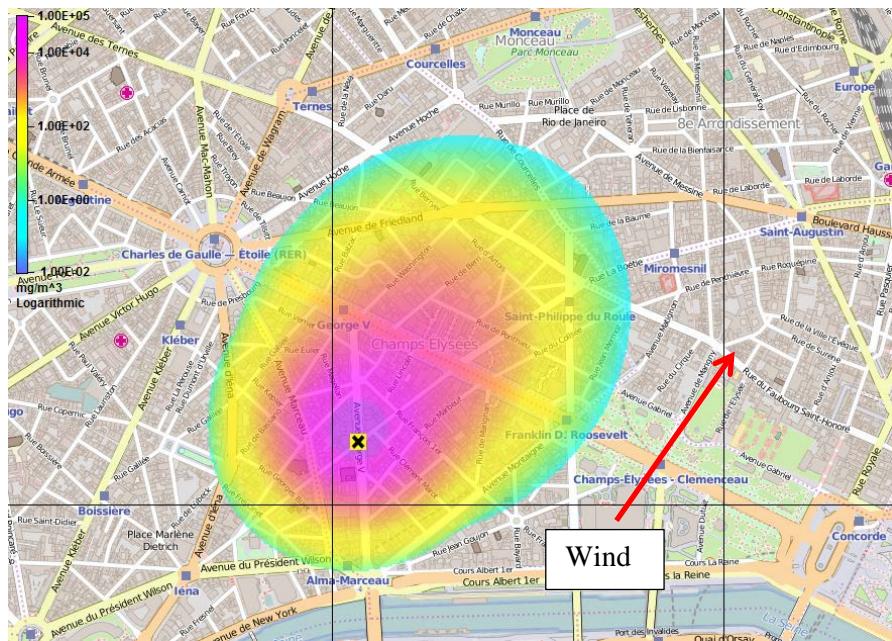
*Figure 5.18 ARGOS concentration plot from the release at source position S2.*
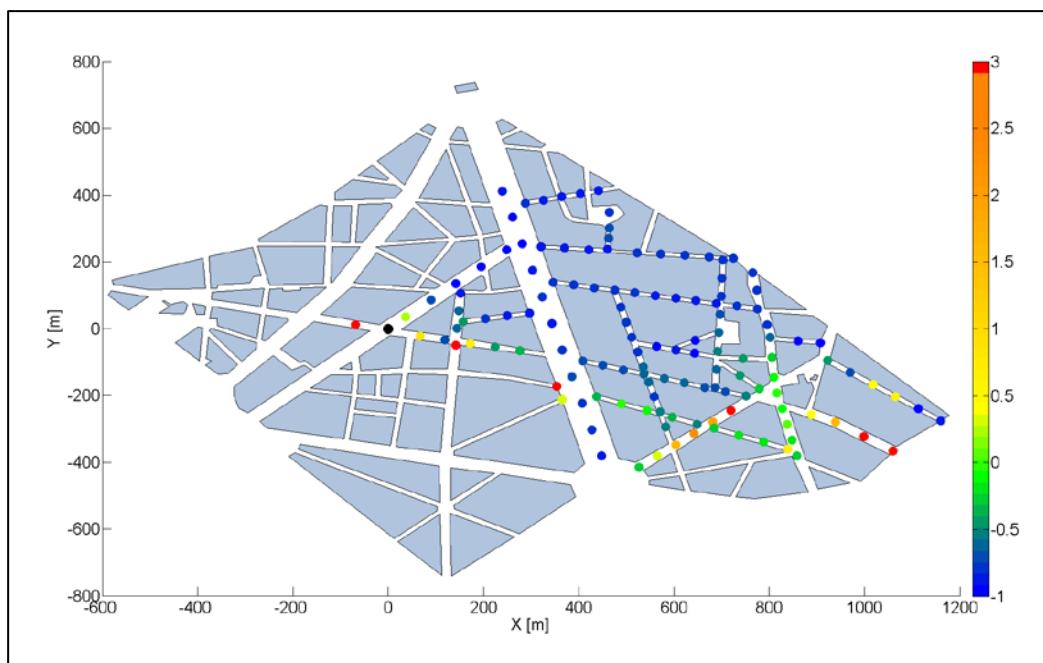
Figure 5.19 Comparison of ARGOS concentrations with wind tunnel measurements. Positive values indicate factors of overprediction and negative values indicate factors of underprediction. The black dot shows the position of the source. The wind direction is from left to right in the figure.

A column plot of street level measurements from the wind tunnel is given in Figure 5.20. This figure shows that the air concentration drops fairly quickly when moving downwind from the source. Only very low concentrations are observed laterally close to the source.
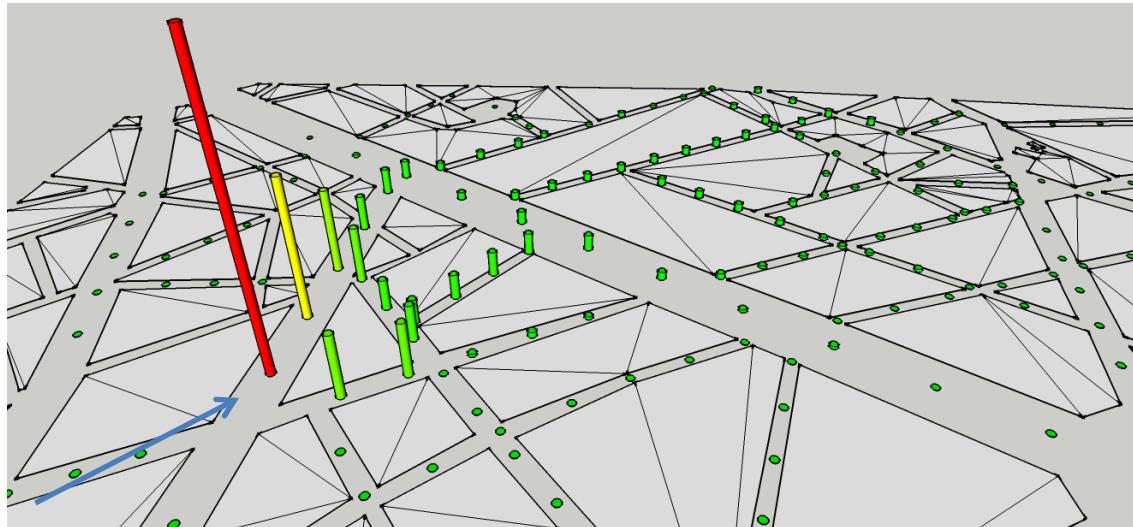

Figure 5.20 Column plot of street level measurements of air, source S2 (taken from J Benson, 2015). The arrow shows the wind direction in the tunnel.

5.2.5.3 Source S3: Position Église Saint-Philippe-du-Roule

In Figure 5.21, the air concentration as a function of distance from the source is shown. The distances are calculated as straight lines as the crow flies. This source position shows better agreement between the wind tunnel concentrations and the concentrations predicted by ARGOS than source positions 1 and 2. Most data are within FAC5 as shown in Figure 5.22. Note that the highest concentrations in the lower left corner represent readings closest to the source. The overpredictions are located laterally relatively close to the source (see Figure 5.24). Farther away from source, ARGOS in general underpredicts the concentration, mostly to the right of the wind direction (downwards in Figure 5.24). An exception is some ARGOS readings along Avenue Montaigne (upper right in the figure) which are close to or above the wind tunnel readings.
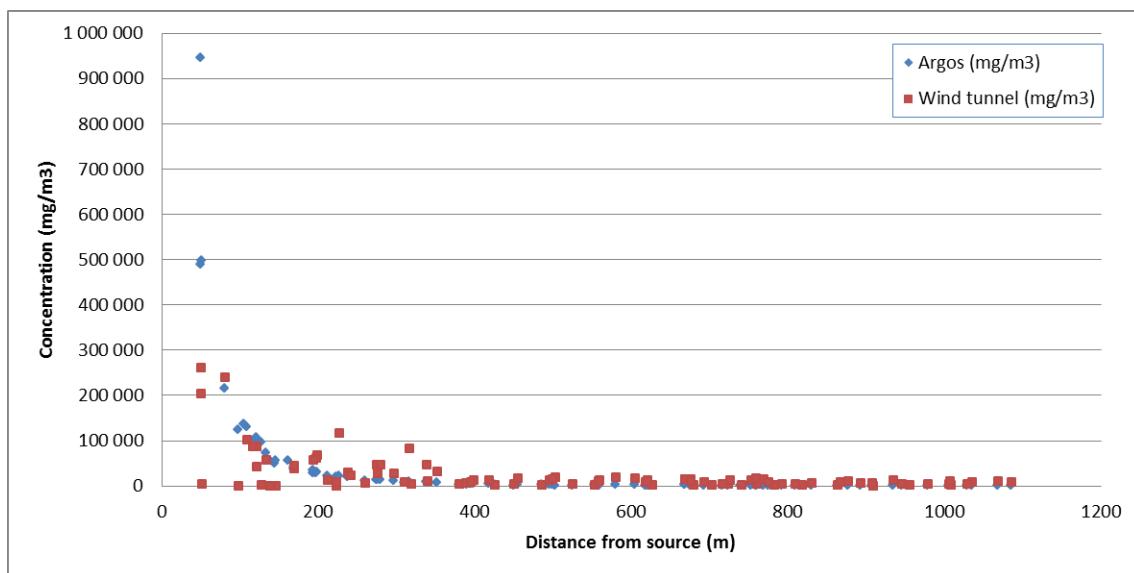
Figure 5.21 Air concentration as a function of distance from the source S3 position.
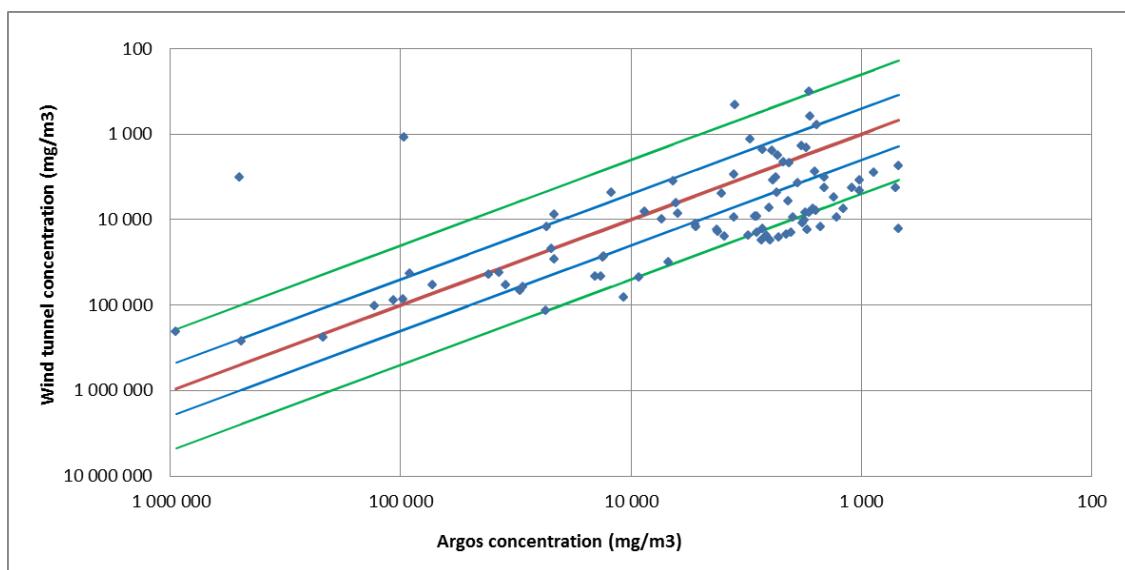

Figure 5.22 Air concentration predicted by ARGOS compared with the air concentration measured in the wind tunnel at different distances from the source S3. Note that the points close to origo represent the highest concentrations found close to the source. The red line represents exact match between predicted and measured concentrations. The blue and green lines represent two times and five times over- and underprediction (FAC2 and FAC5).

Figure 5.23 ARGOS concentration plot from the release at source position S3.
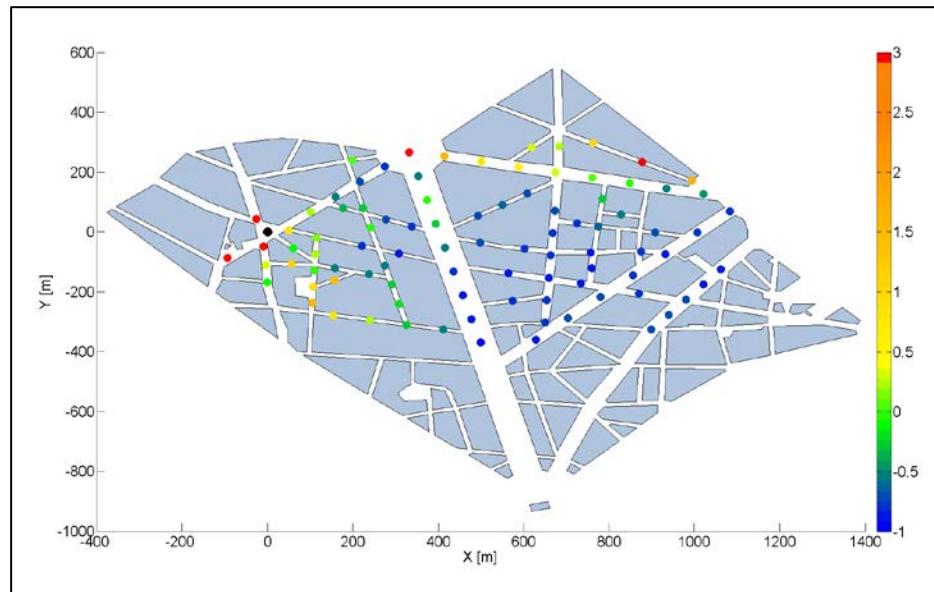

Figure 5.24 Comparison of ARGOS concentrations with wind tunnel measurements. Positive values indicate factors of overprediction and negative values indicate factors of underprediction. The black dot shows the position of the source. The wind direction is from left to right in the figure.
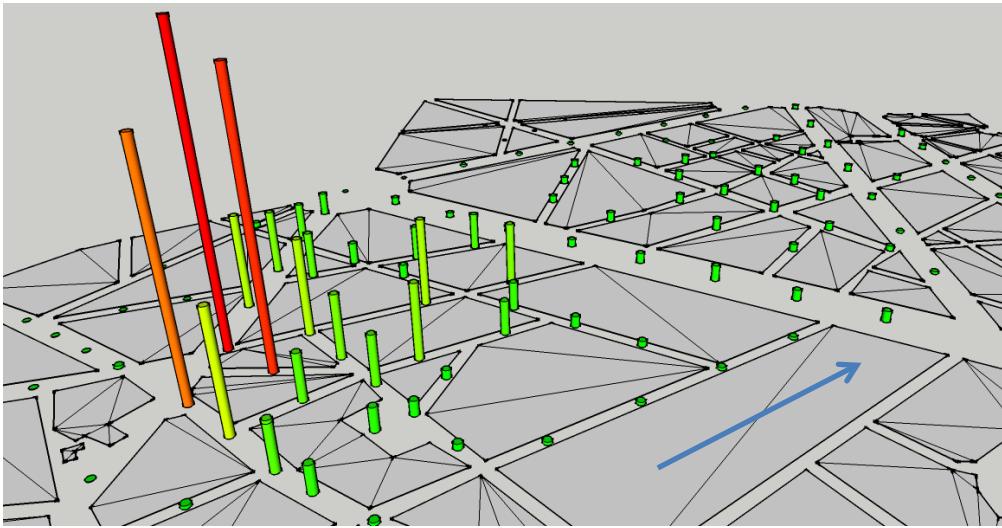
Figure 5.25 Column plot of street level measurements of air, source S3 (taken from J Benson, 2015). The arrow shows the wind direction in the tunnel.

The fraction of the results within a factor of two (FAC2) and within a factor of five (FAC5) are shown in Table 5.7. The results in Table 5.7 show that the ARGOS data fits the wind tunnel data best using the source S3 position and worst using the source S1 position. The reason might be that the wind direction along Champs Elysees does not retain the plume as much as the other source positions. This difference is not taken into account using ARGOS which uses calculations in an urban area, but does not reflect the differences in the street layout as much as the wind tunnel measurements, although a high concentration is predicted along Champs Elysees (see Figure 5.12). In source S3 position, the wind direction is not channelled along large avenues which give results more similar to wind tunnel measurements.

Source position	Fraction within FAC2	Fraction within FAC5
S1	0.08	0.26
S2	0.18	0.47
S3	0.30	0.69

Table 5.7   Fraction of the ARGOS results falling within a factor of two (FAC2) and a factor of five (FAC5).

5.2.6   Realistic Scenario with HCN release

In order to illustrate the ARGOS calculations with a more realistic example, 250 m^3/s of hydrogen cyanide (HCN) was released from source S1 position along Champs Elysees (continuous over 10 min) using the same input parameters as with air. The result is shown in Figure 5.26 (left) as a contour plot at maximum concentration with acute exposure guideline levels (AEGLs) as toxicity limits (10 min exposure). AEGL limits of 30 mg/m^3 (AEGL-3), 19 mg/m^3 (AEGL-2) and 2.8 mg/m^3 (AEGL-1) were used. For comparison, an ARGOS run with Rimpuff only (no URD, i.e. no building data) is also shown in Figure 5.26 (right).
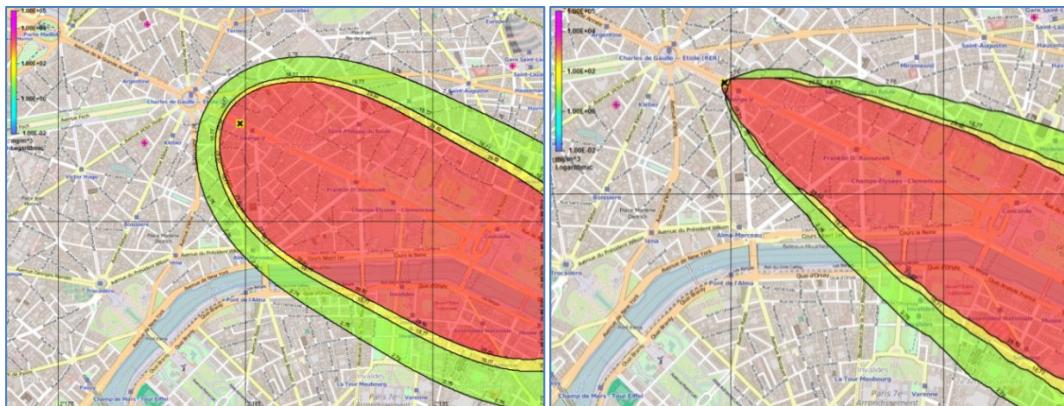
Figure 5.26 Areas of Paris which fall within 10 min exposure AEGL-3 (red plume), AEGL-2 (yellow plume) and AEGL-1 (green plume) exposure limits after a release of 250 m³/s hydrogen cyanide from source S1 position. Calculations using the URD module (left) are compared with Rimpuff (right).

The contour plots in Figure 5.26 show that the areas which fall within the AEGL concentration limits are wider and more oval shaped using the URD compared with Rimpuff, which show a more triangular shaped plume. This is caused by buildings blocking the plume forcing it to move more in lateral directions compared to Rimpuff with no building present. It is also observed upwind concentrations of HCN using URD due to a turbulent wind field at street level. Similar contour plots from source S3 position are shown in Figure 5.27.
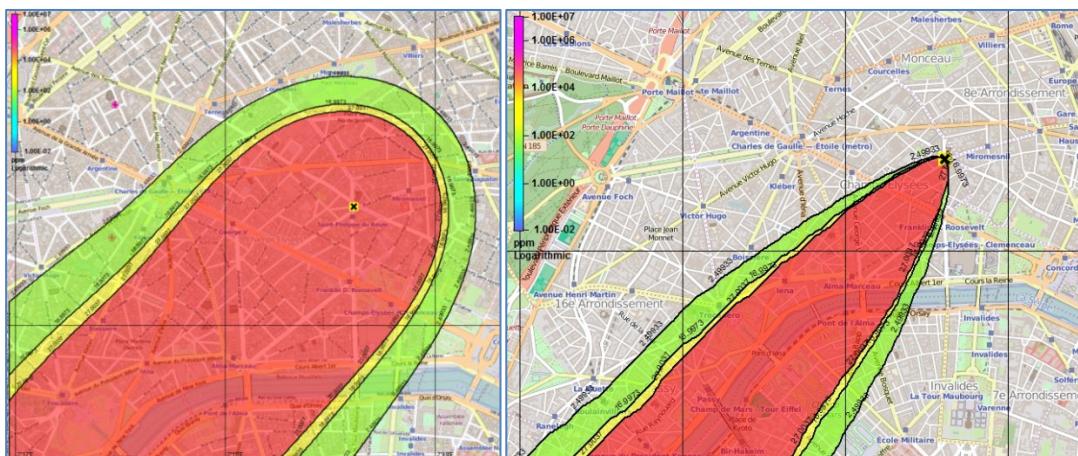

Figure 5.27 Areas of Paris which fall within 10 min exposure AEGL-3 (red plume), AEGL-2 (yellow plume) and AEGL-1 (green plume) exposure limits after a release of 250 m³/s of hydrogen cyanide from source S3 position. Calculations using the URD module (left) compared with Rimpuff (right).

Some differences between the two source positions could be observed. The plume width using URD is somewhat smaller from source S1 position (Figure 5.26, left) compared to source S3 position (Figure 5.27, left). The width of the plume at a distance of 1 km from source S1 position is 1170 m for AEGL-3, 1270 m for AEGL-2 and 1630 m for AEGL-1. For source S3 position, the widths are 1360 m for AEGL-3, 1490 m for AEGL-2 and 1970 for AEGL-1. The

source S3 position gives also higher upwind concentration of HCN compared to source S1 position. Both the wider plume and higher upwind concentrations from source S3 position could be explained by the more complex street pattern close the source with no clear channeling as along Champs Elysees in source S1.

In RIMPUFF, the concentration distribution in an individual puff is Gaussian with standard deviations representing the puff size in all three dimensions. This means that the plume width is larger in ARGOS compared to the actual plume in the wind tunnel.

5.2.7   Conclusions on Argos applied to the Paris case

The following conclusions and recommendations could be made based on the results using ARGOS on the Paris case. Since ARGOS cannot calculate dense gas distribution in an urban environment, only the neutral case (air) has been modelled.

ARGOS gives in general a more unresolved (smoothed) concentration distribution compared to the wind tunnel results (the resolution in ARGOS is 5m x 5m). ARGOS predicts a high concentration in all directions close to the source even in the cases where there is nothing measured in the wind tunnel due to blockage by the buildings. Some observations have further been made related to the three different source positions:

- Source S1: ARGOS generally overpredicts the concentrations (overall average 64000 mg/m^3 higher) compared to the wind tunnel. This is more pronounced close to the source. At the more distant locations some ARGOS concentrations are lower than the wind tunnel concentrations. This source location gives the highest air concentration (max 7.7 E06 mg/m^2) compared to source locations S2 (max 8.1 E05 mg/m^3) and S3 (max 9.5 E05 mg/m^3). According to Nunn [39], the lack of obstacles on the wide Champs Elysees keeps the gas channelled along the street at ground level in high concentrations and discourages vertical mixing.
- Source S2: In this case, the differences (both positive and negative) between ARGOS and wind tunnel concentrations are also larger close to the source (ARGOS predicts the concentration in average $\Delta C=107000$ mg/m^3 higher than the wind tunnel). Farther away from the source, ARGOS generally underpredicts the air concentrations.
- Source S3: In this case the differences between ARGOS and wind tunnel concentrations are smaller compared to the other source locations (ARGOS predicts the concentration in average 14000 mg/m^3 higher than the wind tunnel). This could be explained by the more complex street pattern close the source with no clear channelling as along Champs Elysees in source S1. ARGOS typically overpredicts the concentration close to the source and underpredicts the concentrations farther away from the source.

ARGOS is a model which produces quick results, but with much less resolution than the CFD models. In the tested scenarios in Paris, this in general results in overprediction close to the

source and underprediction farther away from the source. Close to the source this overprediction might be desired in order to be on the safe side.

6   Conclusions and Operational Recommandations

In this study, we wanted to assess the capabilities of current national in-use operational models to handle complex urban dispersion of dense gas release.

Although this WorkPackage WP6000 was not the main contribution to the project, we can draw a number of preliminary conclusions.

Referring to COST action ES1006 on the use of atmospheric dispersion models (ADM) in emergency response tools (ERT) [38], we confirm a number of statements, among which:

- There exists different types of operational tools that require different skill or expertise levels; in ascending orders: Gaussian, Gaussian Puffs (ARGOS, PUMA), Lagrangian particle (QUIC and PMSS). The wind is computed fast (URD in ARGOS, mass consistent and building wakes included in QUIC or PMSS), but the dispersion may take from minutes to hours. The most time consuming and expert part is the time needed to set up the models and couple them with meteorology and source term description.
- The use of FACn statistical measures to give confidence in our outputs will depend strongly on the noise level considered (ARGOS or PMSS results).
- These models are usually conservative, and overestimate the concentration levels close to the source (ARGOS on Paris scenario). They may be too much conservative and lead to wrong decision (evacuate a whole city when only a small part of it may be impacted for a given toxicity effect). Underprediction of the concentrations farther away from the source has been observed in the Paris scenario.

In addition to these remarks, not all our current models are capable to handle dense gas dispersion, and take into account obstacles.

The type of response that should be given to the decision makers is not straightforward: should we present danger zones corresponding to the concentrations/dosages above toxic thresholds or should we give confidence intervals.

QUIC software seems to work well using the included dense gas sub-model (compared to INERIS ammonia release data), and modified-PUMA gives also promising results. These last developments on PUMA have been tested within the scope of this project, dealing with dense puff interaction, in a linearized way to keep the response fast enough. ARGOS heavy puff model works well on INERIS ammonia release, but cannot handle obstacles at the same time.

Regarding obstacles, ARGOS URD wind model with RIMPUFF puff model necessitates to scale up small obstacles (INERIS case with wall) and is more suited to a densely built urban like area (Paris case, with source surrounded by buildings). This model can handle neutral gas only, so no dense gas-obstacle interaction could be tested and validated. On the Paris case, tendency to overestimate by a factor of 3 to 5 close to the source, and underestimate by such in far field, was observed and explanations were proposed.

PMSS was tested against demi-complex array and Paris cases for neutral gas only, and behaves quite satisfyingly with FAC2 of typically 40% and FAC5 of 70%. It was usually observed overestimations of concentrations behind buildings and underestimations in main streets (see the text for more details). This semi-operational tools demand some skill to scale and import shape files (or other numerical format) of the urban area. A dense gas module exists but was not available at the time. QUIC software has shown to give similar results on the demi-complex case.

Only in the study with ARGOS, a real case with HCN was considered (considered neutral). The differences shown by using a traditional puff model urban parameterized (RIMPUFF) and a more advance one (URD) are clearly shown. The more advanced model is taking obstacle blocking and enhanced diffusion into account.

In conclusion, as far as we tested our models, only QUIC has proved able to handle both obstacles and dense gas, PUMA was modified to handle dense gas characteristics but lacks some validation on urban area, and PMSS and ARGOS were partially validated with neutral gas on urban scenarios, but dense gas module remain to be tested/developed.

These tools are not push-button tools and require expert skills. The advantage against CFD is their cheap computer cost, but they still need relatively large set-up times compared to the run-time.

References

[1]   R. Bouet, "Ammonia. Large-scale atmospheric dispersion tests," INERIS - Accident Risks Division, France INERIS-DRA-RBo-199-20410. R. Bouet, 2005.

[2]   O. Gentilhomme, "MODITIC project. Agent characterisation and source modelling (WE 3300)," INERIS, France DRA-13-114532-08877A, 2013.

[3]   A. Robins, P.Hayden, E. M. M. Wingstedt. "MODITIC wind tunnel experiments", FFI-Rapport 2016/01483, Norwegian Defence Research Establishment, 2016.

[4]   J. Burman, B. A. Pettersson Reif, S. Burkhart, O. Parmhed, and A. Robins, "MODITIC WP 1000: Scenario definition and dissemination strategy," FOI, Swedish Defence Research Agency FOI-S--5474--SE, 2016.

[5]   H. W. M. Witlox, "The HEGADAS model for ground-level heavy-gas dispersion—I. Steady-state model," *Atmospheric Environment,* vol. 28, pp. 2917-2932, 1994/10/01 1994.

[6]   H. W. M. Witlox, "The HEGADAS model for ground-level heavy-gas dispersion II. Time-dependent model," *Atmospheric Environment,* vol. 28, pp. 2933-2946, 1994/10/01 1994.

[7]   D. L. Ermak, "A Description of the SLAB Model," Lawrence Livermore National Lab., CA (USA)1989.

[8]   A. P. van Ulden, "On the spreading of a heavy gas released near the ground," in *Proc. 1st. International Symposium on Loss Prevention and Safety Promotion in the Process Industry*, ed The Hague, Netherlands, 1974, pp. 221-226.

[9]   S. S. Beauchemin, H. O. Hamshari, and M. A. Bauer, "Passive Atmospheric Diffusion with Gaussian Fragmentation," *International Journal of Computers and Applications,* vol. 31, pp. 97-108, 2009.

[10]   S. Hanna and P. J. Drivas, *Guidelines for the Use of Vapor Cloud Dispersion Models*, 1987.

[11]   D. Anfossi, G. Tinarelli, S. Trini Castelli, M. Nibart, C. Olry, and J. Commanay, "A new Lagrangian particle model for the simulation of dense gas dispersion," *Atmospheric Environment,* vol. 44, pp. 753-762, 2// 2010.

[12]   S. G. Gopalakrishnan and M. Sharan, "A Lagrangian particle model for marginally heavy gas dispersion," *Atmospheric Environment,* vol. 31, pp. 3369-3382, 10// 1997.

[13]   B.-G. Kim, J. S. Kim, and C. Lee, "Lagrangian stochastic model for buoyant gas dispersion in a simple geometric chamber," *Journal of Loss Prevention in the Process Industries,* vol. 22, pp. 995-1002, 11// 2009.

[14]   M. D. Williams, M. J. Brown, B. Singh, and D. Boswell, "QUIC-PLUME theory guide," *Los Alamos National Laboratory,* 2004.

[15]   N. Brännlund, "Modeling and implementation of dense gas effects in a Lagrangian dispersion model," Swedish Defence Research Institiute FOI-D--0664--SE, 2015.

[16]   R. I. Sykes, C. P. Cerasoli, and D. S. Henn, "The representation of dynamic flow effects in a Lagrangian puff dispersion model," *Journal of Hazardous Materials,* vol. 64, pp. 223-247, Feb 1999.

[17]   R. I. Sykes and R. S. Gabruk, "A Second-Order Closure Model for the Effect of Averaging Time on Turbulent Plume Dispersion," *Journal of Applied Meteorology,* vol. 36, pp. 1038-1045, 1997/08/01 1997.

[18]   R. I. Sykes, S. F. Parker, D. S. Henn, and B. Chowdhury, "SCIPUFF Version 2.2 Technical Documentation," A.R.A.P Report No. 729, 2006.

[19]   S. M. Tauseef, D. Rashtchian, and S. A. Abbasi, "CFD-based simulation of dense gas dispersion in presence of obstacles," *Journal of Loss Prevention in the Process Industries,* vol. 24, pp. 371-376, 7// 2011.

[20]   S. R. Hanna, O. R. Hansen, M. Ichard, and D. Strimaitis, "CFD model simulation of dispersion from chlorine railcar releases in industrial and urban areas," *Atmospheric Environment,* vol. 43, pp. 262-270, 1// 2009.

[21]   M. Siddiqui, S. Jayanti, and T. Swaminathan, "CFD analysis of dense gas dispersion in indoor environment for risk assessment and risk mitigation," *Journal of Hazardous Materials,* vol. 209–210, pp. 177-185, 3/30/ 2012.

[22]   F. Scargiali, F. Grisafi, A. Busciglio, and A. Brucato, "Modeling and simulation of dense cloud dispersion in urban areas by means of computational fluid dynamics," *Journal of Hazardous Materials,* vol. 197, pp. 285-293, 12/15/ 2011.

[23]   F. Scargiali, E. Di Rienzo, M. Ciofalo, F. Grisafi, and A. Brucato, "Heavy Gas Dispersion Modelling Over a Topographically Complex Mesoscale: A CFD Based Approach," *Process Safety and Environmental Protection,* vol. 83, pp. 242-256, 5// 2005.

[24]   Y. Ding, F. B. Meng, B. Chen, H. Ma, J. Lei, and D. Y. Chen, "An experimental study on the fluorescence correlation spectroscopy in laser gradient field," *Acta Phys Sin-Ch Ed,* vol. 50, pp. 2269-2274, 2001.

[25]   G. Zhu, S. P. Arya, and W. H. Snyder, "An experimental study of the flow structure within a dense gas plume," vol. 62, pp. 161-186, // 1998.

[26]   J. S. Puttock, "A model for gravity-dominated dispersion of dense-gas clouds," in *Stably Straified Flows and Dense Gas Dispersion*, P. J.S., Ed., ed: Clarendon Press, Oxford, 1988.

[27]   R. H. S. Winterton, "Newton's law of cooling," *Contemporary Physics,* vol. 40, pp. 205-212, 1999/05/01 1999.

[28]   (2015). *The Engineering ToolBox*. Available: http://www.engineeringtoolbox.com/

[29]   R. Bouet, "Essais de dispersion atmosphérique à grande échelle," INERIS1999.

[30]   R. Bouet, S. Duplantier, and O. Salvi, "Ammonia large scale atmospheric dispersion experiments in industrial configurations," *Journal of Loss Prevention in the Process Industries,* vol. 18, pp. 512-519, 2005.

[31]   O. Gentilhomme, "MODITIC project: Agent characterisation and source modelling," INERIS DRA-13-114532-08877A, 2013.

[32]   T. Godish, *Air quality*: Lewis Publishers, 1991.

[33]   S. Zilitinkevich, P. E. Johansson, D. V. Mironov, and A. Baklanov, "A similarity-theory model for wind profile and resistance law in stably stratified planetary boundary layers," *Journal of Wind Engineering and Industrial Aerodynamics,* vol. 74-6, pp. 209-218, Apr-Aug 1998.

[34]   S. Fischer, R. Forsen, O. Hertzberg, A. Jacobsson, B. Koch, P. Runn*, et al.*, "Vådautsläpp av brandfarliga och giftiga gaser och vätskor: metoder för bedömning av risker," FOA-R--97-00490-990--SE 1997.

[35]   O. Björnham, "Source model of an adiabatic jet," Swedish Defence Research Agency FOI-R--4247--SE, 2016.

[36]   J. Benson, "Dispersion of a Hazard Material in an Urban Area, Project report," Department of Mechanical Engineering Sciences, Faculty of Engineering and Physical Sciences, University of Surrey, UK2015.

[37]   www.engineeringtoolbox.com, accessed 14. September 2016.

[38]   COST, "COST ES1006 Model evaluation case studies: Approach and results, ISBN: 987-3-9817334-2-6," 2015.

[39]   A. Nunn, "Report from Department of Mechanical Engineering Sciences, Faculty of Engineering and Physical Sciences, University of Surrey, UK," 2016.

About FFI

The Norwegian Defence Research Establishment (FFI) was founded 11th of April 1946. It is organised as an administrative agency subordinate to the Ministry of Defence.

FFI's MISSION

FFI is the prime institution responsible for defence related research in Norway. Its principal mission is to carry out research and development to meet the requirements of the Armed Forces. FFI has the role of chief adviser to the political and military leadership. In particular, the institute shall focus on aspects of the development in science and technology that can influence our security policy or defence planning.

FFI's VISION

FFI turns knowledge and ideas into an efficient defence.

FFI's CHARACTERISTICS

Creative, daring, broad-minded and responsible.

Om FFI

Forsvarets forskningsinstitutt ble etablert 11. april 1946. Instituttet er organisert som et forvaltningsorgan med særskilte fullmakter underlagt Forsvarsdepartementet.

FFIs FORMÅL

Forsvarets forskningsinstitutt er Forsvarets sentrale forskningsinstitusjon og har som formål å drive forskning og utvikling for Forsvarets behov. Videre er FFI rådgiver overfor Forsvarets strategiske ledelse. Spesielt skal instituttet følge opp trekk ved vitenskapelig og militærteknisk utvikling som kan påvirke forutsetningene for sikkerhetspolitikken eller forsvarsplanleggingen.

FFIs VISJON

FFI gjør kunnskap og ideer til et effektivt forsvar.

FFIs VERDIER

Skapende, drivende, vidsynt og ansvarlig.

FFI's organisation

FFI Forsvarets
forskningsinstitutt
Norwegian Defence Research Establishment